EFFECT OF RARE EARTH METAL SUBSTITUTION ON THE MAGNETIC AND TRANSPORT PROPERTIES OF Ni-Zn FERRITES

M. Phil. Thesis

By

Md. Alamgir Hossain

DEPARTMENT OF PHYSICS

KHULNA UNIVERSITY OF ENGINEERING & TECHNOLOGY

KHULNA - 9203, BANGLADESH

JANUARY - 2017

EFFECT OF RARE EARTH METAL SUBSTITUTION ON THE MAGNETIC AND TRANSPORT PROPERTIES OF Ni-Zn FERRITES

M. Phil. Thesis

By

Md. Alamgir Hossain

ROLL No. 1355551

SESSION: JULY - 2013

A THESIS SUBMITED TO THE DEPARTMENT OF PHYSICS, KHULNA UNIVERSITY OF ENGINEERING & TECHNOLOGY, KHULNA - 9203 IN PARTIAL FULFILMENT OF THE REQUIRMENT FOR THE DEGREE OF MASTER OF PHILOSOPHY

DEPARTMENT OF PHYSICS

KHULNA UNIVERSITY OF ENGINEERING & TECHNOLOGY

KHULNA - 9203, BANGLADESH

JANUARY - 2017

TO

MY PARENTS

DECLARATION

This is to certify that the thesis work entitled as **"Effect of Rare Earth Metal Substitution on the Structural, Magnetic and Transport properties of Ni-Zn Ferrites"** has been carried out in partial fulfillment of the requirement for M. Phil. degree in the department of Physics, Khulna University of Engineering & Technology, Khulna - 9203, Bangladesh. The above research work or any part of this work has not been submitted anywhere for the award of any degree or diploma. No other person's work has been used without due acknowledgement.

1. Supervisor

(Prof. Dr. S. S. Sikder)

Candidate

(Md. Alamgir Hossain)

2. Co-Supervisor

(Dr. Md. Nazrul Islam Khan)

Acknowledgements

I would like to articulate with due respect my sincere and heartiest gratefulness to my respective research supervisor Prof. Dr. Shibendra Shekher Sikder, Department of Physics, Khulna University of Engineering & Technology (KUET) for his indispensable guidance, keen interest, constructive suggestions, fruitful discussion and constant inspiration throughout the research work. It would have not been possible for me to bring out this thesis without his help and constant encouragement.

I am deeply grateful to my co-supervisor Dr. Nazrul Islam Khan Principal Scientific Officer, Materials Science Division, Atomic Energy Centre, Dhaka, for introducing the present research topic and inspiring guidance and valuable suggestions throughout the research work.

I am indebted to Prof. Dr. Md. Mahbub Alam, Prof. Dr. Abdullah Elias Akhtar and Prof. Dr. Jolly Sultana, Department of Physics, Khulna University of Engineering & Technology (KUET) for their strong support in various ways the entire period of my study in this department.

I am grateful to S. Manjura Haque, Head & Chief Scientific Officer, Material Science Division, Atomic Energy Centre Dhaka, for providing kind opportunity to work her laboratory for experimental work.

I would also like to show my gratefulness to all the members of the material science groups especially Dr. Zakir Hossain and Dr. Saroaut Noor for their pioneering works for the future generation of Department of Physics. I am grateful to Mr. Md. Kamrul Hasan Reza, Associate Professor, Department of Physics, Khulna University of Engineering & Technology (KUET), Mr. Sujith Kumar Shil, Assistant Professor, Mr. Suman Halder, Mr. Suman Debnath , Lecture, Department of Physics, Khulna University of Engineering & Technology (KUET) for their tireless co-operation in my thesis work.

I am thankful to Eng. F. M Kamal S. E. Dr. Md. Mahbubul Haque S. S. O. of MSD of AECD for providing me with technical assistance from time during my research work at the laboratory of AECD. I am also thankful to Ms. Alhamra Parvin, E.O., Ms. Anjummanara Begum J. E. O., Mr. Anawar Hossain S. S. A. Ms. Nazmunnahar Begum (S.A.-II), Ms. Jarna Begum (S.A.-II) of Material Science Division, Atomic

Energy Centre Dhaka (AECD), for their co-operation during the experiments and heartfelt help during the entire period of my research work at the laboratory of AECD.

My special thanks are to the Director, Material Science Division, Atomic Energy Centre Dhaka (AECD) for his kind permission to use the laboratory of Material Science Division, Atomic Energy Centre Dhaka.

A very special thanks to Mrs. Nandita Saha, spouse of Prof. Dr. S. S. Sikder for her heartfelt encouragement, cares and helps throughout the entire period of M. Phil. program.

My gratitude and thanks are also to my father, mother, wife, sisters, uncle, nephew, niece and all of my family members who all were very much co-operative with my higher studies.

I also wish to thank the authority of Khulna University of Engineering & Technology (KUET), for providing me with the necessary permission and financial assistance for conducting this thesis work.

Md. Alamgir Hossain

ABSTRACT

The present work is focused on the influence of substitutions rare earth ions in Ni-Zn ferrites. Three series of ferrite samples of the compositions $Ni_{0.60}Zn_{0.40-x}La_xFe_2O_4$ (where x = 0.05, 0.10 and 0.15), $Ni_{0.60}Zn_{0.40-x}Y_xFe_2O_4$ [x = 0.05, 0.10 and 0.15] and $Ni_{0.60}Zn_{0.40-x}Eu_xFe_2O_4$ [x = 0.05, 0.10 and 0.15] were prepared by using solid state reaction technique. The phase identification was carried out by using the X-ray diffraction (XRD). The XRD analysis revealed that undoped rare earth in sample shows formulation of cubic spinel structure with no extra peak but other three RE (La, Y and Eu) doped samples show additional peaks other spinel structure and corresponding to a second orthoferrite phase. Lattice parameters of all three series slightly decrease with increasing x-content. A slightly increase in bulk density has been found with increasing RE content. The average grain size increases significantly with increasing RE content. The increase in density and grain growth of the samples may be attributed to the liquid phase at constant sintering temperature. A slight increase of Curie temperature, T_c and saturation magnetization M_s of $Ni_{0.60}Zn_{0.40-x}RE_xFe_2O_4$ [RE = La, Y and Eu] series with increasing RE in were observed. The change of M_s with the increase of RE substitution has been explained on the Neel's Collinear two sublattices magnetization model and Yafet-Kittels' non-collinear magnetization model. Initial permeability decreases with the increasing of RE ions. Quality factor signifies the merit of the material from the application point of view. The variation of the quality factor with frequency shows a similar trend for all three samples. From these three series of samples are seen that the real part of initial permeability almost constant up to 4MHz. The AC resistivity decreases with increasing temperature. The dielectric constant is found to decrease continuously with increasing frequency and remains almost constant at higher frequency range. The variation of electrical resistivity and dielectric properties is explained of Fe^{2+}/Fe^{3+} ionic concentration with affect RE ions as well as the electronic hoping frequency between Fe^{2+} and Fe^{3+} ions.

Contents

CHAPTER-III

EXPERIMENTAL PROCEDURE

CHAPTER-IV

RESULTS AND DISCUSSION

CHAPTER-V

CONCLUSIONS

List of Figures

List of Tables

List of Symbols

Rare Earth	=	RE
Lanthanum	=	La
Yttrium	=	Y
Europium	=	Eu
Rare –earth garnets	=	REG
Gadolinium-iron garnet ($Gd_3 Fe_5O_{12}$)	=	GDIG
Inversion parameter	=	δ
Radio frequency	=	RF
Oxygen positional parameter	=	U
Absolute value of impedance	=	$\|Z\|$
Angular frequency	=	ω
Anisotropy field	=	H_K
Anisotropy constant	=	K_1
Average anisotropy	=	<K>
Bohr magneton	=	μ_B
Inter sublattice exchange interaction	=	J_{AB}
Intra-sublattice exchange	=	J_{AA}
Intra-sublattice exchange	=	J_{BB}
Atomic Energy Center Dhaka = AECD		
Bragg's angle	=	Θ
Bulk density	=	d_B
Charge of electron	=	e
Capacitance	=	C
Coercivity	=	H_C
Cross-sectional area of toroids	=	S
Curie temperature	=	T_C
DC resistivity	=	ρ_{dc}
Dielectric constant	=	ϵ'
Diffraction angle	=	θ
Exchange integral	=	J

Exchange coupling constant	=	J_{ij}
Exchange correlation length	=	L_O
Face centered cubic	=	fcc
Frequency	=	f
Ferromagnetism	=	FM
Imaginary part of initial permeability	=	μ''
Impedance	=	Z
Personal Computer	=	PC
Integrated Circuit	=	IC
Lattice parameter	=	a_0
Avogadro's number	=	N_A
Inductance	=	L
Initial permeability	=	μ_i
Inter planner spacing	=	d
Loss factor	=	$\tan\delta$
Saturation Magnetization	=	M_s
Magnetic field	=	H
Magnetic induction	=	B
Magneto crystalline anisotropy constant	=	K_l
Nell temperature	=	T_N
Nelson-Riley function	=	F (ɵ)
Number of turns	=	N
Peak temperature	=	T_P
Permeability of in free space	=	μ_O
Quality factor	=	QF
Reactance	=	X
Real part of initial permeability	=	μ'
Retentivity	=	B_r
Remanent ratio	=	M_r
Resistance	=	R
Resistivity	=	ρ
Saturation magnetization	=	M_S
Saturation induction	=	B_S

Saturation polarization	=	J_S
Susceptance	=	B
Susceptibility	=	χ
X-ray density	=	ρ_x
Thickness of the pellet	=	h
Radius of the pellet	=	r
Electric displacement	=	D
X-ray diffraction	=	XRD
Yafet-Kittel	=	Y-K
Wavelength	=	λ
Scanning Electron Microscope	=	SEM
Vibrating Sample Magnetometer	=	VSM
Nelson Relay Function	=	N-R

CHAPTER I

INTRODUCTION

CHAPTER II

THEROETICAL BACKGROUND

CHAPTER III

EXPERIMENTAL PROCEDURE

CHAPTER IV

RESULTS AND DISCUSSION

CHAPTER V

CONCLUSION

REFERENCE

INTRODUCTION

1.1 Introduction

Ferrites i.e. ferromagnetic cubic spinels are technically important materials. They have been extensively investigated in order to improve good soft magnetic properties. Magnetically soft ferrites are ceramic materials having cubic spinel structure. The general combination of such ferrites is MF_2O_4, where M represents one or several of the divalent transition metals such as Mn, Zn, Ni, Co, Cu, Fe or Mg etc. Ferrimagnetic oxide, ferrite crystallizes with two magnetic sublattices i.e. tetrahedral (A)-site and octahedral (B) - site based on Neel's model. The Ni-Zn ferrites are one of the most versatile, reasonable cost magnetic materials for general use in both low and high frequency devices because of their high resistivity, low dielectric losses, mechanical hardness, high Curie temperature and chemical stability. The typical Ni-Zn ferrites are sintered satisfactory only above 1200°C, where their microstructure and properties being difficult to control because of the validity of ZnO at such high temperatures. High sintering temperature may cause anomalous densification, and high power permeability and low magnetic loss Ni-Zn ferrites at decreased sintering temperatures.

At the beginning of the industrialization, iron and its alloys were used as magnetic materials to serve the need of the electrical industry. With the advent of higher frequencies, the standard techniques of reducing eddy current losses, using lamination or iron powder cores, were no longer efficient or cost effective. This realization stimulated a renewed interest in "Magnetic Insulators" as first reported by S. Hilpert in Germany in 1909. By 1909 Snoek had laid down the basic fundamentals of the physics and technology of practical ferrites materials [1.1]. In 1948, the Neel theory of ferromagnetic provided the theoretical understanding of this type of magnetic material. Polycrystalline soft ferrites prepared from metal oxides are metallic semiconductors and made important contribution, both theoretical and conceptual to the development of electronics. Soft ferrites still remain the best magnetic materials and cannot replaced by any other magnetic materials with respect to their very high frequency application because they are in expensive more stable, easily manufactured [1.2].

The most important advances were made in ferromagnetism in the field of magnetic oxide. The advancement of high frequency ferrites was initiated by the work done by Snoek [1.3] who found that associated with excellent properties in the high frequency range Mn-Zn and Ni-Zn ferrites provide a family of magnetic materials useful for radio and TV sets as carrier telephony as cores of inductors transformer and so forth. The most popular combinations are Ni-Zn [1.4], Ni-Cu-Zn [1.5-1.7], Mg-Zn [1.8] and Mg-Cu-Zn [1.9-1.10] ferrites. Magnetic and electrical properties of ferrites are strongly dependant on distribution of cations in A and B sites and their valence state The properties of Ni-Zn ferrites can be tailored with different metals in such as Co^{2+}, Mg^{2+}, Mn^{2+}, Cu^{2+} etc. Varies additives such as V_2O_5, Bi_2O_3, PbO, MoO, NO_3, Eu_2O_3, P_2O_5, La_2O, W_2O_3, LiO etc. having low melting point, facilitated to reduce the sintering temperature of these oxide materials due to liquid phase either due to the melting point of the additives or due to the eutectic liquid phase formation between the additives and their ferrites. Amount of liquid phase increase with increasing amount of sintering aids which results in increased densification. However, excessive amount of sintering additives will deteriorate electromagnetic properties of the ferrite. So, optimum content of sintering aids is necessary to achieve good sinter ability as well as better electromagnetic properties.

The addition of rare-earth metal in Ni-Zn ferrite composition is known to crucial role in increasing the sintering density and lowering the sintering temperature. The rare earth substituted different ferrites are becoming the promising materials for different applications. Addition of small amount of rare earth ions to ferrite samples produces a change in their properties depending upon the type and the amount of rare earth elements used. Rare earth ions can be divided into two categories; one with the radius closes to Fe ions; while other with ionic radius larger than Fe ions [1.11]. The difference in their ionic radii will lead to micro strains which may cause domain wall motion resulting in deformation of the spinel structure [1.12]. It has been stated that the rare earth ions commonly reside at the octahedral sites by replacing Fe^{3+}ions and have limited solubility in the spinel lattice due to their large ionic radii. If the rare earth ions enter the spinel lattice the RE-Fe interaction also appears (4f-3d coupling) which can lead to changes in the magnetization and Curie temperature [1.13]. The rare earth oxides are good electrical insulators and have resistivities at room temperature greater than $10^6\Omega$-cm [1.14]. Rare earth ion forms the orthoferrite phase.

The occupation of RE ions on B-sites impedes the motion Fe^{2+} in the conduction process in ferrite, thus causing an increase in resistivity. Although enormous research activities have been carried out on spinel soft ferrites in order to improve and optimized their electrical and magnetic properties, there does not exist an ideal ferrite sample that meets the requirements of high permeability and low eddy current loss at reasonably high frequency.

Till now researchers have not yet been able to formulate a rigid set of rules for ferrites about a single property. The most effective sintering for Ni-Zn ferrite the systematic research is still necessary for effects has been under taken to prepare Ni-Zn ferrite doped with La_2O_3, Y_2O_3 and Eu_2O_3. However, attempts have been made to present a systematic review to various experimental and theoretical observed fast related on the study. To carried out on the influence of different rare earth atoms on the properties of ferrites like high saturation magnetization, high permeability, high resistivity, dielectric etc. The results of these researches show that different rare earth behaves differently in spinel structure ferrite. The systematic research is still necessary for a more comprehensive understanding and properties of such materials.

1.2 The Aims and Objectives of the Present Work

The effect of rare earth ions on the structural, magnetic and transport properties of $Ni_{0.6}Zn_{0.4-x}RE_x Fe_2O_4$ ferrites where RE = La, Y and Eu. Rare earth ion formed orthoferrite ($REFe_2O_4$) phase and the formation of these secondary phases in ferrite during sintering process was governed by the type and the amount of RE^{3+}ion used.

The main objectives of the present research work are made as follows:

(i) $Ni_{0.6}Zn_{0.4-x}La_xFe_2O_4$ [x = 0.05, 0.10, 0.15]

(ii) $Ni_{0.6}Zn_{0.4-x}Y_xFe_2O_4$ [x = 0.05,0.10,0.15] and

(iii) $Ni_{0.6}Zn_{0.4-x}Eu_x Fe_2O_4$ [x = 0.05, 0.10, 0.15]

It is ferromagnetic in nature and posses a cubic structure and can be used in various electromagnetic devices due to their high resistivity and high frequency tolerance. At present, Bangladesh is totally dependent upon the imported ferrite cores and other soft magnetic materials. If we can develop rare earth doped ferrites in our country that may alleviate present problems of our country. Even though, improvements and innovation continue to take place; many new applications,

theories and preparation technologies are currently under development in the field of ferrites.

- To synthesis a series of rare earth metals Ni-Zn ferrites.
- To investigate the structure of the composition using XRD and SEM.
- To study electrical and magnetic properties of the sample using LCR meter, VSM.
- To study effect of La^{3+}, Y^{3+} and Eu^{3+} substitution for Fe^{3+} on structural and transport properties of the optimized Ni-Zn ferrite.
- Optimize the concentration of rare earth doped for the best magnetic and transport properties.

Finally, it is expected to use powder particles as starting materials may give uniform microstructure exhibiting better magnetic and electrical transport properties. With the substitution of rare earth metals in the Ni-Zn ferrite system permeability and magnetic properties are expected to be improved. Thus this system will have further good technological application in high frequency range. In our research in soft magnetic materials and in rare earth metal doped ferrites, Bangladesh may develop a profitable electronic industry.

1.3 Experimental Reason for This Research Work

Rare earth metal doped ferrites sample have been prepared by standard solid state reaction technique. High purity powders of NiO (99.9%), ZnO (99.9%), La_2O_3 (99.9%), Y_2O_3 (99.9%), Eu_2O_3 (99.9%) will be mixed thoroughly in an appropriate amount mixing will be performed in both dry and acetone. The mixed powders will be calcined at high temperature. After calcinations toroid and disk shaped sample will be prepared and will be sintered at various temperatures. The experimental methods that have been used in this work are as follows:

(i) The prepared sample would be characterized in terms of their crystal structure, unit cell parameters and phase presents in the prepared sample with the help of XRD.

(ii) Sintering of the samples has been carried out in a microprocessor controlled high temperature furnace.

(iii) Surface morphology of the samples has been investigated using scanning electron microscope (SEM).

(iv) Permeability, magnetic loss factor and quality factor as function of frequency have been determining using impedance analyzer.

(v) Magnetizations of the samples have been measured as a function of field using vibrating sample magnetometer (VSM).

(vi) AC electrical resistivity as a function temperature has been studied with the help of electrometer.

(vii) Dielectric properties as a function of frequency have been studied with the help of inductance meter.

1.4 Application of Ferrites

Ferrites are primarily used as inductive components in a large variety of electronic circuits such as low noise amplifiers, filters, voltage controlled oscillators, impedance matching networks for instance. The basic components to produce the inductance are very soft ferrite and a metallic coil. Multilayer chip inductors for high frequency circuit's applications use sheets made of dielectric ceramics instead of ferrite industry. Ferrites are used widely due to their following application.

(i) Ferrites are part of low power and high flux transformers which are used in television.

(ii) Small antennas are made by winding a coil on ferrite rod used in transistor radio receiver

(iii) In computer, non volatile memories are made of ferrite materials. They store in formation even if power supply fails. Non-volatile memories are made up of ferrite materials as they are highly stable against severe shock and vibrations.

(iv) Ferrites are used in microwave devices like circulators, isolators, switch phase shifters and in radar circuits.

(v) Ferrites are used in high frequency transformer core and computer memories i.e. computer hard disk, floppy disks, credit cards, audio cassettes, video cassettes and recorder heads.

(vi) Ferrites are used to produce low frequency ultrasonic waves by magnetostriction.

(vii) Nickel alloys are used in high frequency equipments like high speed relays, wideband transformers and inductors. They are used to

manufacture transformers, inductors, small motors, synchros and relays. They are used for precision voltage and current transformers and inductive potentiometers.

(viii) They are used as electromagnetic wave absorbers at low dielectric values.

(ix) Ferrites are important components for the latest products, such as cellular phones, video cameras, note book computers, hard temperatures and floppy drives.

(x) Ferrites for the applications in producing multilayer-type chips mainly because these oxides can be sintered at relatively low with a wide range of compositions.

1.5 Review of the Earlier Research Work

Spinel ferrites are extremely important for academic and technological applications [1.15-1.17]. The physical properties such as structural, electrical and magnetic properties are governed by the type of magnetic ions residing on the A site and B-site of the spinel lattice and the relative strength of inter and intra sub lattice interactions. In recent years, the design and synthesis of non magnetic particles have been the focus of fundamental and applied research owing to their enhanced or unusual properties [1.18]. Many investigators have been carried out on the different rare earth atoms like La, Sm, Gd, Nd, Dy, Tb, Cs, Th, Y, Eu on the properties of ferrites. The results of the researches show that different rare earth cations in Ni-Zn based alloy ferrites along with some different ferrites is reviewed below.

Rezlescu *et. al.* [1.19] investigated the effect of Fe replaced by RE [Yb, Eu, Sm, Tm, Gd, Dy and Ce] ions on the properties of $(Ni_{0.7}Zn_{0.3})\ Fe_2O_4$ ferrite. The results showed that the electrical resistivity of a ferrite increased by substituting a small quantity of Fe_2O_3 with RE_2O_3. Sun *et. al.* [1.20] investigated the effects of rare earth ions on the properties of $(Ni_{0..5}$-Zn) $Fe_{1.98}RE_{0.02}O_4$ [RE = Y, Eu and Gd] nominal compositions. The partial substitution of Fe^{3+} with a small amount of RE ions increased the electrical resistivity and relative loss factor, whereas, it slightly decreased the Curie temperature. Results had shown that Y and Eu substitution tend to decrease initial permeability, μ_i while Gd did not reduce μ_i.

The structural and magnetic properties of Ni-Zn ferrite films with high saturation magnetization have been synthesized by Guo *et. al.* [1.21]. They observed

the XRD patterns and confirm the samples were well crystallized and single phase. SEM images indicated that all the samples consisted of particles nanocrystaline in nature. They have observed a large real part of permeability, μ_i a very high resonance frequency f_r of 1.2 GHz. Lattice parameter and saturation magnetization of Ni-Zn ferrites have been investigated by Naughton *et. al.*1.22]. The lower saturation magnetization was attributed to a combination of the large lattice parameter decreasing the per- exchange interactions between the Ni^{2+} and Fe^{3+} ions and incomplete ordering of the cations between the octahedral and tetrahedral sites in the spinel structure.

Sun *et. al.* [1.23] reported the effect of the Fe substitution by La and Gd on the structure, magnetic and dielectric properties of $(Ni_{0.5}Zn_{0.5}Fe_{2-x})$ RE_xO_4 ferrites. It was found that the relative density of sintered bodies decreased and the lattice parameter increased with increasing RE in substitution. La and Gd both tend to increase the cut-off frequency, decrease the μ_i and magnetic loss tangent (tanδ) which could be explained by a combination of low density, small grain size, secondary phase ($REFeO_3$) formation and more lattice defects. The low tanδ values resulted mainly from the reduction in eddy current loss due to the higher electrical resistivity with increasing RE ions.

Costa *et. al.* [1.24] investigated the effect of Sm on the microstructure, relative density and magnetic properties of $(Ni_{0.5}Zn_{0.5})$ Sm_x $Fe_{2-x}O_4$ ferrites. Results showed that the increased relative density and decreased average grain size with rare earth substitutions. It also showed that the increase in coercive field and decrease in permeability with rare earth substitution and show a bi-phasic microstructure constituted of a matrix of dark grains and a second phase ($SmFeO_3$).

Khan *et. al.* [1.25] and Low [1.26] reported that Ni-Cu-Zn ferrites are well established soft magnetic materials for MLCI application because of their relatively low sintering temperature, high permeability in the rf-frequency region and high electrical resistivity. Khan *et. al.* [1.5] studied complex permeability spectra of Ni-Cu-Zn ferrites. The particle size increase with increasing the sintering temperature and it was also found that the real part of initial permeability of the low frequency region decreases.

Haque *et. al.* [1.27] reported the magnetic properties of $Mg_{1-x}Zn_x$ Fe_2O_4 ferrites prepared by solid state reaction method. They observed that the lattice parameter increases linearly with the increase in Zn content. The Curie temperature

(T_c) decreases with increase in Zn content. The μ_i increases with the addition of Zn^{2+} ions but the resonance frequency shift towards the lower frequency.

Roy *et. al.* [1.28-1.29] reported the impact of La^{3+} and Sm^{3+} substitution showed improved resistivity Ni-Cu-Zn ferrites. They also discussed relative density and grain size of ferrites increased with increase Sm^{3+} substitution. Increased densification may be due to the appearance of excess Ni, Zn and Cu composed with Fe in the composition. A significant increase in μ_i of the ferrites was found at small fraction of Sm^{3+} substitution about 0.05. Similarly this substitution may improve the electromagnetic properties in ferrites. Nonmagnetic Y^{3+} ions were introduced into Ni ferrites. Their result revealed that the structural and transport properties of Ni ferrites could be improved by doping of Y^{3+} ions.

Sattar *et. al.* [1.30] investigated Cu-Zn ferrites doped with rare earth ions like La, Sm, Nd, Gd and Dy. They found that all samples were of high relative density and low porosity. The magnetization of the samples with Sm and La were higher than that of the undoped ones. The magnetization values of the sample with Nd may be higher or lower than that of the undoped ones depending on the applied magnetic field. The samples with La, Sm and Nd had higher values of relative permeability (μ_r) than that of undoped samples while those with Gd and Dy had lower values μ_r than that of undoped ones.

Ahmed *et. al.* [1.31] reported the effect of rare earth ions on the structural, magnetic and electrical properties of $(Mn_{0.5}\ Zn_{0.5})RE_{0.05}\ Fe_{1.95}O_4$ ferrites where RE = Tb, La, Ce, and Th. Rare earth ions formed orthoferrite ($REFeO_3$) phase and formation of these secondary phase in ferrite during sintering process was governed by the type and the amount of RE^{3+} in used. It was found that the molar magnetic susceptibility for rare earth substituted samples were smaller than pure ferrite. T_c and electrical resistivity increased with increasing rare earth ions in Mn-Zn ferrites.

Saroaut Noor *et. al.* [1.32-1.34] investigated composition dependence of $Co_{1-x}Cd_xFe_2O_4$ sintered at 1000°C/3 hrs. They found variation of lattice parameter with Cd content obey's Vegard's law and the linear variation of X-ray densities with Cd-content. The (μ_i) increases with Cd-content and sintering temperature has lattice effect on permeability, saturation magnetization (M_s) increases with increasing Cd-content at $x \geq 0.4$ and then it decreases .The hysteresis behavior and initial permeability (μ_i) reveal the soft ferromagnetic nature of the studied sample. DC electrical resistivity is found to increase with the increase of Cd-content.

Zhao *et. al.* [1.35-1.36] worked on the effect of substitution of Fe^{3+} by Nd^{3+} ions on structure and magnetic properties of Co $Fe_{2-x}Nd_xO_4$ferrites. It was stated that the value of M_s for Nd^{3+} doped samples was less than that of the pure cobalt ferrite whereas, the coercivity increased with Nd^{3+} content. They are also reported influence of Gd on magnetic properties of $(Ni_{0.7}Mn_{0.3})Gd_xFe_{2-x}O_4$ ferrites. It was found the crystallite sizes decreased when Gd ions were doped into Ni-Mn ferrites. With Gd-substitution when $x > 0.6$ all Gd ions could not enter into the ferrite lattice but resided at the grain boundary. The values of H_c and M_s were zero for all the samples calcined at 600°C. In addition, the H_c 800°C was higher than those sintered 850°C with GD content less than 0.08.

Abdeen [1.37] studied electric conduction in Ni-Zn ferrite. The real AC and DC electrical conductivities increase as the temperature increases indicating the studied samples are semiconductors in nature. The AC electrical conductivity increases with increasing angular frequency below T_C and above T_C it is independent of nature. The values of T_C decrease with increasing of Zn content and activation energy below and above T_C decreases with increasing Zn-content. Ahmed *et. al.* [1.38] investigated the influence of zinc ion substitution on densification in Ni-Zn ferrite. They found rapid densification with increasing Zn^{2+} concentrations.

Sun *et. al.* [1.39] reported the initial permeability and relative loss factor increased while the cut off frequency decreased with increasing Zn content in $(Ni_{1-x}Zn_x)Fe_2O_4$ ferrites. Zn substituted $(Cu_{1-x}Zn_x)Fe_2O_4$ ferrites had been prepared by Ajmal *et. al.* [1.40]. They found that sintered density increased with increasing Zn concentration. Both saturation magnetization and magnetic moment increased with increasing Zn concentration up to $x = 0.02$ and then decreased with further addition of Zn.

Nakamura [1.41] reported on frequency dispersion of permeability in ferrite composite materials. The permeability increases with increasing density of composite materials. As the ferrite content decreases both the real and imaginary parts of the low frequency permeability is significantly reduced, and the peak frequency of imaginary part of permeability shifts toward higher frequency. Nakamura *et. al.* [1.42] reported on low temperature sintering Ni-Cu-Zn ferrite and its permeability spectra. The post sintering density and the complex permeability Ni-Cu-Zn ferrite ceramic can be controlled by altering the particle size of the sintering oxide materials and calcinations temperature. Rezlescu *et. al.* [1.43] investigated the influence of rare earth ions like

Yb, Er, Dy, Tb, Gd and Sm substitution on structure, magnetic and electrical properties of ($Li_{0.3}Zn_{0.4}$) $Fe_{1.96}RE_{0.04}O_4$ ferrites. They found that RE_2O_3 facilitated the formation of secondary phases at grain boundary which suppressed the grain growth. The results also showed that the Curie point shifted to lower temperature and increased the electrical resistivity. Gabal *et. al.* [1.44] studied the structural, magnetic properties of La-substituted $Ni_{0.50}Cu_{0.25}Zn_{0.25}Fe_{2-x}La_xO_4$ nanocrystalline ferrites. He also discussed the hysteresis loop measurements indicating a decrease in the measured saturation magnetization with increasing La content. Coercivity shows a size dependent behavior. The measured susceptibility exhibited a decrease in the Curie temperature by the addition of lanthanum. After going through the literature survey, it comes to know that no systematic information is available in the literature on the structural, magnetic, electric and dielectric properties of different rare earth ions doped with the $Ni_{0.25}Cu_{0.20}Zn_{0.55}Fe_{2-x}RE_xO_4$ ferrite.

Jacobo *et. al.* [1.45] worked on ($Zn_{0.5}Ni_{0.5}RE_{0.02}Fe_{1.98}O_4$) ferrites, with RE = Y, Gd and Eu. The results showed a small increase in the hyperfine field parameters and a strong decrease of the total resonant area with respect to the pure Ni-Zn ferrite. Curie temperatures decreased and coercive fields increased with substitution rare earth ions. By adding much large ionic radii rare earth ions resulted in local distortion and disorder, enough to induce a softening of the network (electron density).

In the present work, the attempt is made to systematically investigate the structural, magnetic, electric and dielectric properties of rare earth (RE= La^{3+}, Eu^{3+} and Y^{3+}, x =0.05 0.10 and x = 0.15) substituted $Ni_{0.60}Zn_{0.40-x}RE_xFe_2O_4$ spinel ferrites and it is prepared by Standard Ceramic Method. This composition can be used for technological applications.

1.6 Outline of the Thesis

The thesis has been configured into five chapters which are as follows:

Chapter 1: Introduction

In this chapter, presents a brief introduction to Ni-Zn ferrites and organization of thesis. This chapter incorporates background information to assist in understanding the aims and objectives of this investigation, and also reviews recent reports by other investigators with which these results can compared.

Chapter II: Theoretical Background

In this chapter, a briefly describe theories necessary to understand magnetic materials as well as ferrites, classification of ferrites, cation distribution, super exchange interaction, two sublattices modules etc. have been discussed in details.

Chapter III: Experimental Background

In this chapter, the experiment procedures are briefly explained along with description of the sample preparation, raw materials. This chapter deals with mainly the design and construction of experimental and preparation of ferrite samples. The fundamentals and working principles of measurement set up are discussed.

Chapter IV: Results and Discussion

In this chapter, results and discussion are thoroughly explained. The various experimental and theoretical studies namely Effect of Rare Earth Metal Substitution on the Structural, Magnetic and Transport properties of Ni-Zn Ferrites are presented and discussed step by step.

Chapter V: Conclusion

In this chapter, the results obtained in this study are summarized. Suggestions for future works on these studies are included.

References are added at the end of each chapter.

THEROETICAL BACKGROUND

2.1 Rare Earth Ferrites

The rare earth substituted different ferrites are becoming the promising materials for different applications. Addition of small amount of rare earth ions to ferrite samples producing a change in their magnetic and electrical as well as structural properties depending upon the types and the amount of rare earth elements used. Rare earth elements are a group of seventeen chemical elements that occur together in the periodic table. The group consists of yttrium and the 15 lanthanide elements (lanthanum, cerium, praseodymium, neodymium, promethium, samarium, europium, gadolinium, terbium, dysprosium, holmium, erbium, thulium, ytterbium, and lutetium). Scandium is found in most rare earth element deposits and is sometimes classified as a rare earth element. The International Union of Pure and Applied Chemistry include scandium in their rare earth element definition.

The rare earth elements are all metals, and the group is often referred to as the "rare earth metals." These metals have many similar properties and that often causes them to be found together in geologic deposits. They are also referred to as "rare earth oxides" because many of them are typically sold as oxide compounds. Rare earth elements are not as "rare" as their name implies. Thulium and lutetium are the two least abundant rare earth elements - but they each have an average crustal abundance that is nearly 200 times greater than the crustal abundance of gold [2.1]. However, these metals are very difficult to mine because it is unusual to find them in concentrations high enough for economical extraction.

The most abundant rare earth elements are cerium, yttrium, lanthanum and neodymium [2.2].They have average crustal abundances that are similar to commonly used industrial metals such as chromium, nickel, zinc, molybdenum, tin, tungsten and lead [2.1]. Again, they are rarely found in extractable concentrations.

The rare earth ions can be divided into two categories; one with the radius closes to Fe ions; while the other with ionic radius larger than Fe ions [2.3].The difference in their ionic radii will lead to micro strains, which may cause domain wall motion resulting in deformation of the spinel structure. It has been stated that ions commonly reside at the octahedral sites by replacing Fe^{3+} ions and have limited solubility in the spinel

lattices due to their large ionic radii [2.4]. The rare earth ions have unpaired 4f electrons and the strong spin orbit coupling of the angular momentum.

Moreover, 4f shell of rare earth ions is shielded by $5S^2 5P^6$ and almost not affected by the potential field of surrounding ions. Doping rare earth ions into spinel type ferrites, the occurrence of 4f-3d couplings which determine the magneto-crystalline anisotropy in spinel ferrite can also improve the electric and magnetic properties of spinel ferrites [2.5-2.8]. Spinel ferrites ceramic are widely used in microwave devices to control transmission path, frequency, amplitude and phase of microwave signals. Accurate dielectric and magnetic properties measurement at the operational frequency and temperature ranges are needed for optimized development of these devices, as well as to assist in the manufacture of the ferrite [2.9]. The structured magnetic materials have an interesting area of study because of its possible applications in a variety of widely areas ranging from information technology to biotechnology [2.10]. The properties of ferrites are being improved due to the increasing trends in ferrite technology. It is believed that there is a bright future for ferrite technology. Ferri magnetism in ferrite is largely governed by Fe-Fe interaction, i.e. the spin coupling of the 3d electron. If the rare earth ions the spinel lattice, the RE-Fe interactions also appears 4f-3d coupling, which can lead to changes in the specific magnetization and Curie temperature.

2.2 Classification of Ferrites and its Relevance

Ferrites exhibit dielectric properties. Exhibiting dielectric properties means that even through electromagnetic waves can pass through ferrites, they do not readily conduct electricity. This also gives them an advantage over irons, nickel and other transition metals that have magnetic properties in many applications because these metals conduct electricity. Another important factor which is of considerable importance in ferrites and is completely insignificant in metals is the porosity. Such a considerable helps us to explain why ferrites have been used and studied for several years.

Ferrites are essentially ceramic materials, compound of iron, boron, barium strontium, lead, zinc, magnesium or manganese. The ingredients are mixed, prefired, milled / crushed, dried, shaped and finally pressed and fired into their final hand in brittle state. Ferrites are a class of chemical compounds with the formula AB_2O_4, where A and B represent various metal cations usually including iron. These ceramic

materials are used in applications ranging from magnetic components in micro electronics. At high frequencies ferrites are considered superior to other magnetic materials because they have low eddy current losses and high DC electrical resistibility. The DC electrical resistivity of ferrites at room temperature can vary depending upon the chemical composition between about 10^{-2} Ω-cm and higher than 10^{11} Ω-cm [2.11].

Ferrites are classified into two categories based on their coercive field strength. They are:

(i) Soft ferrite with coercive field strength < 10 Oe

(ii) Hard ferrite with coercive field strength > 125Oe

According to crystallographic structures ferrites can be classified into three different types [2.12]

(i) Spinel ferrites (Cubic ferrites)

(ii) Hexagonal ferrites

(iii) Garnets

The present research work is a spinel ferrites, therefore it has been discussed in detail the spinel ferrites only.

2.2.1 Spinel Ferrites

They are also called cubic ferrite. Spinel is the most widely used family of ferrite. High values of electrical resistivity and low eddy current losses make them ideal for their use at microwave frequencies. The spinel structure of ferrite as possessed by mineral spinel $MgAl_2O_4$ was first determined by Bragg and Nishikawa in 1915 [2.13, 2.14]. The chemical composition of a spinel ferrite can be written in general as $MeFe_2O_4$ where Me is a divalent metal ion such as Co^{2+}, Zn^{2+}, Fe^{2+}, Mg^{2+}, Ni^{2+}, Cd^{2+}, Cu^{2+} or a combination of these ions.

The unit cell of spinel ferrite is fcc with eight formula units per unit cell. The formula can be written as $M_8Fe_{16}O_{32}$. The anions are the greatest and they form an fcc lattice. Within these lattices two types of interstitial positions occur and these are occupied by the metallic cations. There are 96 interstitial sites in the unit cell, 64 tetrahedral (A) and 32 octahedral (B) sites. The sites are so narrow because they are surrounded by four and six ions at equal distances respectively. The lattice characteristics of a spinel includes a face centre cubic (fcc) site for two oxygen atoms and two cationic sites occupying A and B sites [2.15-2.16] in a spinel, there are 64 A

sites, 32 B sites and 32 oxygen sites in a unit cell. Due to their exchange coupling, spinel ferrites are ferrimagnetically aligned where all of the moment of A sites are aligned parallel with respect to one another while moments of A and B sites are anti parallel to each other. The change neutrality requires the presence of the cations within the structure to counter balance the change of these oxygen anions. These cations rest on two types of interstitial sites to preserve the change neutrality namely A and B sites. The magnetic properties of spinel ferrites are generally influenced by composition and cation distributions. Variation of cation distribution between the cationic sites lead to different electrical and magnetic properties even if the composition of cations over A and B sites is determined by their ionic radius, electronic configuration and electrostatic energy in the spinel lattice.

2.2.2 Hexagonal Ferrites

This was first identified by Went, Rathenau, Gorter and Van Oostershout 1952 [2.17] and Jonker, Wijn and Braun 1956. Hexa ferrites are hexagonal or rhombohedral ferromagnetic oxides with formula $MFe_{12}O_{19}$, where M is an element like Barium, Lead or Strontium. The third type o ferrites are often called the barium ferrites. These compound usually cation BaO, in addition to Fe_2O_3, as the basic component oxide. They are also known as magneto plumbites. The common chemical formula of barium ferrites is l (BaO).m (MO).N $(Fe_2O_3)_n$ or $Ba^{3+}.Mm^{2+}Fe_{2n}^{3+}O^{2-}_{l+m+3n}$, where l is much more complex than the previous two in both in terms of composition of barium ferrites may be complex than the previous two in both in terms of composition of barium ferrites may be changed one is to vary the M^{3+}ions. Mg, Mn, Fe, Co, Ni, Cu and Zn are found suitable for the formation of hexagonal ferrites. Another way to alter the values of l, m and n. Basic compositions are found at 1-0-6(M), 1-2-8 (M_2W), 2-2-6 (M_2Y) and 3-2-12(M_2 ⟶). In these ferrites, oxygen ions have closed packed hexagonal crystal structure. They are widely used as permanent magnets and have high coercivity. They are used at very high frequency. Their hexagonal ferrite lattices are similar to the spinel structure with closely packed oxygen ions, but there are also metal ions at some layers with the same ionic radii as that of oxygen ions. Hexagonal ferrites have larger ions than that of garnet ferrite and are formed by the replacement of oxygen ions. Most of these larger ions are barium, strontium or lead.

2.2.3 Cubic Ferrites Garnets

The mineral garnet refers to group of mixed oxides, of which the widely known on has the chemical formula $Mn_3Al_2Si_{13}O_{12}$, or equivalently 3 MnO. Al_2O_3.3 Si_2O_3 single magnetic garnets have the general formula.

$$3M_2O_3.\ 5\ Fe_2O_3 = 2\ M_3^{3+}Fe_5^{3+}O_{12}$$

It is to be noted that in magnetic garnets the 24 positive charge units per formula units are divided unequally between the ferrites ions (15 units) and another species of trivalent ions (9 units). Technically metal garnets are those with M = Sm, Eu, Gd, Tb, Dy, Ho, Er, Tm, Yb and Yttrium. They are known as rare garnets. A code system has been adopted to name them. REG stands for the rare –earth garnets, GDIG for gadolinium-iron garnet ($Gd_3\ Fe_5O_{12}$) etc. Garnets crystallize in the cubic system with two fifths of the ferrite ions forming a bcc lattice, like ferrospinels, the garnets too. Pach a large number (160) of ions in eight units formula unit cell. The lattice constant is nearly 12.5^0A about 50% larger than those ferrospinel. Also the crystal structure of garnets is more complicated than the spinel structure because of the size ($0.85\text{-}1.10^0$ A) of the M^{3+} ions. They are too large to be accommodated at the interstitial sites between the oxygen ions. Hence the oxygen ions are prohibited from forming a close packed structure as in the spinel. The general formulas for the unit cell of a pure iron garnet have eight formula units of $M_3Fe_5O_{12,}$ where M is trivalent rare earth ions (Y, Gd, Dy). Their cell shape is cubic and the edge length is about 12.5^0A. They have complex crystal structures. They are important due to their application in memory structure.

2.3 Types of Spinel Ferrites

The spinel ferrites have been classified into three categories due to the distribution of cations on tetrahedral (A) and Octahedral (B) sites.

(i) Normal spinel ferrites

(ii) Inverse spinel ferrites

(iii) Intermediate or Mixed spinel ferrites.

2.3.1 Normal Spinel Ferrites

If there is only one kind of cations on octahedral (B) sites, the spinel is normal. In these ferrites the divalent cations occupy tetrahedral (A) sites while the trivalent cations are one octahedral (B) site. Square brackets are used to indicate the ionic distribution of the octahedral (B) sites. The divalent cations (M^{2+}) are in tetrahedral A-sites and two trivalent (Fe^{3+}) cations are in octahedral B- site which is represented as $(M^{2+})_A[Fe^{3+}Fe^{3+}]_BO_4$. A typical example of normal spinel ferrite is bulk $ZnFe_2O_4$.

2.3.2 Inverse Spinel Ferrites

In this structure half of the trivalent (A) sites and half octahedral (B) sites, the remaining cations being randomly distributed among the octahedral (B) sites. In this case divalent (M^{2+}) cations are octahedral (B) sites and the trivalent (Fe^{3+}) cations are equally divided between A and B sites. The divalent (M^{2+}) cations are in octahedral B-sites and the trivalent (Fe^{3+}) cations are equally divided between A and B sites (The divalent and trivalent ions normally occupy the B sites in a random fashion i.e. they are disordered) arrangement is as $(Fe^{3+})_A[M^{2+}Fe^{3+}]_BO_4$. A typical example of inverse spinel ferrite is Fe_3O_4 in which divalent cations of Fe occupy the octahedral (B) site.

2.3.3 Intermediate or Mixed Spinel Ferrites

X-ray and neutron diffraction experiments and magnetization measurements show that there is a whole range of cation distribution between the normal and inverse structures. Spinel with ionic distribution, intermediate between normal and inverse are known as mixed spinel. Compounds formed under these combinations are termed classical hexagonal ferrites. Still another way is to substitute for Ba with Pb or Sr and or substitute for Fe with Al, Ga, Cr or Mn. A fourth way to vary the composition of barium ferrites is to mix two or more of the classical hexagonal ferrite in different proportion.

The arrangement of the form $(Fe^{3+}_{1-\delta}M^{3+}_{\delta})_A[Fe^{3+}_{1+\delta}M^{2+}_{1-\delta}]_BO^{2-}_4$ where δ is called inversion parameter. Quantity δ depends on the method of preparation and nature of the constituents of the ferrites. For complete normal spinel δ = 1, for complete inverse spinel ferrites δ = 0, of mixed spinel ferrite δ ranges these two extreme values. For completely mixed ferrites δ = 1/3. If these are unequal numbers of each

kind of cation on octahedral sites, the spinel is called mixed. The factors affecting the cation distribution over A and B sites are as follows:

(i) The size of the cations

(ii) The electronic configuration of cations

(iii) The electronic energy

(iv) The saturation magnetization of the lattice

Smaller cations (trivalent ions) prefer to occupy the A-sites. The cations have special preference for A and B sites and the preference depends on the following factors:

(i) Ionic radius

(ii) Size of interstices

(iii) Sintering temperature and

(iv) Orbital preference for the specific coordination.

The preference of cations is according to Verway- Heilmar scheme [2.18]

(i) Ions with strong preference for A-sites Zn^{2+}, Cd^{2+}, Ga^{2+}, In^{3+}, Ge^{4+}.

(ii) Ions with strong preference for B-sites Ni^{2+}, Cr^{3+}, Ti^{4+}, Sn^{4+}.

(iii) Indifferent ions are Mg^{2+}, Al^{3+}, Fe^{2+}, Co^{2+}, Mn^{2+}, Fe^{3+}, Cu^{2+}.

Moreover the electrostatic energy also affects the cation distribution in the spinel lattice.

The cations of the smallest positive charge reside on the B-sites having six anions in surrounding i.e. the most favorable electrostatic conduction. It has been observed that X-ray powder diffraction, in conjunction with appropriate computational method, has enough sensitivity to determine the degree of inversion δ, and oxygen positional parameter U. A difference of one electron between two different cations can be enough to render them distinguishable.

2.4 Types of Ferrites with Respect to Hardness

Materials with low coercivity are said to be magnetically soft. They are used in transformer and inductor cores, recording heads, microwave devices and magnetic shielding. The wide variety of magnetic materials can be divided into two groups, the magnetically soft and the magnetically hard. Soft magnetic materials are those materials that are easily magnetized and demagnetized. They have low magnetocrystalline anisotropy resulting in reduced coercivity and high permeability. They typically have intrinsic coercivity less than 1000 Am^{-1}. They are used primarily

to enhance and/or channel the flux produced by an electric current. The important parameter, often used as figure of merit for soft magnetic materials, is the high relative permeability. The other main parameters of interest are the coercivity, the saturation magnetization and the electrical conductivity.

The types of applications for soft magnetic materials fall into two main categories: AC and DC. In DC applications the material is magnetized in order to perform an operation and then demagnetized at the conclusion of the operation, e.g. an electromagnet on a crane at a scrap yard will be switched on to attract the scrap steel and then switched off to drop the steel. In AC applications the material will be continuously cycled being magnetized in one direction to the other throughout the period of operation, e.g. a power supply transformer, a high permeability will desirable for each type of application but the significance of the other properties varies. The main consideration for material selection is most likely to be the permeability. For example, in shielding applications the flux must be channeled through the material. Where the material is used to generate a magnetic field or to create a force then the saturation magnetization may also be significant.

The important consideration is how much energy is lost in the system as the material is cycled around its hysteresis loop. The energy loss can originate from three different sources:

(i) Hysteresis loss, which is related to the area contained within the hysteresis loop

(ii) Eddy current loss, which is related to the generation of electric current in the magnetic material and the associated resistive losses and

(iii) Anomalous loss, which is related to movement of domain walls within the material.

Hysteresis losses can be reduced by the reduction of the coercivity, with a consequent reduction in the area contained within the hysteresis loop. Eddy current losses can be reduced by decreasing the electrical conductivity and is important by the laminating the material, which on influence on overall conductivity and is important because of skin effects at higher frequency. Finally, anomalous losses can be reduced, within which there will be no hindrance to the motion of domain walls.

2.4.1 Soft Ferrites

Soft ferrites are those that can be easily magnetized or demagnetized. These are characterized by low coercive forces and high magnetic permeabilities. The low

coercivity means the materials magnetization can easily reverse direction without dissipating much energy (hysteresis losses), while the materials high resistivity prevents eddy currents in the core, another source of energy loss, generally exhibit small hysteresis losses. At high frequency metallic soft magnetic materials simply cannot be used due to the eddy current losses. Therefore soft ferrite, which is ceramic insulators, becomes the most desirable material.

These materials are ferromagnetic with a cubic crystal structure and the general composition $MO.Fe_2O_3$ where M is a transition metal such as nickel, manganese, magnesium, zinc, cobalt or cadmium. The magnetically soft ferrites first came into commercial production in 1948. Additionally, parts of the family of soft ferrites are the microwave ferrites e.g.Ytrium iron garnet .These ferrite are used in the frequency range from 100 MHz to 500GHz. For waveguides, for electromagnetic radiation, and in microwave device such as phase shifters. Application of soft ferrite include: cores for electro-magnets, electric motors, transformers, generators, and other electrical equipment. Because of their comparatively low losses at high frequencies they are extremely used in the cores of RF transformers and inductors in the applications such as a switched mode power supplies.

2.4.2 Hard Ferrites

Hard ferrites are difficult to magnetized or demagnetized. Hard magnets are characterized by high remanent inductions and high coercivities. The higher coercivity means the materials are very resistant to becoming demagnetized an essential characteristic for a permanent magnet. They also conduct magnetic flux will and have a high magnetic permeability. This enables these so-called ceramic magnets to store stronger magnetic fields than iron itself. They are cheap and are widely used in household products such as refrigerator magnets. They generally exhibit large hysteresis losses. Hard ferrite referred to as permanent magnets retain their magnetism after being magnetized.

Hard ferrite likes Ba-ferrite, Sr-ferrite, Pb-ferrite are used in communication device operating with high frequency currents because of their high resistivity, negligible eddy currents and lower loss of energy due to Joule heating and hysteresis. These are found useful in many applications including fractional horse-power motors, automobiles, audio- and video-recorders, earphones, computer peripherals, and clocks.

2.5 Magnetic Exchange Interaction

In physics, the exchange interaction is a quantum mechanical effect without classical analogue which increases or decreases the expectation value of the energy or distance between two or more identical particles when their wave functions overlap. For example, the exchange interaction results in identical particles with specially symmetric wave function (bosons) appearing closer together than would be expected distinguishable particles, and identical particles with spatially anti symmetric wave functions (fermions) appearing further apart. The exchange interaction is the mechanism responsible for ferromagnetism, among other consequences.

The electron spin of the two atoms S_i and S_j which is proportional to their product .The exchange energy can be written as universally in terms of Heisenberg Hemiltonian [2.19]

$$H = -\sum J_{ij}\ S_i.S_{j\,=} -\sum J_{ij}\, S_i\, S_j \cos\varphi, \qquad (2.1)$$

Where J_{ij} is the exchange integral represents the strength of the coupling between the spin angular momentum i and j and φ is the angle between the spins. It is well known that the favored situation is the one with the lowest energy and it turns out that there are two ways in which the wave functions can combine there are two possibilities for lowering the energy by H.

These are:

(i) If J_{ij} is positive and the parallel spin configuration ($\cos\varphi = 1$) the energy is minimum.

(ii) If J_{ij} is negative and the spins are antiparallel ($\cos\varphi = -1$) energy is maximum. This situation leads to antiferromagnetism.

2.5.1 Super Exchange Interaction

The magnetic interaction in magnetic oxide ferrites cannot be explained on the basis of direct interaction because of the following facts:

(i) The magnetic ions are located too far apart from each other shielded by the non magnetic anion i.e., oxygen. This is because these are not band type semiconductor [2.20] .The non magnetic anion such as oxygen is situated in the line joining magnetic cations.

(ii) Superexchange interaction appears, i.e. indirect exchange via anion p-orbital that may be strong enough to order the magnetic moments.

This P orbital of an anion (center) interact with the d orbital of the transitional metal cations.

Three major types of superexchange interactions in spinel ferrites are: J_{AB}, J_{BB}, and J_{AA}. Ferromagnetic oxides are one kind of magnetic system in which there exist at least two in equivalent sublattice for the magnetic ions. The antiparallel alignment between these sub lattices (ferrimagneting ordering) may occur provided the inter sublattice (J_{AB}) exchange interaction are antiferromagnetic and some requirements concerning the signs and strength of the intra-sublattice ($J_{AA,}$ J_{BB}) exchange interactions are fulfilled.

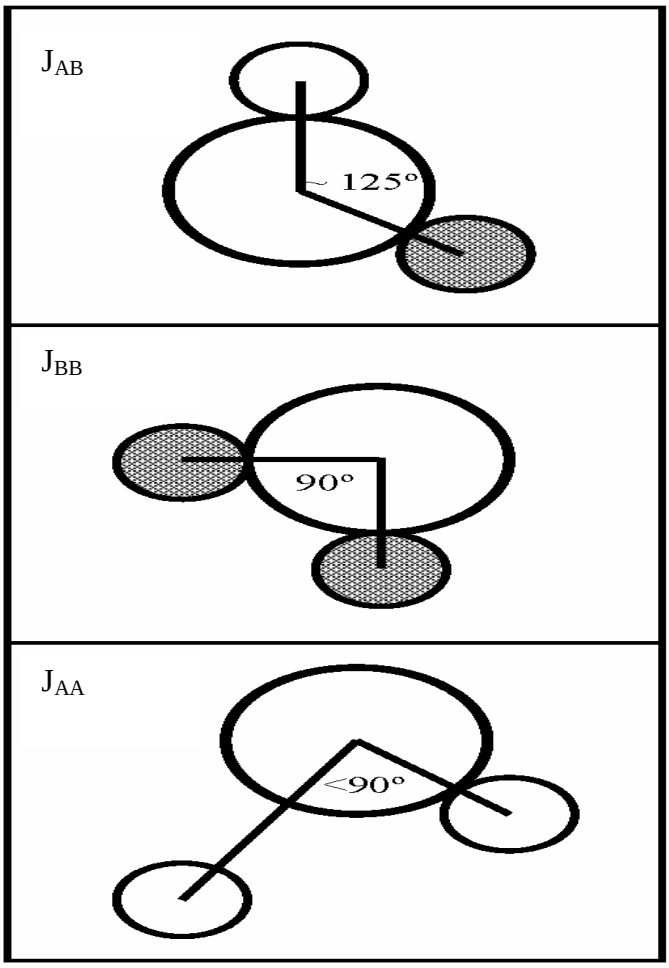

Figure 2.1 Three major types of super exchange interactions in spinel ferrites are as follows: J_{AB}, J_{BB} and $J_{AA.}$ The small empty circle is A-site, the small solid circle is B-site, and the large empty circle is oxygen anion.

Since usually in ferromagnetic oxides the magnetic cations are surrounded by bigger oxygen anions (almost excluding the direct overlap between cation orbital) magnetic interactions occur via indirect superexchange interactions depends both on the electronic structure of the cations and their geometrical arrangement [2.21]. In most of ferromagnetic oxides the crystallographic and electronic structure give rise to antiferromagnetic inter and intra-sublattice competing interactions.

The magnitude of negative exchange energies between two magnetic ions M and M' depend upon the distances from these ions to the oxygen ion O^{2-} via which the superexchange take place and on the angle M-O-M' (φ). According to the superexchange theory the angle φ = 180° gives rise to the greatest exchange energy, and this energy decrease very rapidly as the distance between the ions increases. The magnetic properties of the spinel ferrites are governed by the type of magnetic ions residing on the A and B-sites and the relative strengths of the inter-sublattice (J_{AB}) and intra-sublattice (J_{AA}, J_{BB}) exchange interactions.

2.6 Two sublattice in Spinel Ferrite

The term "Magnetic sublattice" is widely used in the study of magnetic structures of the whole spectrum of magnetic materials [2.22]. In the case of ferromagnetic materials, the "Magnetic sublattice'' is exactly the same as the crystal structure and no problem arises. In the case of antiferromagnetics, the importance of the direction of the magnetic moment is evident and makes clear the existence of two magnetic sublattices, as for example, in MnO. The difference between the two magnetic sublattices is the direction of their magnetic moment. However, ferromagnetic materials are considerably more complex and the application of the molecular field theory to spinels has pointed to the problem of a clear definition of the concept of magnetic sublattices. In spinel ferrites the metal ions are separated by the oxygen ions and the exchange energy between spins of neighboring metal ions is found to be negative, that is, antiferromagnetic. This is explained in terms of superexchange interaction of the metal ions via the intermediate oxygen ions [2.21]. There are a few points to line out about the interaction between two ions in tetrahedral (A) site.

(i) The distance between two ions (~3.5 A^0) is very large compared with their ionic radius (0.67A° for Fe^{3+}).

(ii) The angle A-O^{2-}A ($\Phi = 79^\circ 38'$) is unfavorable for superexchange interaction [2.11], and

(iii) The distance from one A ion to O^{2-} is not the same as the distance from the other A ion to O^{2-}as there is only one A nearest neighbor to an oxygen ion (in fig M and M' are A ions, r = 3.3 A° and q = 1.7 A°) [2.11]. As a result, two nearest A ions are connected via two oxygen ions.

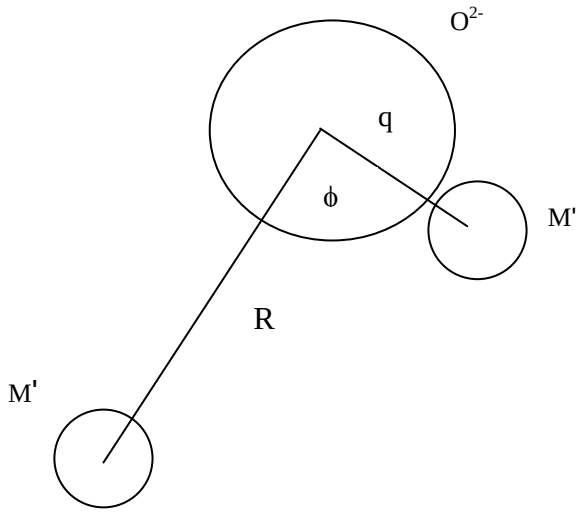

Figure 2.2 Schematic representation of ions M and M' and the O^{2-} ion through which the superexchange is made. R and q are the centre to centre distances from M and M' respectively to O^{2-} and ϕ is the angle between them

Both $M_B(T)$ and $M_A(T)$ are given in terms of the Brillouin function $B_{Si}(X_i)$;

$$M_B(T) = M_B(T = 0)\, B_{SB}(\chi_B) \quad (2.2)$$

$$M_A(T) = M_A(T = 0)\, B_{SA}(\chi_A) \quad (2.3)$$

With, $$\chi_A = \frac{\mu_B g_A S_A M_B N_{AB}}{K_B T} \quad (2.4)$$

$$\chi_B = \frac{\mu_B g_B S_{AB} M_B}{K_B T} \left[\frac{M_B N_{BB} + M_A N_{AB}}{K_B T}\right] \quad (2.5)$$

The molecular field coefficients Nij, are related to the exchange constants Jij by the following expression:

$$J_{ij} = \frac{n_i g_i g_j \mu_B^2 N_{ij}}{2Z_{ij}}\ , \quad (2.6)$$

with n_j the number of magnetic ions per mole in the j^{th} sublattice, g the Lande factor, μ_B is the Bohr magneton and Z_{ij} the number of nearest neighbors on the j^{th} sublattice that interact with the i^{th} ion.

According to Neel's theory and using $J_{AA} = 0$, equating the inverse susceptibility $1/\chi = 0$ at $T = T_c$ we obtain for the co-efficients of molecular field theory N_{AB}= and N_{BB} of the following expression:

$$N_{BB} = \frac{T_C}{C_B} - \frac{C_A N_{AB}^2}{T_C} \qquad (2.7)$$

Where C_A and C_B are the Curie constants for each sublattice. N_{AB} and N_{BB} two unknown parameters provided that M_A and M_B are a known function of T. For simple cases, the Goodenough-Kanamorj rules readily allow the prediction of the net magnetic exchange expected for the coupling between ions. Complication begins to arise in various situations.

(i) When direct exchange and superexchange mechanism compete with one another.

(ii) When the cation-anion-cation bond angle deviates away from 180^0

(iii) When the electron occupancy of orbital is non-static or dynamical and

(iv) When spin orbit coupling become important.

Double exchange is a related magnetic coupling interaction proposed by Clarenoe Zener to account for electrical transport properties. It differs from superexchange in the following manner: In superexchange the electrons actually do not move between the two metal positive ions. The occupancy of the d-shell of the two metal ions is the same or differs by two. In double exchange, the electrons are itinerant, i.e. they actually move between the positive ions via the intermediate (e.g. oxygen); this results in the material doping magnetic exchange coupling as well as metallic conductivity.

2.6.1 Neel's Collinear Model of Ferrites

Neel [2.22] assumed that a ferromagnetic crystals lattice could be split into two sublattices such as A (tetrahedral) and B (Octahedral) sites. He supposed the existence of only one type of magnetic ions in the material of which a fraction λ appeared on A sites and the rest fraction M on B sites. Thus

$$\lambda + \mu = 1 \qquad (2.8)$$

The remaining lattice sites were assumed to have ions of zero magnetic moment. A-ions as well as B ion have neighbors of both A and B types, there are several interactions between magnetic ions as A-A, B-B, A-B and B-A . It is supposed that A-A and B-A interactions are identical and predominant over A-A or B-B interactions and favour the alignment of the magnetic moment of each A ion more- [2.23]. Neel defined the interactions within the material from the Weiss molecular field viewpoint as

$$H=H_0+H_m \tag{2.9}$$

Where H_0 is the external applied field and H_m is the internal field arises due to the interaction of other atoms or ions in the material. When the molecular field concept is applied to ferromagnetic material we have

$$H_A = H_{AA} + H_{AB} \tag{2.10}$$

$$H_B = H_{BB} + H_{BA} \tag{2.11}$$

Here molecular field H_A on A site is equal to the sum of the molecular field H_{AA} due to neighboring A ions and H_{AB} due to neighboring B-sites. Molecular field components can be written as

$$H_{AA} = r_{AA} M_A, \; H_{AB} = r_{AB} M_B \tag{2.12}$$

A similar definition holds for molecular field

$$H_B = r_{BB} M_B, H_{BA} = r_{BA} M_A, \tag{2.13}$$

Here r's are molecular field Co-efficients and M_A and M_B are magnetic moments of A and B sublattices. For unidentical sublattices

$$r_{AB} = r_{BA} \text{ but } r_{AA} \neq r_{BB} \tag{2.14}$$

In the presence of the applied magnetic field H_a, the total magnetic field can be written as,

$$H_a = H_0 + H_A$$

$$H_a = H_0 + r_{AA} M_{A+} r_{AB} M_B \tag{2.15}$$

and $$H_a = H_0 + H_B$$

$$H_B = H_0 + r_{BB} M_{B+} r_{AB} M_A \tag{2.16}$$

2.6.2 **Non-Collinear Model of Ferrimagnitism**

In general, all the interactions are negative (antiferromagnetic) with $|J_{AB}| >> |J_{BB}| > |J_{AA}|$. In such situation, collinear or type of ordering is obtained. Yafet and Kittel [2.24] theoretically considered the stability of the ground state of magnetic ordering, taking all the three exchange interactions into account and concluded that

beyond a certain value of $\frac{J_{BB}}{J_{AB}}$, the stable structure was a non-collinear triangular configuration of moment where in the B-site moments are oppositely canted relative to the A-sites moments. Later on Leyons *et.al.* [2.25] extending these theoretical considerations showed that for normal spinel the lowest energy correspond to conical spinel structure for the value of $\frac{3J_{BB}\ S_B}{2\ J_{AB}\ S_A}$ greater than unity. Initially one can understand why the collinear Neel structure gets perturbed when J_{BB} / J_{AB} increases. Since all these three exchange interactions are negative (favoring anti ferromagnetic alignment of moments) the inter- and intra-sublattice exchange interaction complete with each other in aligning the moment direction in the sublattice. This is one of the origins of topological frustration in the spinel lattice. By selective one can effectively decreases the influence of J_{AB} vis-a vis J_{BB} and thus perturb the Neel ordering.

It was found that ferrites which have been substituted sufficiently with nonmagnetic atoms showed significant departure from Neel Collinear Model. These theoretical models have been used to explain these departures:

- A paramagnetic centre model in which a number of magnetic nearest neighbours determine whether a magnetic ion remains paramagnetic or contributes to the magnetization.
- A uniform spin canting relative to the average magnetization and
- A localized canting where the canting angle of a magnetic ion spins depends on the local magnetic environment.

The discrepancy in the Neel's theory was resolved by Yafet and Kittel [2.24] and they formulated the non-collinear model of ferrimagnetism. They concluded that the ground state at 0K might have one of the following configurations:

- Have an antiparallel arrangement of the spins on two sites.
- Consists of triangular arrangements of the spins on the sublattices.
- An antiferromagnetic in each of the sites separately.

2.7 Theory of Initial Permeability

Initial permeability describes the relative permeability of a material at low values of B. The maximum value for μ in a material is frequently a facing of between 2 and 5 or more above its initial value. Low flux has the advantage that every ferrite

can be measured at that density without risk of saturation. This consistency means that comparison between different ferrite is easy.

For high frequency application, the desirable property of a ferrite is the high initial permeability with low loss. The present goal of the most of the recent ferrite researches is to fulfill this requirement. The initial permeability μ_i is defined as the derivative of induction B with respect to the initial field H in the demagnetization state.

$$\mu_i = \frac{dB}{dH}/H \to 0, B \to 0 \qquad (2.17)$$

At microwave frequency and also in low anisotropic materials, dH and dB may be in different directions. The permeability is thus a tensor character. In the case of amorphous materials containing a large number of randomly oriented magnetic atoms the permeability will be scalar. As we have

$$B = \mu_0 (H+M) \qquad (2.18)$$

and susceptibility

$$\chi = \frac{dM}{dH} = \frac{d}{dxH}\left(\frac{B}{\mu_0} - 1\right) = \frac{1}{\mu_0}(\mu - 1) \qquad (2.19)$$

The magnetic energy density

$$E = \frac{1}{\mu_0}\int H.dB \qquad (2.20)$$

For time harmonic fields $H = H_0$ Sin wt. The dissipation can be described by a phase difference between B^+ and B.

Permeability is namely defines as the proportional constant between the magnetic field induction B and applied intensity H:

$$B = \mu H \qquad (2.21)$$

If a magnetic material is subjected to an AC magnetic field as given below:

$$H = H_0 e^{i\omega t} \qquad (2.22)$$

Then it is observed that the magnetic flux density B experiences a delay. The delay is caused due to presence of various losses and is thus expressed as

$$B = B_0 e^{i(\omega t - \delta)} \qquad (2.23)$$

Where δ is the phase angle and marks the delay of B with respect to H. The permeability is then given by

$$\mu = \frac{B}{H} = \frac{B_0 e^{i(\omega t-\delta)}}{H_0 e^{i\omega t}}$$

$$= \frac{B_0 e^{-i\delta}}{H_0} = \frac{B_0}{H_0} Cos\delta - i \frac{B_0}{H_0} \sin\delta \quad (2.24)$$

$$\mu = \mu' - i\mu'' \quad (2.25)$$

Where $$\mu' = \frac{B_0}{H_0} \cos\delta \quad (2.26)$$

$$\mu'' = \frac{B_0}{H_0} \sin\delta \quad (2.27)$$

The real Part μ’ of complex permeability μ represent the component of B induction which is in phase with H, so it corresponds to the normal permeability. If there is no losses , we should have μ = μ', The imaginary part μ" corresponds to that part of B which is delayed by phase angle δ from H arranging up to 90° from H . The presence of such a component requires a supply of energy to maintain the alternating magnetization regardless of the origin of delay. The ratio of μ" to μ’ as is evident from equation gives:

$$\frac{\mu'}{\mu''} = \frac{\frac{B_0}{H_0}\sin\delta}{\frac{B_0}{H_0}\cos\delta} = \tan\delta \quad (2.28)$$

This tan δ is called the loss Factor or loss tangent. The Q-Factor or quality factor is defined as the reciprocal of this loss factor, i.e.

$$Q = \frac{1}{\tan\delta} \quad (2.29)$$

And the relative quality factor = $\frac{\mu'}{tan\delta}$ = $\mu' Q$ (2.30)

The behavior of μ' and μ" versus frequency is called the permeability spectrum. The initial permeability of a ferromagnetic or ferrimanetic substance is the combined effects of the wall permeability and rotational permeability mechanisms.

2.8 Magnetization Process

A review of magnetization process, namely the response of ferro-or ferri magnetic material (bulk) to an applied field with a semi-microscopic approach is presented. In ferro- or ferri-magnetic material, the magnetization curves, especially in low magnetic fields differ widely from sample to sample and as a function of the magnetic history of the sample i.e., of the previous fields which have been successively applied.

2.8.1 Magnetization Curve

For unmagnetized bulk materials, there is a zero net magnetic moment. It can be predicted that there will be an infinite number of degree of magnetization between the unmagnetized and saturation conditions, when the material is subjected to an external magnetic field. These extreme situations are corresponds respectively to random orientation of domains complete alignment is one direction with elimination of domain walls. If we start with a demagnetized specimen and increase the applied magnetic field, the bulk material will progressively magnetized by the domain dynamics. The magnetization of the sample will follow the course as shown in figure 2.7 [2.26]. The slop from the origin to a point on the curve r the ratio $\frac{M}{H}$ is defined as magnetic susceptibility. This curve is called magnetization curve. This curve is generally perceived as being made of three major portions.

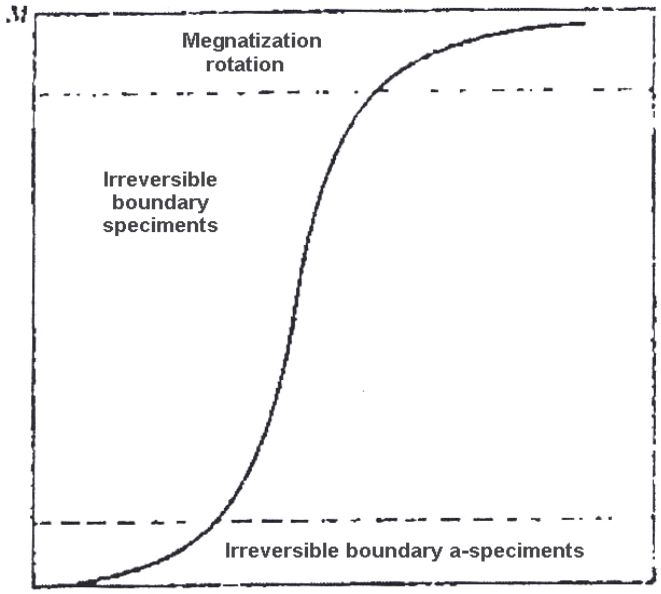

Figure2.3 Domain dynamics during various parts of the magnetization curve

The first, the lower section, is the initial susceptibility region and characterized by reversible domain wall movements and rotations. By reversible means that after the magnetization slightly with an increase in field the origin magnetization can be reversed if the field is reduced to initial value. The condition of the displacement walls to an initial permeability is entirely dependent on the sort of material studied.

In the second stage magnetization curve if the field is increased, the intensity of the magnetization increases more drastically is called the irreversible magnetization range. This range is obtained mainly by the reversible domain wall motion from one stable state to another.

If the field is increased further, the magnetization curve less step and its process become reversible once more. In the third section of magnetization curve, the displacement of domain walls have all ready been completed and the magnetizations take place by rotation magnetization. This range is called rotation magnetization range. Beyond this range the magnetization gradually approaches to saturation magnetization shown in figure-2.4

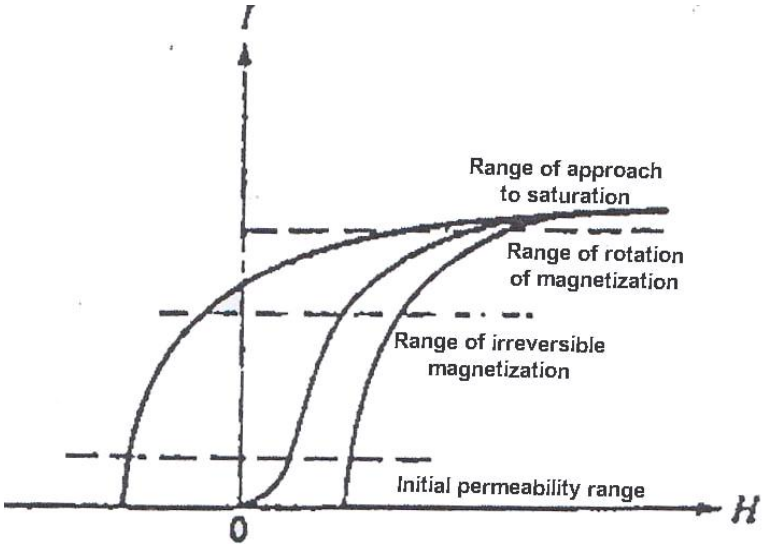

Figure-2.4 Magnetization curve and the classification of magnetization mechanism

2.9 Transport Properties

Ferrites are ferromagnetic semiconductors that could be used in electronic devices. The increasing demand for low loss ferrites resulted in detailed investigations on conductivity and on the influence of various substitutions on the electrical conductivity, thermoelectric power, etc. The conduction mechanism in ferrites is quite different from that in semiconductors. In ferrites, the temperature dependence of mobility affects the conductivity and the carrier concentration is almost unaffected by temperature variation. In semiconductors, the band type conduction occurs, where in

ferrites, the cations are surrounded by closed pack oxygen anions and as a first approximation can well be treated as isolated from each other.

There will be a little direct overlap of the anion charge clouds or orbital. In other words, the electrons associated with particular ion will largely remain isolated and hence a localized electron model is more appropriate than a collective electron (band) model. This accounts for the insulating nature of ferrites. These factors led to the hopping electron model [2.26]. An appreciable conductivity in these ferrites is found to be due to the presence of iron ion ions with different valence states at crystallographically different equivalent lattice sites [2.27]. Conduction is due to exchange of 3d electron, localized at the metal ions, from Fe^{3+} to Fe^{2+}. Various models have been suggested to account for the electrical properties. These are as follows:

- Hopping model of electrons
- Small polaron model

2.9.1 AC Resistivity of Ferrites

AC resistivity is an important property of ferrites material. Ferrites material has high intrinsic resistivity. It can be changed with change of frequency and temperature.

2.9.2 Conduction Mechanism

Ferrites are ferrimagnetic semiconductors and exhibit interesting properties that could be used in electronic devices. That is why ferrites attracted the attention of the physicist. The increasing demand for low loss ferrites resulted in detailed investigations on conductivity and on the influence of various substitutions on the electrical conductivity, thermoelectric power, etc.

The conduction mechanism in ferrites is quite different from that in semiconductors. In ferrites the temperature dependence of mobility affects the conductivity and the carrier concentration is almost unaffected by temperature variation. In semiconductors the band type conduction occurs, where in ferrites, the cations are surrounded by closed pack oxygen anions and as a first approximation can well be treated as isolated from each other. There will be a little direct overlap of the anion charge clouds or orbital. In other words the electrons associated with particular ion will largely remain isolated and hence a localized electron model is more

appropriate than a collective electron (band) model. This accounts for the insulating nature of ferrites.

These factors led to the hopping electron model [2.26]. An appreciable conductivity in these ferrites is found to be due to the presence of iron with different valence states at crystallographically different equivalent lattice points [2.28]. Conduction is due to exchange of 3d electrons, localized at the metal ions, from Fe^{3+} to Fe^{2+} [2.28]. Assuming that all the Fe^{2+} ions in the B-site to participate in the in hopping transport, the number of charge carriers (n) worked out to be ~ $10^{22}/cm^3$. Since mobility is low, even though n is large.

2.9.3 Hoping Model's of Electron

Jonker [2.29] suggested that in materials like ferrites there is a possibility of exchanging the valency of a considerable fraction of metal ions and especially that of iron ions.

In the presence of lattice vibrations however the ions occasionally come close enough together for transfer to occur with a high degree of probability. Thus only the lattice vibrations induce the conduction and the consequence the carrier mobility shows temperature dependence characterized by activation energy. For such a process of jumping of electrons and holes the motilities are given by:

$$\mu_1 = el_1 f_1 \left[\frac{e^{-\frac{E_1}{k_B T}}}{kT} \right] \quad \text{and} \tag{2.31}$$

$$\mu_2 = el_2 f_2 \left[\frac{e^{-\frac{E_2}{k_B T}}}{kT} \right], \tag{2.32}$$

where subscripts represent the parameters for electrons and holes, I represent jumping length, f_1 and f_2 lattice frequencies active in the jumping process, E_1 and E_2 are activation energies involved in the required lattice deformation.

The general expression for the total conductivity in this case where we have two types of charge carriers can be given as;

$$\sigma = n_1 e\, \mu_1 + n_2 e \mu_2 \qquad (2.33)$$

The temperature dependence of conductivity arises only due to mobility and not due to the number of charge carriers in the sample. It was concluded that for hopping conduction:

- The mobility has a minimum value much lower than the limiting value (0.1 cm^2/Vs) taken as minimum for band conduction [2.30].
- The independence of Seebeck coefficient on temperature is due to fact that in hopping model the number of charge carriers is fixed.
- Thermally activated process with activation energy E_a called hopping activation energy.
- Occurrence of n-p transitions with charge carriers in the Fe^{2+} or oxygen concentration in the system.

EXPERIMENTAL PROCEDURE

3.1 Methodology of Rare Earth Ferrite Preparation

The preparation of rare-earth ferrites with optimum magnetic properties is a complex and difficult job to do. Knowledge and control of the chemical composition, homogeneity and microstructure are very crucial. As the most of the properties needed for ferrite applications are not intrinsic but extrinsic, preparation of samples has to encounter added complexity. Influence of rare earths on the properties of different ferrites. Rare earth ions can improve densification and increase permeability and resistivity. In $Ni_{0.60}Zn_{0.40-x}\ RE_xFe_2O_4$ Ferrites where RE enters into the B-sites by displacing a proportionate number of Fe^{3+} form 'B' to 'A' sites. Rare earth ion formed orthoferrite ($REFeO_3$) phase and the formation of this secondary phase in ferrite during sintering process was governed by the type of and the amount of RE^{3+} ions used.

The rare-earth ferrite is completely defined by its chemistry and crystal structure but also requires knowledge and control of parameters of its microstructure such as density, lattice parameters, porosity and their intra- and inter-granular distribution. It is well known that almost all rare-earth ferrites decompose at the elevated temperature if we want to melt them under normal conditions. This happens because the oxygen splits off at higher temperature reducing Fe^{3+} and Fe^{+2}. This necessarily implies that ferrite preparation by melting, as in case of metals, is not possible. The normal methods of preparation of ferrites comprise of the conventional ceramic method or powder metallurgy, chemical co-precipitation method, sol-gel method, wet method etc. In this work Conventional Ceramic Method has been employed for the preparation of $Ni_{0.60}Zn_{0.40-x}\ RE_x$ ferrites for its relative similarity and availability.

3.1.1 Composition of the Studied Ferrites

A series of mixed ferrites of various compositions were fabricated by solid state reaction technique keeping in view of their ionic radial and valences for maintaining the charge neutrality.

In the present work, conventional ceramic method has been employed for a series of various compositions of Ni-Zn ferrites are synthesized, characterized and investigated. The powder preparation process is sintering facility available at

Materials Science Division, Atomic Energy Centre, Dhaka has been utilized in the preparation of samples. In the present research several compositions of RE (La, Y and Eu) substituted ferrites are synthesized, characterized and investigated. The ferrites under investigation are:

(i) $Ni_{0.60}Zn_{0.40-x}La_xFe_2O_4$(x = 0.05, 0.10 and 0.15)

(ii) $Ni_{0.60}Zn_{0.40-x}Y_xFe_2O_4$(x = 0.05, 0.10 and 0.15)

(iii) $Ni_{0.60}Zn_{0.40-x}Eu_xFe_2O_4$(x = 0.05, 0.10 and 0.15)

3.1.2 **Sample Preparation Technique**

The sample preparation of polycrystalline ferrites with optimum desired properties is still a complex and difficult task. Ferrites with optimized properties have always demanded delicate handling and cautious approach in materials synthesis and appropriate knowledge of thermodynamics control of the chemical composition and homogeneity. The samples were synthesized by solid state reaction method. The starting materials for the preparation of the studied composition were in the form of powder oxides [Fe_2O_3, NiO, ZnO Eu_2O_3, Y_2O_3 and La_2O_3] of In Framat Advance Materials USA. The purity of our materials is up to 99.9%. The reagent oxide powders where weighted precisely according to their molecular weight

These are mainly divided into two groups:

(i) Conventional ceramic method which involves milling of reactant followed by sintering at elevated temperature range such as Solid State Reaction Method [3.1], High Energy Ball Milling [3.2],

(ii) Non Conventional method such as Sol- gel Method [3.3], Chemical Co-precipitation Method [3.4], Microwave Sintering Method [3.5], Auto Combustion Method [3.6] etc.. In the present investigation Solid State Reaction Method has been employed for the preparation of rare-earth ferrite samples for its relative simplicity and availability. The overall preparation process generally comprised of the following four major steps.

(i) Preparing a mixture of materials.

(ii) Pre-firing the mixture to form ferrite at wet milling.

(iii) Pre-sintering and

(iv) Sintering

In this method, different metal oxide and rare earth metal oxides are mixed and calcined to get ferrite powders. However mechanical mixing of different oxides is hardly intimate and homogeneous and hence its results in composition fluctuation at every stage of processing that also persist after sintering [3.7]. Solid state process requires calcinations temperature more than 600^0C for phase formation and sintering temperature more than 1000^0C to achieve better densification. This high sintering temperature evaporation of Zn leads to the formation of chemically inhomogeneous material [3.8]. The ferrite is not completely defined by its chemistry and crystal structure but also requires knowledge and control of parameters of its microstructure such as grain size, porosity, intra and intergranular distribution.

3.1.2.1 Preparing a Mixture of Materials

The extend of this work in this step greatly, depending on the starting materials, when component oxide are used, the corresponding step involves a mere mixing of the oxides by wet milling. To avoid iron contamination, mixing is done with stainless steel balls in a steel ball milling machine and a fluid such as distilled water is used to prepare the mixture into slurry. Ferric oxide, Fe_2O_3 and whatever oxides, MO are required are taken in powder form with the captions in the ratio corresponding to that in the final product. Metal carbonate may also be used; during the later firing, CO_2 will be given off and they will be converted to oxides.

3.1.2.2 Pre-sintering the Mixture to Form Ferrite

The pre-sintering is very crucial because in this step of sample preparation a ferrite is formed from its component oxides. The slurry prepared in step (1) is dried, palletized and then transferred to a porcelain crucible for pre-firing at temperature at 1000°C. This was performed in a furnace named Gallen Kamp at Materials Science Division, Atomic Energy Centre, Dhaka. This is done in air, and the temperature goes up to about 1250°C down to 200°C in about 20hours of time. Solid-state reactions take place between the component oxides in this stage, leading to the formation of ferrites actually achieved by counter diffusion. This means that the diffusion involves two or more species of ions which move in opposite direction initially across the interface of two contacting particles of different component oxides. During the pre-sintering stage, the reaction of Fe_2O_3 with metal oxide (MO or M'_2O_3 where M is

divalent and M' is the trivalent metal atom) takes place in the solid state to form spinel according to the reactions [3.8]:

$$MO+Fe_2O_3 \rightarrow MO.\ Fe_2O_3\ (spinel)$$

$$2M'_2O_3 + 4Fe_2O_3 \rightarrow\ 4M'Fe_2O_4\ (spinel) + O_2$$

The NiO creep into Fe_2O_3 as below, to form an intermediate phase $Ni_2Fe_2O_4$ at low temperature:

$$Fe_2O_4+NiO \rightarrow\ Ni\ Fe_2O_4$$

After that Lanthanum (La), Yttrium(Y) and Europium (Eu) ions are introduced successively by

(i) $0.60Ni + (0.40\text{-}x)\ Zn + x\ La + Fe_2O_3 \rightarrow\ Ni_{0.60}\ Zn_{0.40\text{-}x}\ La_xFe_2\ O_4$
(where, x = 0.05, 0.10 and 0.15)

(ii) $0.60Ni + (0.40\text{-}x)\ Zn + x\ Y + Fe_2O_3 \rightarrow\ Ni_{0.60}\ Zn_{0.40\text{-}x}\ Y_x\ Fe_2O_4$
(where, x = 0.05, 0.10 and 0.15)

(iii) $0.60Ni + (0.40\text{-}x)\ Zn + x\ Eu + Fe_2O_3 \rightarrow\ Ni_{0.60}\ Zn_{0.40\text{-}x}Eu_xFe_2O_4$
(where, x = 0.05, 0.10 and 0.15)

As far as the final composition of the ferrite is concerned step (2) is most crucial because subsequent steps would not change the composition substantially. However, the 'raw' ferrite thus formed has two defects its composition is not homogeneous and it contains pores. In order to produce chemically homogeneous, dense and magnetically better material of desired shape and size, sintering at an elevated temperature is needed.

3.1.2.3 Converting the Raw Ferrite into Powder and Pressing the Powder

These undesirable features of the raw ferrites are eliminated in the following two steps:

(i) **Grinding:** The ferrite produced via pre-sintering is usually in the lump form. In this step, it is first ground into powder in a steel ball mill. Grinding eliminates intra particle pores, homogenizes the ferrite, reduces the particle size to << 1μm and promote mixing of any un-reacted oxides.

(ii) Pressing or Extrusion: The dry powder is mixed with an organic binder and pressed into compacts of desired shapes either by the conventional method in a die-punch assembly or by hydrostatic or isostatic compaction. Most

shapes, such as toroidal cores, are pressed (at 1-10 ton/cm^2, 14-140MPa), but rods and tubes are extruded.

3.1.2.4 **Sintering**

Sintering is the final and a very critical step of preparing a ferrite with optimized properties. The sintering time, temperature and the furnace atmosphere play very important role on the magnetic property of final materials. Sintering commonly refers to processes involved in the heat treatment by which a mass of compacted powder is transformed into a highly densified object by heating it in a furnace below its melting point. Ceramic processing is based on the sintering of powder compacts rather than melting/ solidifications/cold working (characteristic for metal), because ceramics melt at high temperatures.

(i) As solidified microstructures cannot be modified through additional plastic deformation and re-crystallization due to brittleness of ceramics.

(ii) The resulting course grains would act as fracture initiation sites.

(iii) Low thermal conductivities of ceramics (< 30 - 50 W/mK) in contract to high thermal conductivity of metals (in the range 50 – 300 W / mK) cause large temperature gradients, and thus thermal stress and shock in melting-solidification of ceramics.

Sintering is the bonding together of a porous aggregate of particles at high temperature. The thermodynamic driving force is the reduction in the specific surface area of the particles. The sintering mechanism usually involves atomic transport over particle surfaces, along grain boundaries and through the particle interiors. Any un-reacted oxides form ferrite, inter diffusion occurs between adjacent particles so that they adhere (sinter) together, and porosity is reduced by the diffusion of vacancies to the surface of the part. Strict control of the furnace temperature and atmosphere is very important because these variables have marked effects on the magnetic properties of the product. Sintering may result in densification, depending on the predominant diffusion pathway. It is used in the fabrication of metal and ceramic components, the agglomeration of ore fines for further metallurgical processing and

occurs during the formation of sandstones and glaciers. Sintering must fulfill three requirements:

(i) To bond the particles together so as to impart sufficient strength to the product.

(ii) To densify the grain compacts by eliminating the pores and

(iii) To complete the reactions left unfinished in the pre-sintering step.

The theory of heat treatment is based on the principle that when a material has been heated above a certain temperature, it undergoes a structural adjustment or stabilization when cooled at room temperature. The cooling rate plays an important role on which the structural modification is mainly based.

The principle goal of sintering is the reduction of compact porosity. Sometimes the initial spaces between compacted grains of ceramics are called "voids", to differentiate term from the isolated spaces pores, which occur in the final stages of sintering. The sintering process is usually accompanied by other changes within the materials, some desirable and some undesirable. The largest- changes occur in:

(i) Binding the particles together so as to impart sufficient strength to the products.

(ii) Densification the green compacts by eliminating the pores.

(iii) Homogenization the materials by completing the relation left unpressed in the pre-sintering step

(iv) Making strength of elastic modulus

(v) Forming hardness and fracture tough

(vi) Making homogeneous distribution of grain number, grain size and shape.

(vii) Developing the average pore size and shape.

(viii) Getting a stable chemical composition and crystal structure.

Sintering is a widely used but very complex phenomenon. The fundamental quantification of change in pore fraction and geometry during sintering can be attempted by several techniques, such as: dilatometer, buoyancy, gas absorption, porosimitry indirect methods (e.g. hardness) and quantitative microscopy etc. The description of the sintering process has been derived from model experiments (e.g.

sintering of a few spheres) and by observing powdered compact behavior at elevated temperatures. The following phenomena were observed:

(i) Increase of inter- particle contact area with time.

(ii) Rounding- off of sharp angles and points of contacts

(iii) In most cases the approach of particle centers and overall densification

(iv) Decreases in volume of inter connected pores.

(v) Continuing isolation of pores

(vi) Grain growth and decreases in volume of isolated pores.

3.1.2.5 **Flow Chart of Sample Preparation**

The following block diagram in Figure 3.1 represents the method employed for the rare - earth ferrites:

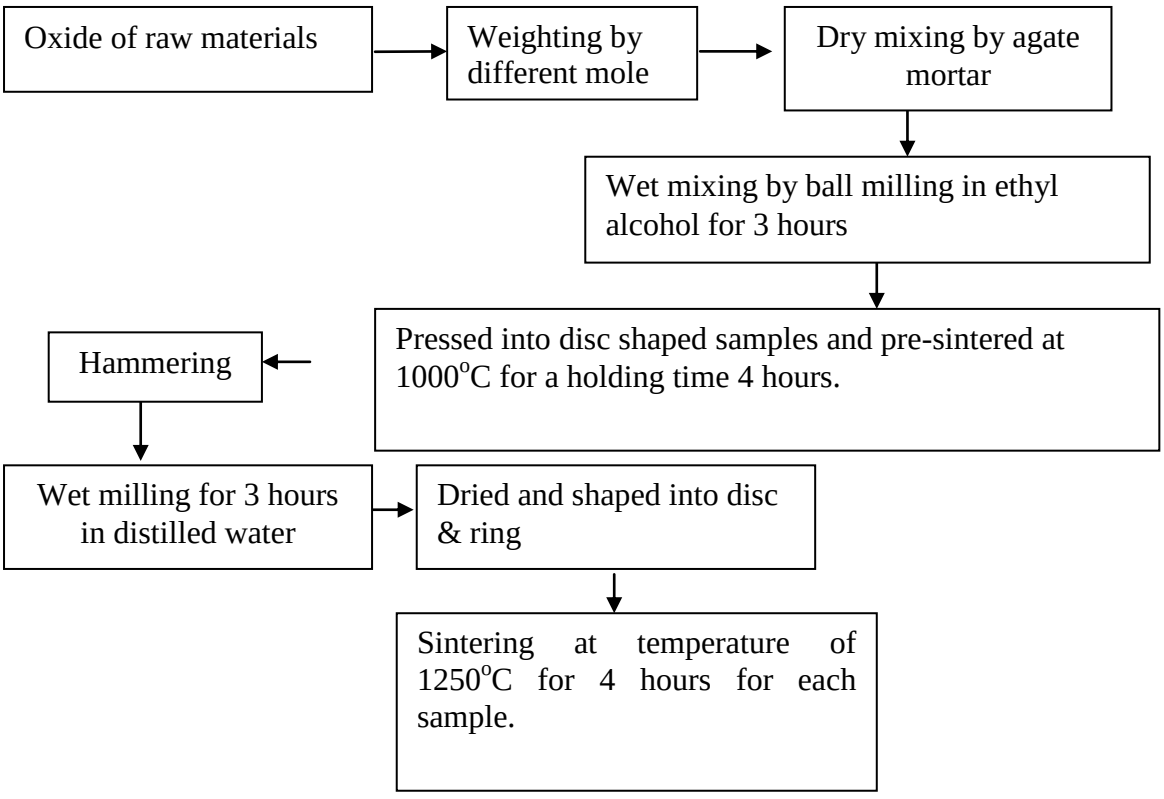

Figure 3.1: Flow chart of rare-earth ferrite sample preparation technique by usual ceramic method.

3.1.3 Method of Sample Preparation

A goal common to all the ferrites is the common formation of the spinel structure. Today, the large majority of ferrite powders are made by the Conventional Ceramic Process or Solid State Reaction Method.

3.1.3.1 Solid State Reaction Method

The weight percentage of the oxide to be mixed for various samples was calculated by using formula:

$$\text{Weight \% of oxide} = \frac{M.wt \cdot of\ oxide \times required\ \ weight\ of\ the\ sample}{Sum\ of\ Mol.wt.of\ each\ oxide\ in\ a\ sample}$$

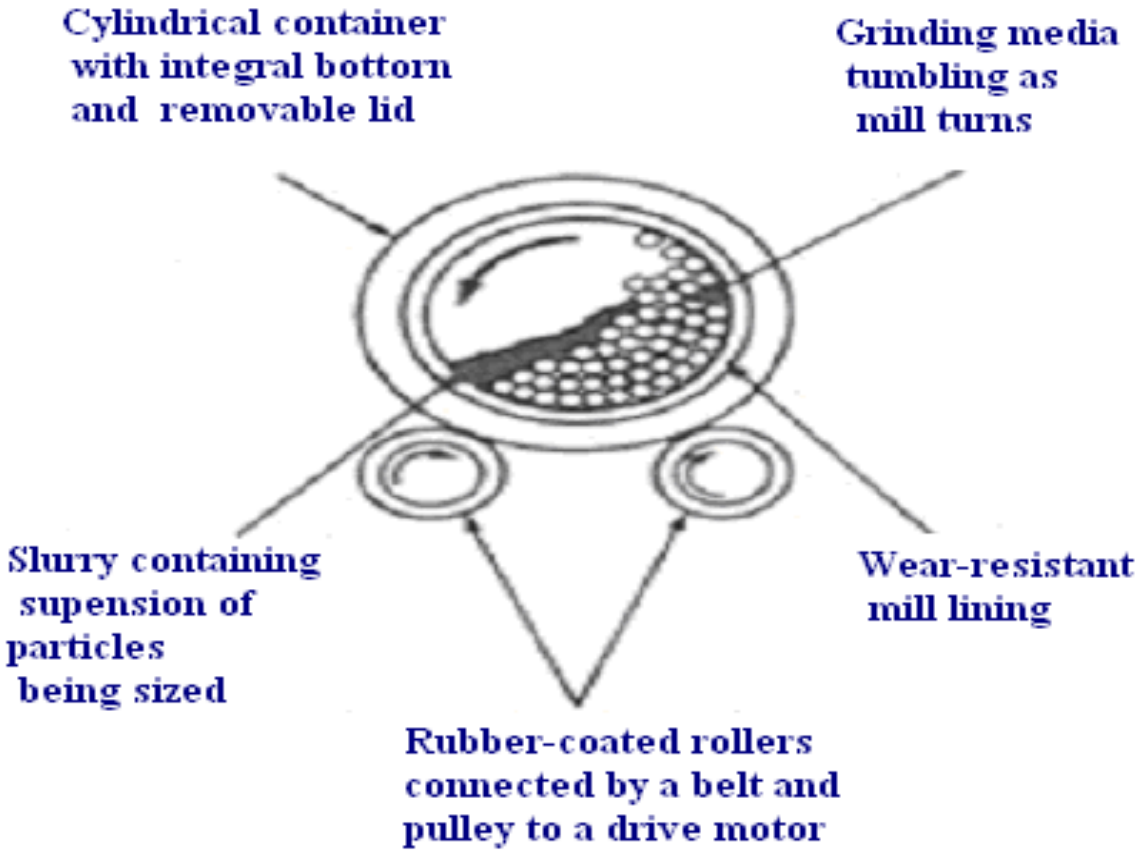

Figure 3.2 Rubber-lined mill with stainless-steel balls

The constituent in required stoichiometric proportions of materials were thoroughly mixed using ceramic mortar and pestle for 3 hrs and then ball milled in a planetary ball mill in ethyl alcohol media for 3 hrs with stainless steel balls of different sizes in diameter Figure 3.2. The slurry was dried and the powder was

pressed into disc shape. The disc shaped sample was pre-sintered at 1000°C for 3 hrs. The sample was then cooled down to room temperature at the same rate as that of heating.

After that samples were crushed again and subsequently wet ball milled for 3 hrs in distilled water to reduce it to small crystallites of uniform size. In order to produce chemically homogeneous and magnetically better material this pre-fired lump material was crushed. These oxide mixtures were milled thoroughly for 4 hours to obtain homogeneous mixture. The mixture was dried and a small amount of saturated solution of polyvinyl alcohol (PVA) were added as a binder and pressed into pellet and toroid shape respectively under pressure 1.75 ton-cm^{-2} and 1.2 ton-cm^{-2} using hydraulic press Fig. 3.3. The prepared samples (Fig 3.4) were sintered at 1250°C for 4 hours with a microprocessor controlled muffle furnace. The samples were polished in order to remove any oxide layer formed during the process of sintering.

Figure 3.3 Hydraulic press used to make different shaped samples.

Figure 3.4 Toroid and disk shapes

Mainly, we made three types of samples cylindrical, tablet and toroidal. Specimen was prepared by a hydraulic press with a pressure at 1 – 10ton/cm^2, 14-140MPa. The die was designed and made in the workshop of AECD. This is made of nonmagnetic stainless steel.

3.2 X-ray Diffraction

X-ray diffraction (XRD) provides precise knowledge of the lattice parameter as well as the substantial information on the crystal structure of the material under study. To study the crystalline structure of solids, X-ray diffraction (XRD) is a versatile and non-destructive technique that provides detailed information about the materials. A crystal lattice is a regularly arranged three-dimensional distribution (cubic, rhombic etc.) of atoms in space. They are fashioned in such a way that they from a series of parallel planes separated from one another by a distance d (inter-planer or inter –atomic distance) which varies according to the nature of the material. XRD is a rapid analytical technique primarily used for phase identification of a crystalline material and can provide information on unit cell dimensions. The analyzed material is finely ground, homogenized and average bulk composition is determined.

X-rays are the electromagnetic waves whose wavelength is in the neighborhood of 1Å. The wavelength of an X-ray is that the same order of magnitude as the lattice constant of crystals and it is this which makes X-ray so useful in structural analysis of crystals. When X-ray beam is incident on a material, the photons primarily interact with the electrons in atoms and get scattered. Diffracted waves from different atoms can interfere with each other and the resultant intensity distribution is strongly modulated by this interaction. If the atoms are arranged in a periodic fashion, as in crystals, the diffracted waves will consist of sharp interference maxima (peaks) with the same symmetry as in the distribution of atoms. Measuring the diffraction pattern therefore allows us to deduce the distribution of atoms in a material. It is to be noted here that, in diffraction experiments, only X-rays diffracted via elastic scattering are measured.

The peaks in an X-ray diffraction pattern are directly related to the atomic distance. Let us consider an incident X-ray beam interacting with the atoms arranged in a periodic manner as shown in two dimensions in Figure 3.5. The atoms, represented as spheres in the illustration, can be viewed as forming different sets of planes in the crystal. For a given set of lattice planes with an inter-plane distance of d, the condition for a diffraction (peak) to occur can be simple written as

$$2d \sin n\theta = n\lambda \tag{3.1}$$

This is known as Braggs's law.

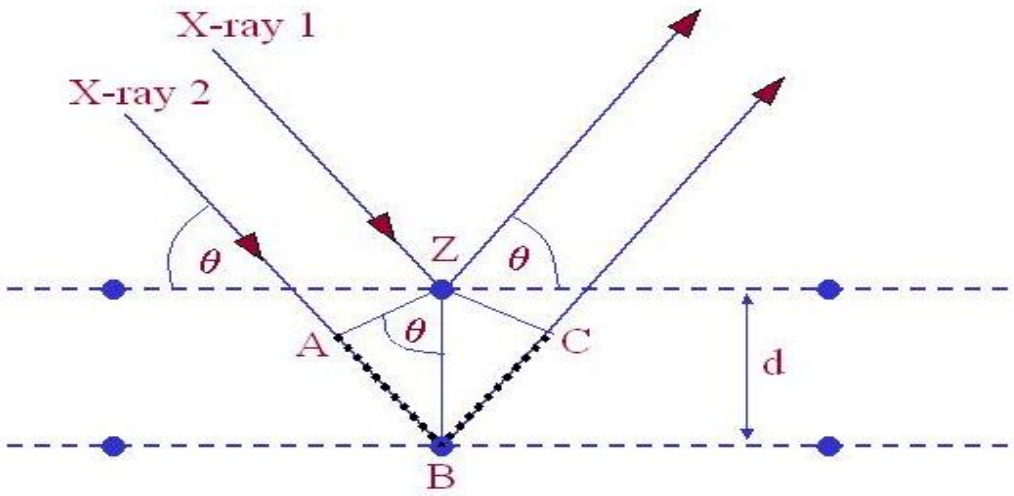

Figure 3.5 Bragg's diffraction pattern

In the equation (3.1), λ is the wavelength of the X-ray, θ is the scattering angle, and n is an integer representing the order of the diffraction peak. The Bragg's Law is one of the most important laws used for interpreting X - ray diffraction data. From the law, we find that the diffraction is only possible when $\lambda < 2d$ [3.9].

In the present work A PHILIPS PW3040 X'Pert PRO X-ray diffractometer was used to study the crystalline phases of the prepared samples in the Materials Science division, Atomic Energy Centre, Dhaka.

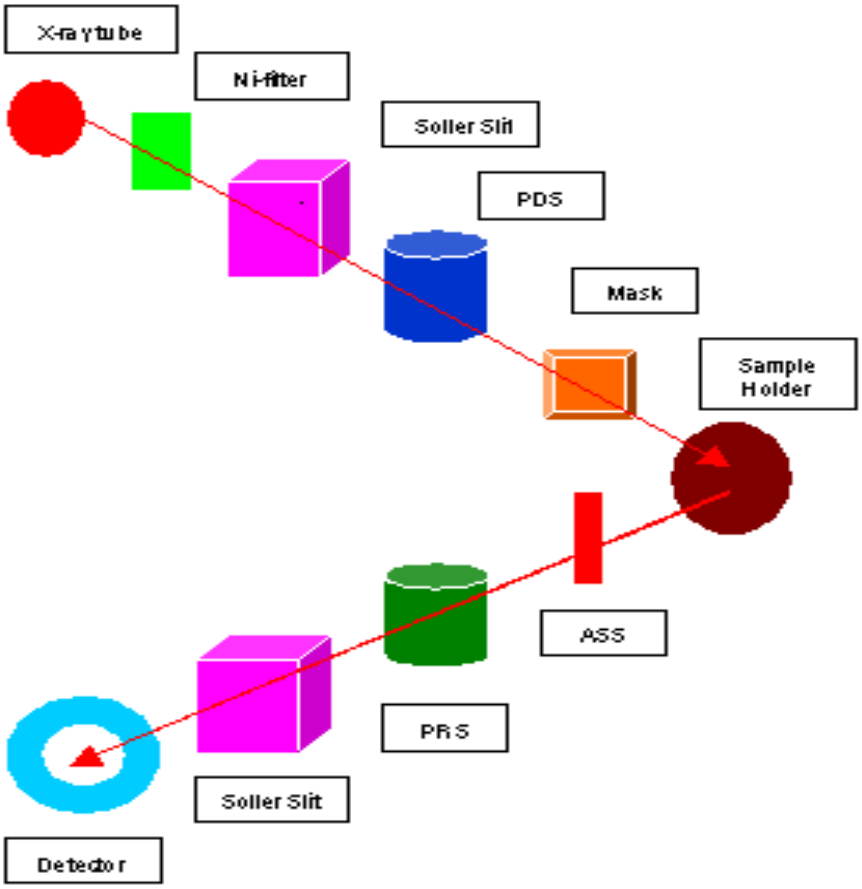

Figure 3.6 Block diagram of the PHILIPS PW3040 X'Pert PRO XRD system

Figure 3.6 shows the inside view of the PHILIPS X'Pert PRO XRD system. The powder diffraction technique was used with a primary beam powder of 40 kV and 30 mA for Cu-K_α radiation. A nickel filter was used to reduce Cu-K_β radiation and finally Cu-K_α radiation was only used as the primary beam. The experimental has been performed at room temperature. A 2θ scan was taken from 25^o to 75^o to get possible fundamental peaks with the sampling pitch of 0.02^o and time for each step

data collection was 1.0 sec. Both the programmable divergence and receiving slits were used to control the irradiated beam area and output intensity from the powder sample, respectively. An anti scatter slit was used just after the tube and in front of the detector to get parallel beam only. All the data of the sample were stored in the computer memory and later on analyzed them using computer "software" X'Pert HJGHS CORE". For XRD experiment each sample was set on a glass slide and fixed the sample by putting adhesive typed the two ends of the sample.

For each composition, the cylindrical samples of weight more than 2 gm are converted into powder. For XRD experiment each sample was set on a glass slide and fixed the sample by putting adhesive tape at the two ends of the sample X-ray diffraction patterns were carried out to confirm the crystal structure. Instrumental broadening of the system was determined from θ - 2θ scan of standard Si. At (311) reflections position of the peak, the value of instrumental broadening was found to be 0.07°. This value of instrumental broadening has subtracted from the pattern. After that using the X-ray data, the lattice constant (a) and hence the X-ray densities were calculated.

3.2.1 Different Parts of the PHILIPS X' Pert PRO XRD System

Figure 3.7 shows the inside view of the X'- pert PRO XRD system. A complex of instruments of X- ray diffraction analysis has been established for both materials research and specimen characterization. These include facilities for studying single crystal defects, and a variety of other materials problems.

The PHILIPS X' Pert PRO XRD system comprised of the following parts

(i) Cu-Tube" with maximum input power of 60 kV and 55 mA

(ii) "Ni- Filter" to remove Cu-K_α component

(iii) "Solar Slit" to pass parallel beam only

(iv) "Programmable Divergent Slits(PDS)" to reduce divergence of beam and control irradiated beam area

(v) "Mask" to get desired beam area

(vi) "Sample holder" for powder sample.

(vii) "Anti Scatter Slit (ASS)" to reduce air scattering back ground.

(viii) "Programmable Receiving Slit (PRS)" to control the diffracted beam intensity and

(ix) Solar Slit to stop scattered beam and pass parallel diffracted beam only.

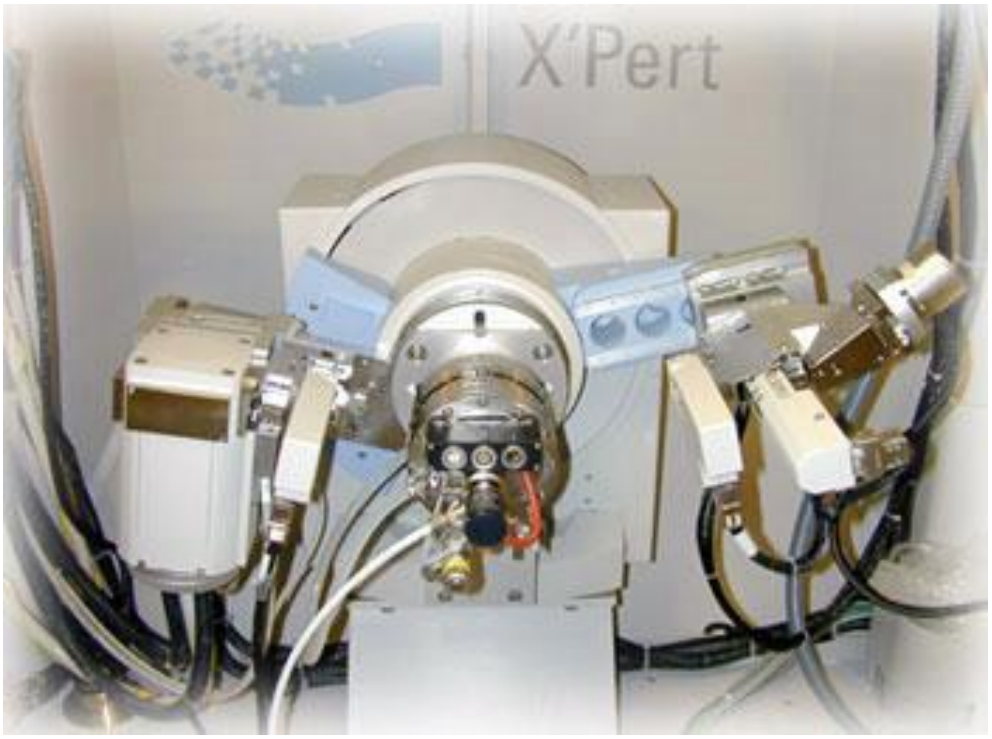

Figure 3.7 Internal arrangement of a PHILIPS X' Pert PRO X-ray diffractometer

3.2.2 Interpretation of the XRD Data

The XRD data consisting of θ_{hkl} and d_{hkl} values corresponding to the different crystallographic planes are used to determine the structural information of the samples like lattice parameter and constituent phase. Lattice parameters of rare earth-ferrites samples were determined. Normally, lattice parameter of an alloy composition is determined by the Debye-Scherrer method after extrapolation of the curve. We determine the lattice spacing (interplaner distance), d using these reflections from the equation which is known as Bragg's Law.

$$2d_{hkl} \operatorname{Sin}\theta = \lambda$$

$$\text{i. e. } d_{hkl} = \frac{\lambda}{2\sin\theta}, \qquad (3.2)$$

Where λ is the wavelength of the X-ray, θ is the diffraction angle and n is an integer representing

3.2.2.1 **Lattice Parameter**

The lattice parameter for each peak of each sample was calculated by using the formula:

$$a = d_{hkl} \times \sqrt{h^2 + k^2 + l^2} \quad , \tag{3.3}$$

Where h, k, l are the indices of the crystal planes. We get d_{hkl} values from the computer using software "X'- Pert HJGHS CORE". So we got eight 'a' values for eight reflection planes such as a, a_1, a_2, a_3 ….. etc. Determine the exact lattice parameter for each sample, through the Nelson-Riley extrapolation method. The values of the lattice parameter obtained from each reflected plane are plotted against Nelson-Riley function [3.9]. The Nelson-Riley function F (θ), can be written as

$$F(\theta) = \frac{1}{2}\left[\frac{\cos^2\theta}{\sin\theta} + \frac{\cos^2\theta}{\theta}\right] \quad , \tag{3.4}$$

where θ is the Bragg's angle. Now drawing the graph of 'a' vs. F (θ) and using linear fitting of those points will give us the lattice parameter 'a_0'. This value of 'a_0' at F (θ) = 0 or θ = 90° .These 'a_0's are calculated with an error estimated to be ± 0.0001Å.

3.2.2.2 **X-ray Density, Bulk Density**

X-ray density, ρ_x was also calculated usual from the lattice constant. The relation between ρ_x and 'a' is as follows,

$$\rho_x = \frac{ZM}{Na^3}, \tag{3.5}$$

where M is the molecular weight of the corresponding composition, N is the Avogadro's number ($6.023X10^{23}$ $mole^{-1}$), 'a' is the lattice parameter and Z is the number of molecules per unit cell,(Z = 8 for the spinel cubic structure). The bulk density was calculated considering a cylindrical pellet of mass (m) and volume (V) of the pellets using the relation

$$\rho_B = \frac{m}{V} = \frac{m}{\pi r^2 h}, \tag{3.6}$$

where m is the mass of the pellet sample, r is the radius and h is the thickness of the pellet.

3.2.2.3 **Porosity**

Porosity is a parameter which is inevitable during the process of sintering of oxide materials. It is noteworthy that the physical and electromagnetic properties are strongly dependent on the porosity of the studied samples. Therefore an accurate idea of percentage of pores in a prepared sample is prerequisite for better understanding of the various properties of the studied samples to correlate the microstructure property relationship of the samples under study. The porosity of a material depends on the shape, size of grains and on the degree of their storing and packing. The difference between the bulk density ρ_B and X-ray density ρ_x gave us the measure of porosity. Percentage of porosity has been calculated using the following relation [3.10]

$$P = (1-\frac{\rho_B}{\rho_x})\times 100\% \qquad (3.7)$$

3.3 **Permeability Measurement**

From the frequency dependence of complex permeability, evolution of permeability and magnetic loss component at different stages of ferrite sample as affected by thermal treatment at different temperature was determined using toroids shape sample prepared with insulating Cu wire. The 4192 LF Impedance Analyzer directly measures the value of inductance, L and loss factor

$$D = \tan\delta \qquad (3.8)$$

From inductance the value of real part of complex permeability, μ' can be obtained by using the relation

$$\mu' = \frac{L}{L_0}\ , \qquad (3.9)$$

Where L is the inductance of the toroid and L_o is the inductance of the coil of same geometric shape in vacuum, Lo is determined by using the relation,

$$L_0 = \frac{\mu_0 N^2 S}{\pi \bar{d}} \qquad (3.10)$$

Here μ_o is the permeability of the vacuum, N is the number of turns (here N = 5), S is the cross-sectional area of the toroid shaped sample, S = dh, where, $d = \frac{d_1 \sim d_2}{2}$ $\bar{d}$ is the average diameter of the toroid sample given as $\bar{d} = \frac{d_1 + d_2}{2}$, Where, d_1 and d_2 are the inner and outer diameter of the toroid samples.

3.4 Agilent Precision Impedance Analyzer (Agilent, 4192A)

The Agilent Technologies 4294A precision impedance analyzer greatly supports accurate impedance measurement and analysis of a wide variety of electronic devices (components and circuits) as well as electronic and non-electronic material Fig: 3.6. We made use of the excellent experimental facilities available at the Materials Science Division, Atomic Energy center, Dhaka. Moreover, the 4294A's high measurement performance and capable functionally delivers a powerful tool to circuit design and development as well as materials research and development (both electronic and non electronic materials) environments:

(i) Accurate measurement over wide impedance range and wide frequency range

(ii) Powerful impedance analysis functions

(iii) Ease of use and versatile PC connectivity

The following are application examples:

(i) Impedance measurement of two terminal components such as capacitors, inductors, ferrite beads, resistors, transformers, crystal / ceramic resonators, multi-chip modules or array/network components.

Semiconductor components:

(i) C – r characteristic analysis of varac for diodes.

(ii) Parasitic analysis of a diode, transistor or IC package terminal/leads.

(iii) Amplifier input/output impedance measurement.

(iv) Impedance evaluation of printed circuit boards, relays, switches, cables, batteries etc.

Dielectric materials: Permittivity and loss tangent evaluation of plastics, ceramics, printed circuit boards and other dielectric material.

Magnetic materials : Permeability and loss tangent evaluation of ferrite, amorphous and other magnetic materials.

Semiconductor material: Permittivity, conductivity and C – V characteristics of semiconductor materials.

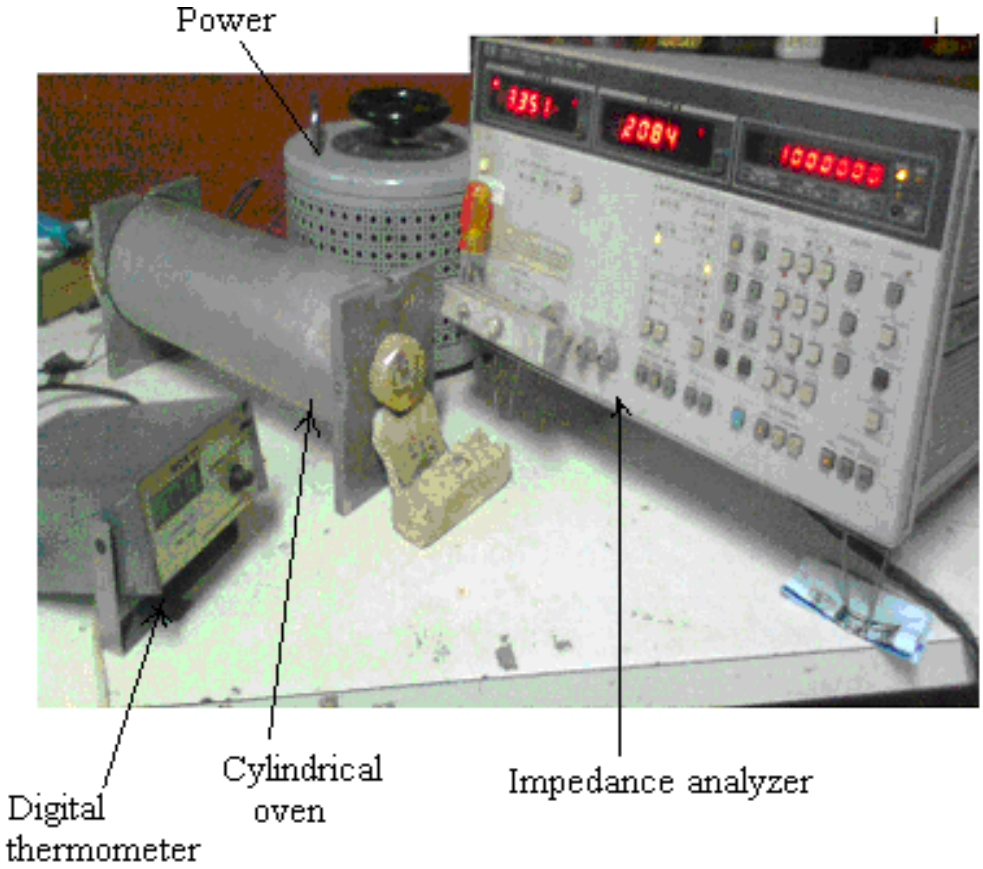

Figure 3.8 Impedance Analyzer Model-Hewlett-Packard 4192A

3.5 Magnetization Measurement Technique

Magnetization in ferrite samples originate due to the difference in the magnetic moments for the two sub-lattices. The larger the difference, the greater is the resultant magnetization, because of the anti-parallel arrangements of the moments in two sub-lattices. The magnetic moment of each sub-lattice arises due to the presence of magnetic ions such as Fe^{2+}, Fe^{3+}, Mn^{2+}, Cu^{2+}, Ni^{2+}, Co^{2+} etc. In our case, only iron ion has magnetic moment since Mg and Zn are non-magnetic. Different ions occupy different 2 sites. So, as a whole, the two sub-lattices have their individual resultant magnetic moments. The differences in magnetic moment between the two sub-lattices give rise to net magnetic moment which in turn yields magnetization. In the present study magnetization has been performed using a Vibrating Sample Magnetometer (VSM).

3.5.1 **Vibrating Sample Magnetometer of Model EV7 System**

The principle of VSM is the measurement of the electromotive force induces by magnetic sample when it is vibrate at a constant frequency in the presence of a static and uniform magnetic field. A small part of 10-50mg was weighed and made to avoid movements inside the sample holder

Figure 3.9 Vibrating Sample Magnetometer

.

Figure 3.9 shows Vibrating Sample Magnetometer (VSM) of Model EV7 system. The magnetic properties measurement system Model EV7 is a sophisticated analytical instrument configured specially for the study of the magnetic properties of small samples over a broad range of temperature from 103K to 800k and magnetic field from-20KO_e to +20KO_e. Vibrating Sample Magnetometer is a versatile and sensitive method of measuring magnetic properties developed by S. Foner [3.11] and is based on the flux change in a coil when the sample is vibrated near it.

The VSM is designed to continuously measure the magnetic properties of materials as a function of temperature and field. In this type of magnetometer, the

sample is vibrated up and down in a region surround by several pickup coils. The magnetic sample is thus acting as a time-changing magnetic flux, varying magnetic flux is accompanied by an electric field and the field induces a voltage in pickup coils. This alternating voltage signal is processed by a control unit system, in order to increase the signal to noise ratio. The result is a measure of the magnetization of the sample.

3.5.2 **Working Procedure of Vibrating Sample Magnetometer**

If a sample is placed in a uniform magnetic field, created between the poles of an electromagnet, a dipole moment will be induced. If the sample vibrates with sinusoidal motion a sinusoidal electrical signal can be induced in suitable placed pick-up coils. The signal has the same frequency of vibration and its amplitude will be proportional to the magnetic moment, amplitude, and relative position with respect to the pick-up coils system. Figure 3.10 shows the block diagram of vibrating sample magnetometer.

The sample is fixed to a sample holder located at the end of a sample rod mounted in an electromechanical transducer. The transducer is driven by a power amplifier which itself is driven by an oscillator at a frequency of 90 Hz. So, the sample vibrates along the Z axis perpendicular to the magnetizing field. The latter induce a signal in the pick-up coil system that is fed to a differential. The output of the differential amplifier is subsequently fed into a tuned amplifier and an internal lock in amplifier that receives signal supplied by the oscillator.

The output of this lock-in amplifier, or the output of the magnetometer itself, is a DC signal proportional to the magnetic moment of the sample being studied. The electromechanical transducer can move along X, Y and Z directions in order to find the saddle point. Calibration of the vibrating sample magnetometer is done by measuring the signal of a pure Ni standard of known saturation magnetic moment placed in the saddle point. The basic instrument includes the electromechanical system and the electronic system (including a personal computer). Laboratory electromagnets or superconducting coils of various maximum field strengths may be used.

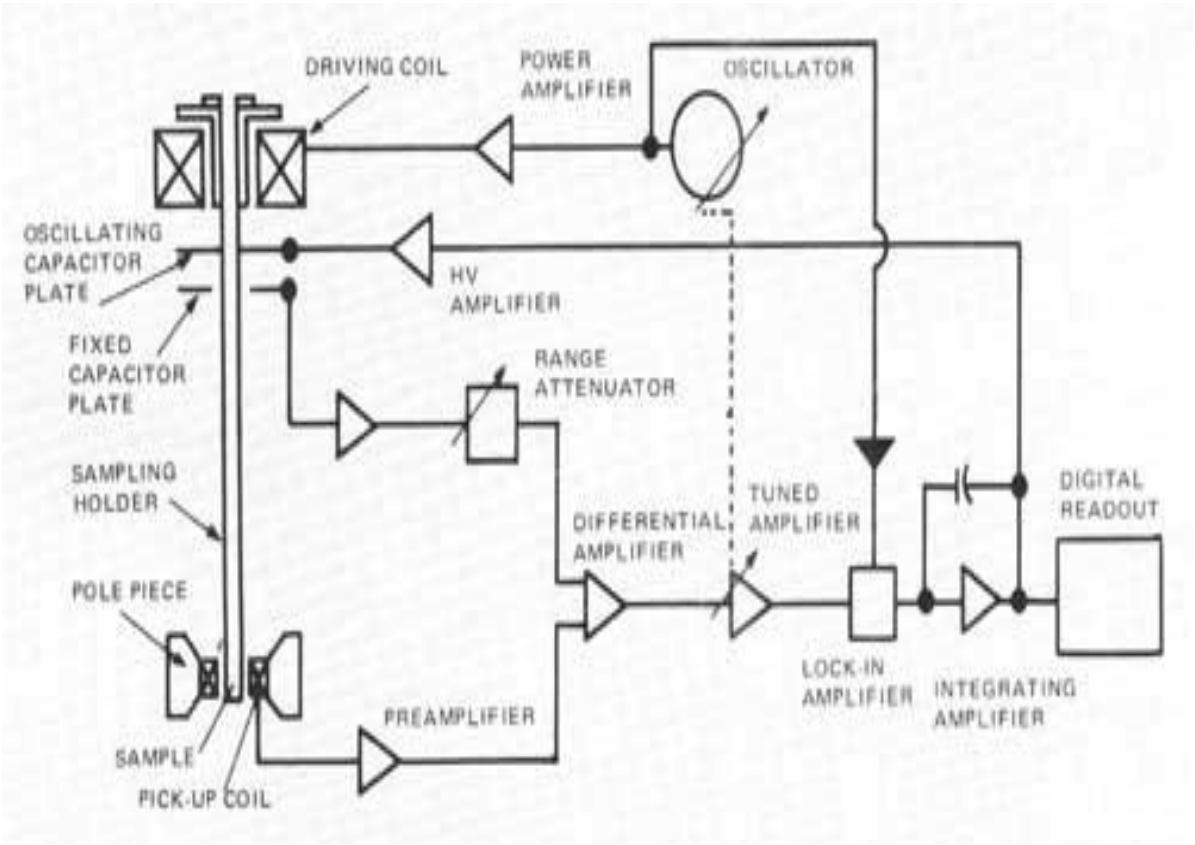

Figure 3.10 Block Diagram of a Vibrating Sample Magnetometer

3.6 **Transport Property**

3.6.1 **DC Resistivity**

Resistivity is an intrinsic property of a material. The technical importance of ferrites lies primarily in their high resistivity. Technical ferrites are resistivity of 1 to 10^{12} Ω-cm. In magnetic material to low resistivity gives raise T_c eddy current losses. The losses are inversely proportional to the resistivity. So measurement of resistivity is very crucial for ferrite material. The electrical resistivity measurements carried out by a two probe method on silver painted sample a Keithley Electrometer using pellet samples of diameter 8.3-8.8mm and of thickness 1.2 - 2.5 mm by applying silver electrodes on the surfaces. Samples were prepared by sintering the samples at 1250°C for Ni- Zn ferrites for 3hours. The samples were polished using metallurgical polishing machine with the help of silicon carbide papers with grit size 600. After that the samples were clean with acetone and then again polished with special velvet type

polishing cloth named as α-gam, for finer polishing using fine alumina powder of grain size 0.05 micron dispersed in a liquid.

The powders were of various sizes starting with 1 micron to 0.05 micron. Samples are then cleaned in an ultrasonic cleaner and dried in surface at room temperature for several hours. Then the samples are again cleaned with acetone and silver paste was added to both the sides of the polished pellet samples together with two thin copper wires of 100 micron diameter for conduction. Again the samples are dried at room temperature to eliminate any absorbed moisture.

The AC resistivity was measured as a function of frequency in the range 1 kHz-13MHz at room temperature by Electrometer Keithley model 6514 and impedance analyzer. The electrical resistivity has been calculated using the formula:

$$\rho = \frac{RA}{l} = \frac{\pi r^2 R}{l}, \ [\because A = \pi r^2] \qquad (3.11)$$

Where R is the resistance of the Pellet, r is the radius of the pellet and *l* is the thickness of the pellet. Sintered ferrite pellet specimens were used to determine resistivity. Electrodes were painted on the surface of the sample using a conducting silver paste.

3.6.2 **Dielectric Constant**

Dielectric constant measurements were done by using WAYNE KERR INDUCTANCE ANALYZER 3255B. The overall dielectric constant (ε') of an insulator material as given by the relation:

$$D = \varepsilon_0 E = \varepsilon_0 \varepsilon' E \qquad (3.12)$$

where, D represents the electric displacement, E the electric field in the dielectric, ε' the dielectric constant and ε_0 permittivity of the vacuum. The electric displacement describes the extent to which the electric field has been altered by the presence of the dielectric material. The dielectric constant ε' is an intrinsic property of a material and a measure of the ability of the material to store electric charge relative to vacuum.

It is measured directly from the capacitance of a capacitor in which the material is used as electrode separator or dielectric. The capacitive cell, the dielectric constant (ε'), total charge (q) and capacitance © can be developed as follows:

$$\varepsilon' = \frac{D}{\varepsilon_0 E} = \frac{\frac{Q}{A}}{\frac{\varepsilon_0 V}{d}}$$

$$\therefore Q = \frac{\varepsilon_0 \varepsilon' A V}{d} = CV \qquad (3.13)$$

Where $C = \frac{\varepsilon_0 \varepsilon' A}{d}$ (3.14)

Here A represents the area of the capacitive cell, d its thickness, C is the capacitance of the material, V the voltage across the cell and $\varepsilon_0\left(\frac{F}{m}\right)$ the material permittivity in vacuum.

Thus $\varepsilon^{/}$ represents the ratio of the permittivity or charge storage capacity relative to air or vacuum as dielectric

$$\varepsilon' = \frac{cd}{\varepsilon_o A}, \qquad (3.15)$$

where c is the capacitance of the pellet in farad, d is the thickness of the pellet in meter, A the cross-sectional area of the flat surface of the pellet in m^2 and ε_o the constant of permittivity for free space. Dielectric measurement as a function of frequency in the range 100Hz-13MHz at room temperature were carried out by using Hewlett Packrat impedance analyzer in conjunction with a laboratory made furnace which maintain the desired temperature with the help of a temperature controller.

RESULTS AND DISCUSSION

4.0 Introduction

The rare earth oxides are recently becoming the promising and potential additives for the improvement of the properties of ferrites. Rare earth element has large magnetic moments, large magnetocrystalline anisotropy and very large magnetostriction at low temperatures due their localized nature of 4f electrons being totally screened by 5s and 5p orbital. But the solubility of rare-earth in the spinel lattice is limited. It has been demonstrated that even a low content of rare earth substitution in the spinel ferrite shows phase segregation and diffusion of rare–earth species to the grain boundaries as extra crystalline phase like orthoferrites ($REFeO_3$) [4.1-4.2]. Now-a-days the rare-earth oxides are becoming promising additives to change the magnetic properties of ferrites. The investigation studied the effect of rare-earth metals substitution on the properties of Ni-Zn ferrites [4.3-4.4]. It has been accepted that rare-earth ions commonly reside at octahedral site [4.5] and have limited solubility in the spinel lattice due to their large ionic radii. But the exact value of their solubility in the spinel lattice is not known.

Most of the research works performed earlier by RE substitution have been done with basic ferrite compositions that are strongly ferromagnetic having long-range ferromagnetic ordering with high T_c. Dilute$Ni_{0.60}Zn_{0.40}Fe_2O_4$ with nonmagnetic Zn content higher than percolation limit where frustration and competing interaction start to play dominant role has hither to not been studied in much detail except a detail study carried out by $Ni_{0.60}$ $Zn_{0.40-x}RE_xFe_2O_4$ [RE = la, Y, Eu] where x = 0.05, 0.10, 0.15 samples are prepared solid state reaction method sintered at 1250^0 for 3 hrs. The effects of La^{3+}, Y^{3+} and Eu^{3+} substitution on the density, microstructure, permeability, Curie temperature, magnetic loss, resistivity, saturation magnetization and dielectric constant of Ni-Zn-RE ferrites.

4.1 X-Ray Diffraction Analysis

X-ray diffraction is a useful technique to evaluate the various phases of the synthesized ferrites as well as their unit cell parameters. In the present study X-ray diffraction technique has been utilized to discern these parameters X-ray diffraction (XRD) studies of the samples were performed by using Philips PERT PRO X-ray Diffraction using Cu-K_α radiation in the range of $2\theta = 20^0$ to 65^0 in steps of 0.02^0.

4.1.1 Phase Analysis

Structural characterization and identification of phases are prior for the study of ferrite properties. Optimum magnetic and transport properties of the ferrites necessitate having single phase cubic spinel structure. XRD patterns for the sample$Ni_{0.60}Zn_{0.40}Fe_2O_4$ sintered at 1250^0C for 3 hours shownFigure 4.1. The XRD patterns for all the samples were indexed for fcc spinel structure and Bragg diffraction planes are shown in the patterns. All the samples show good crystallization with well defined diffraction lines. It is obvious that the characteristic peaks for spinel ferrites i.e. (111), (200), (311),(222),(400),(422), (511) and (440), which represent either all odd or even indicating that the samples are spinel cubic phase. The samples have been characterized as cubic spinel structure without any extra peaks corresponding to any second phase.

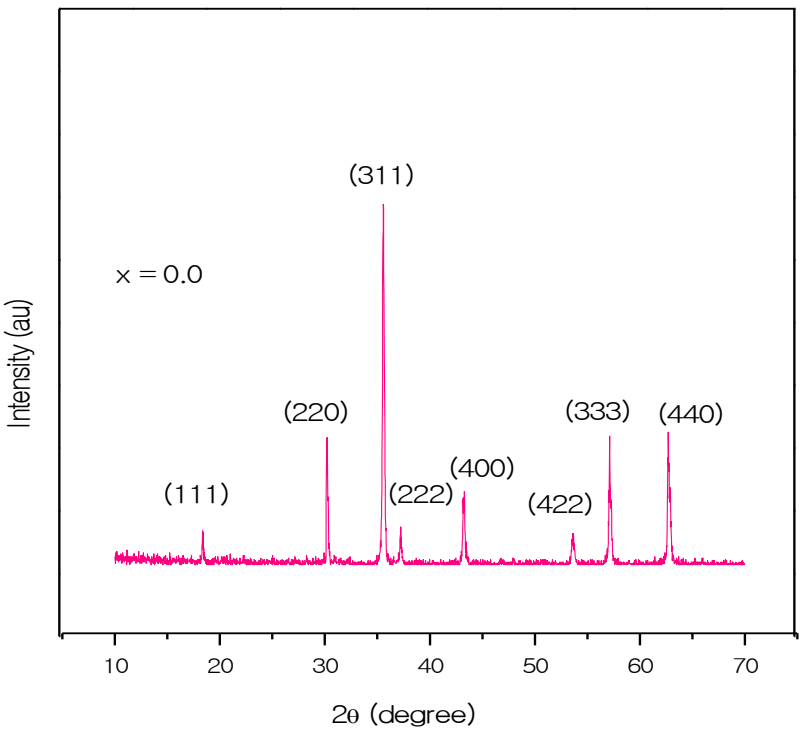

Figure 4.1 X-ray diffraction patterns of $Ni_{0.60}Zn_{0.40}Fe_2O_4$ ferrites sintered at 1250^0C/3hrs.

The La substituted $Ni_{0.60}Zn_{0.40-x}La_xFe_2O_4$ ferrites were extensively characterized by XRD shown in Figure 4.2. The structural model was taken as the

spinel phase was obtained for $Ni_{0.60}\ Zn_{0.40-x}La_xFe_2O_4$ samples with x = 0.05, 0.10 and 0.15. However, a very weak reflection peak at $2\theta = 27.03^0$ is about to emerged for x = 0.05, 0.10 and 0.15 is more prominent indicated by the arrow. The peak is identified as the weak reflection peak of the $LaFeO_3$ phase. Figure 4.3 shows the graphical representation of the measured XRD values, calculated diagram, and the back ground for $Ni_{0.60}\ Zn_{0.40-x}Y_xFe_2O_4$ ferrites where x = 0.05, 0.10 and 0.15. The structure model was taken as the spinel phase. To identify the possible formation of a second phase $YFeO_3$ in the substituted ferrites, the slow step scan XRD analysis was conducted on the samples after different steps of processing. $YFeO_3$ phase was in all Y^{3+} substituted ferrites in the replace of Zn^{2+}. The amount of $YFeO_3$ that is peak intensity increased with increasing Y^{3+} concentrations indicated by arrow. This apparently indicated that Y^{3+} did not form a solid solution with spinel ferrites or it had very solid solubility.

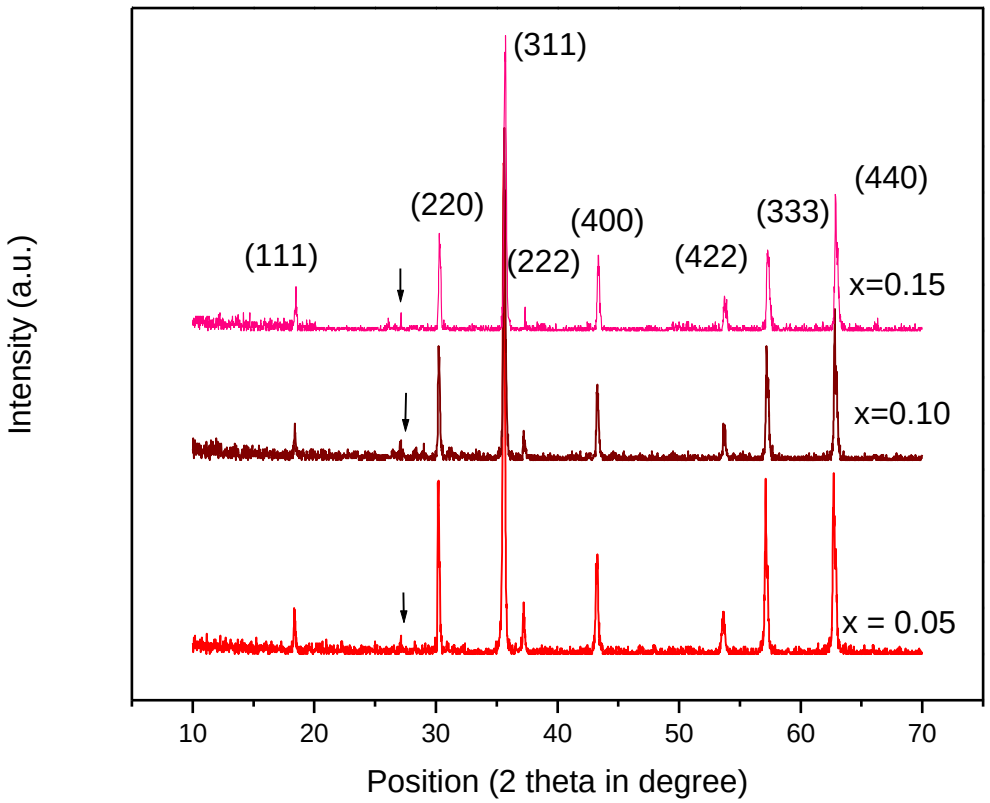

Figure 4.2 X-ray diffraction patterns of $Ni_{0.60}Zn_{0.40-x}La_xFe_2O_4$ [x= 0.05, 0.10 and 0.15] ferritessintered at 1250^0C/3hrs

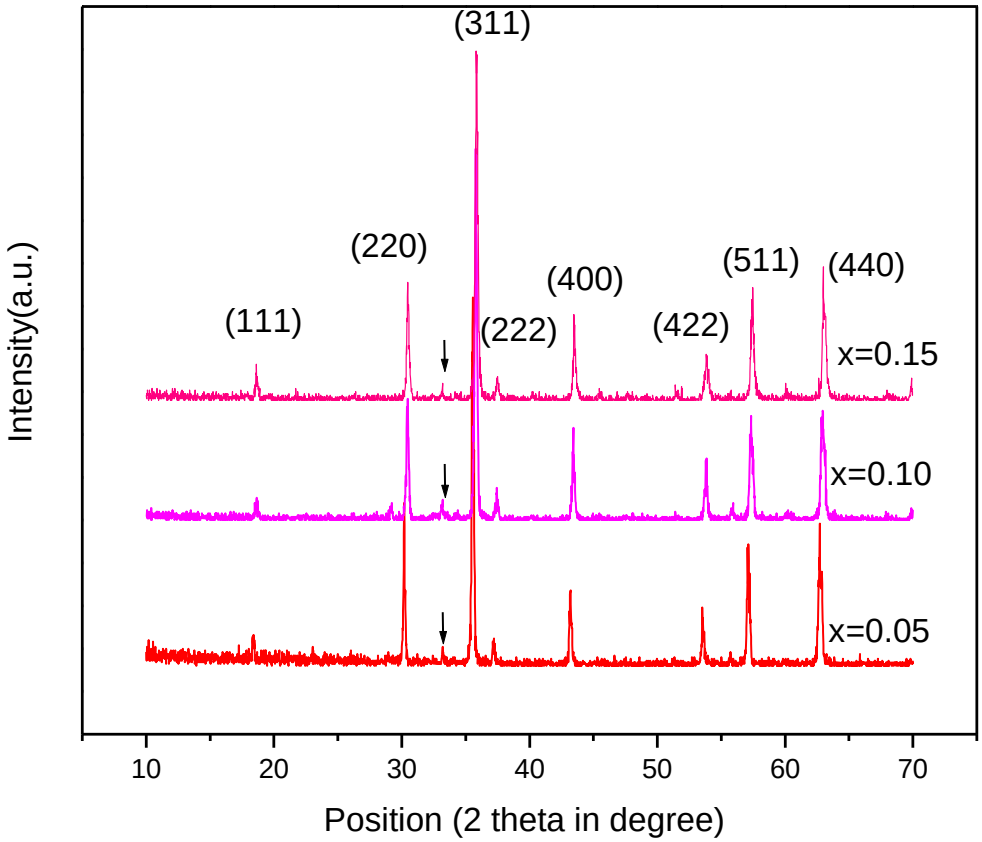

Figure 4.3 X-ray diffraction patterns of $Ni_{0.60}Zn_{0.40-x}Y_xFe_2O_4$ [x= 0.05, 0.10 and 0.15]ferrites sintered at 1250^0C/3hrs.

XRD patterns are demonstrated in the Figure 4.4 for Eu^{3+} doped samples of $Ni_{0.60}Zn_{0.40-x}Eu_xFe_2O_4$[x = 0.05, 0.10 and 0.15] ferrites sintered at 1250^0 C for 3 hrs. It is clearly noticed that undoped Eu^{3+} sample shows formulation of cubic spinel structure with no extra peak as shown in the Figure 4.1, where Eu^{3+} doped samples how additional peaks other than spinel structure and probably corresponding to a second phase of $EuFeO_3$ (Ortho ferrite) shown in Figure 4.4. Determination of exact phase could not be possible, since the number of extra peaks other than spinel is not sufficient for accurate analysis. XRD analysis evidenced that the compounds containing La^{3+}, Y^{3+} and Eu^{3+}ions are pluri-phasic. Rare earth is formed orthoferrite ($REFeO_3$) phase and the formation of these secondary phases in ferrite during sintering process was governed by the type and the amount of RE^{3+}[La^{3+}, $Y^{3+}$and Eu^{3+}] ions used.

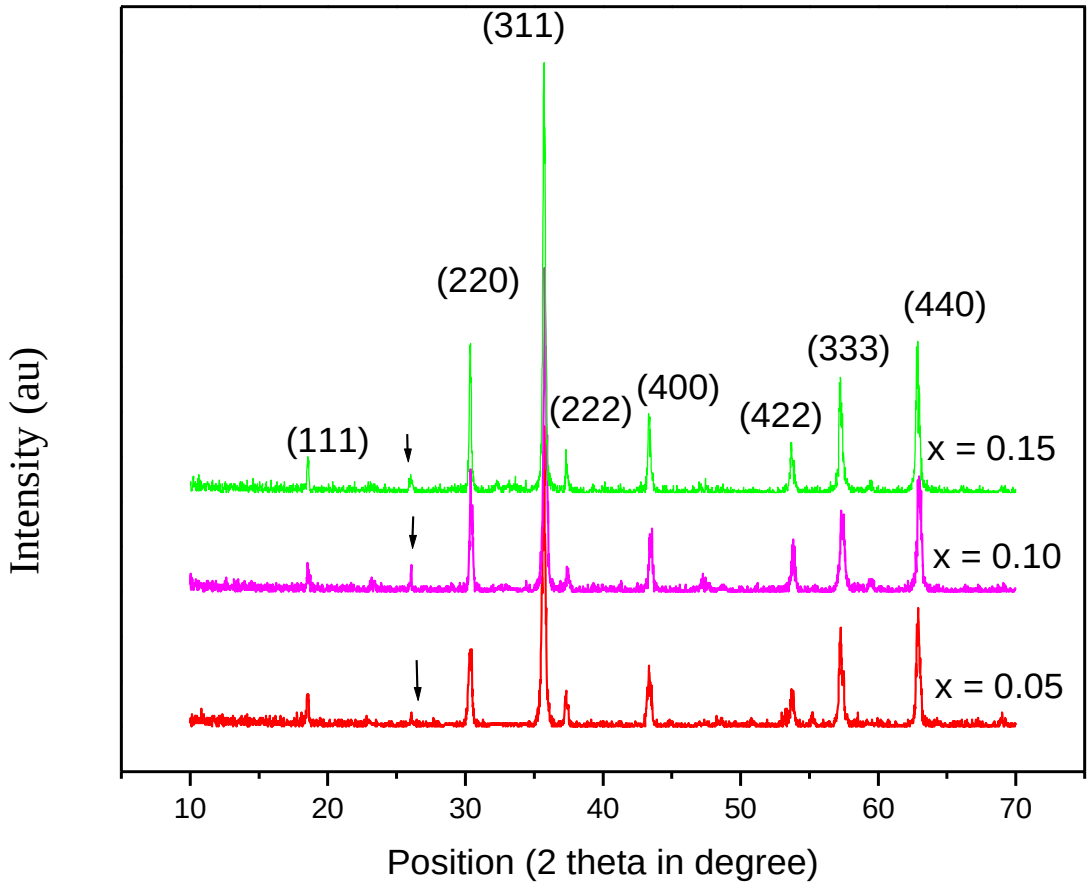

Figure 4.4 X-ray diffraction patterns of $Ni_{0.60}Zn_{0.40-x}Eu_xFe_2O_4$ [x = 0.05, 0.10 and 0.15]ferrites sintered at 1250^0C/3hrs.

The phase formation behavior of $Ni_{0.60}Zn_{0.40-x}RE_xFe_2O_4$ ferrites where (RE = La, Y, Eu] where x =0.00, 0.05, 0.10, and 0.15 sintered at 1250^0C were studied by XRD. All the samples show well crystallization with we defined diffraction patterns exhibited that all the samples were identified as a single phase of cubic spinel structure. The XRD patterns for all the samples were indexed for fcc spinel structure and the Bragg planes are shown in the patterns. The XRD patterns of the samples are given in Figure 4.1 to Figure 4.4. The peaks (220), (311), (222), (400), (422), (333) and (440) correspond to spinel phase which are characteristic of spinel structures with a single phase. The lattice parameter 'a' corresponding to each plane was calculated by using the X-ray data.

4.1.2 Lattice Parameters

The values of lattice parameters have been determined from each plane of XRD pattern using Nelson Relay function (4.6) F (θ) = $\frac{1}{2}$ [$\frac{cos^2\theta}{sin^2\theta} + \frac{cos^2\theta}{\theta}$], where θ is the Bragg's angle, by extrapolating lattice parameter's values of F (θ) = 0 or θ = 90^0. The lattice parameters are plotted against the Nelson Relay function, F (θ) shown in Figure 4.5 for La content, Figure 4.6 for Y content and Figure 4.7 for Eu content.

The lattice parameter (a_0) decreases at x = 0.05, 0.10 and 0.15 due to the replacement of Zn^{2+} ions (radius=0.68Å) by the larger La^{3+}ions (radius = 1.03Å) in the octahedral sites shown in Table-4.1. The decrease in 'a_0' is probably due to a distribution in the spinel lattice because of the relatively large radius of La^{3+}. This is evidence by the appearance of the minor $FeLaO_3$ phase, besides the major spinel phase. These changes in lattice parameters with La content indicate that the present system obeys the Vegard's law [4.7] partially. Table 4.2 shown in a minor decrease in 'a_0' of $Ni_{0.60}Zn_{0.40-x}Y_xFe_2O_4$ ferrite with Y substitution, which might be due to the compressive pressure exerted on the ferrite lattice by $YFeO_3$. However, no significant decrease in 'a_0' is observed in the present experiment. There is a slight decrease Y^{3+} (radius = 0.90Å) in the octahedral sites, indeed, lattice parameter was in the same range of different.

Table 4.3 shows a decrease in lattice constant (a_0) is observed with the increasing Y content in the lattice. This indicates that the present system obeys the Vegard's law. This may be due to Eu^{3+}ions (radius = 1.12Å) having bigger that Zn^{2+} ions of radius 0.68Å, which when Zn^{2+} substituted resides on A-site and displaces all small ions from A site to B site. This decrease can be attributed to the vacancy created by Zn^{2+} deficiencies with increasing its content. The unit cell is expected to reduce its size by contraction of the lattice resulting in decrease of lattice parameter gradually.

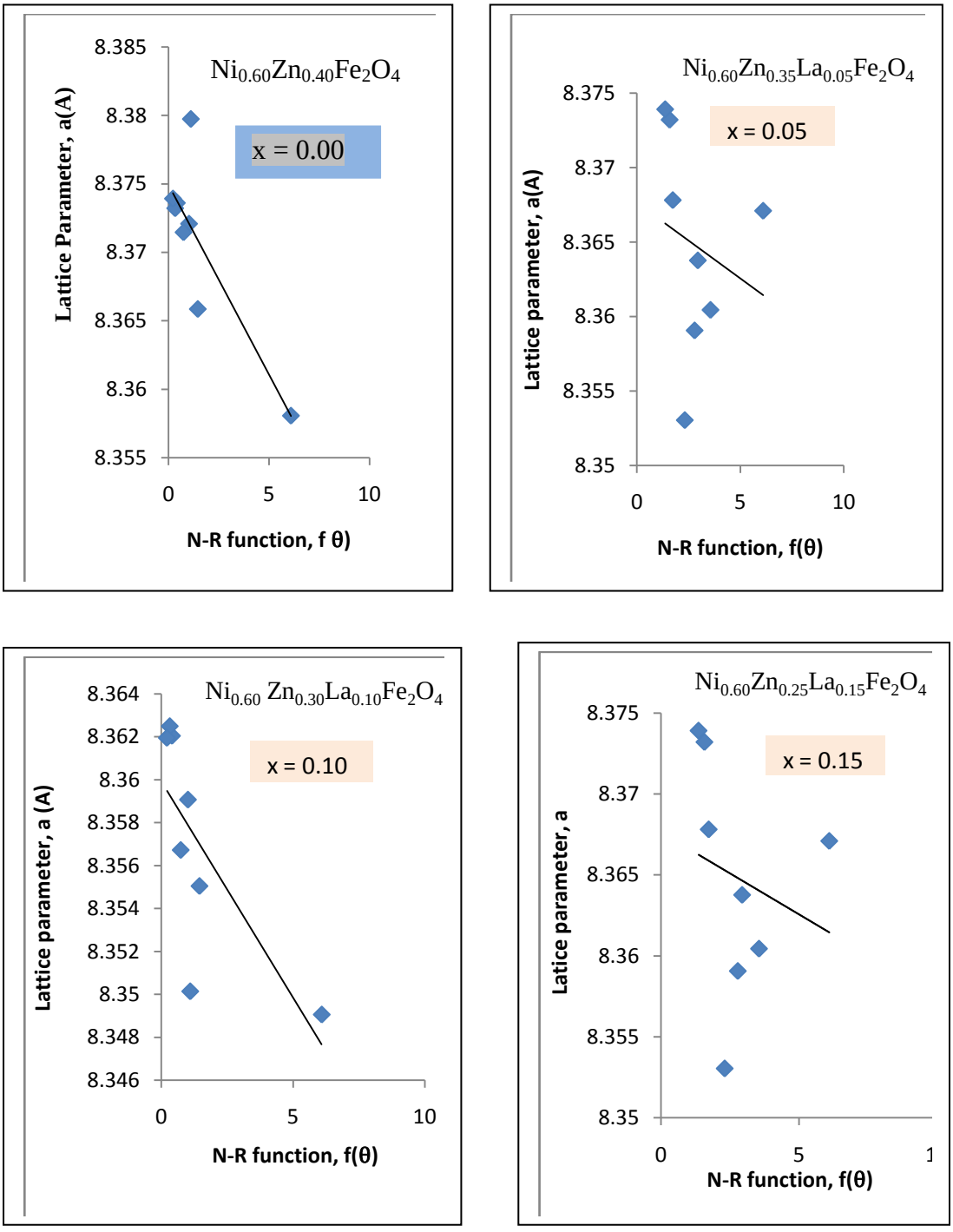

Figure 4.5 Variation of lattice parameter 'a' with N-R function and determination of exact lattice parameter a_0 of $Ni_{0.60}Zn_{0.40-x}La_xFe_2O_4$ [x = 0.00, 0.05, 0.10, 0.15]

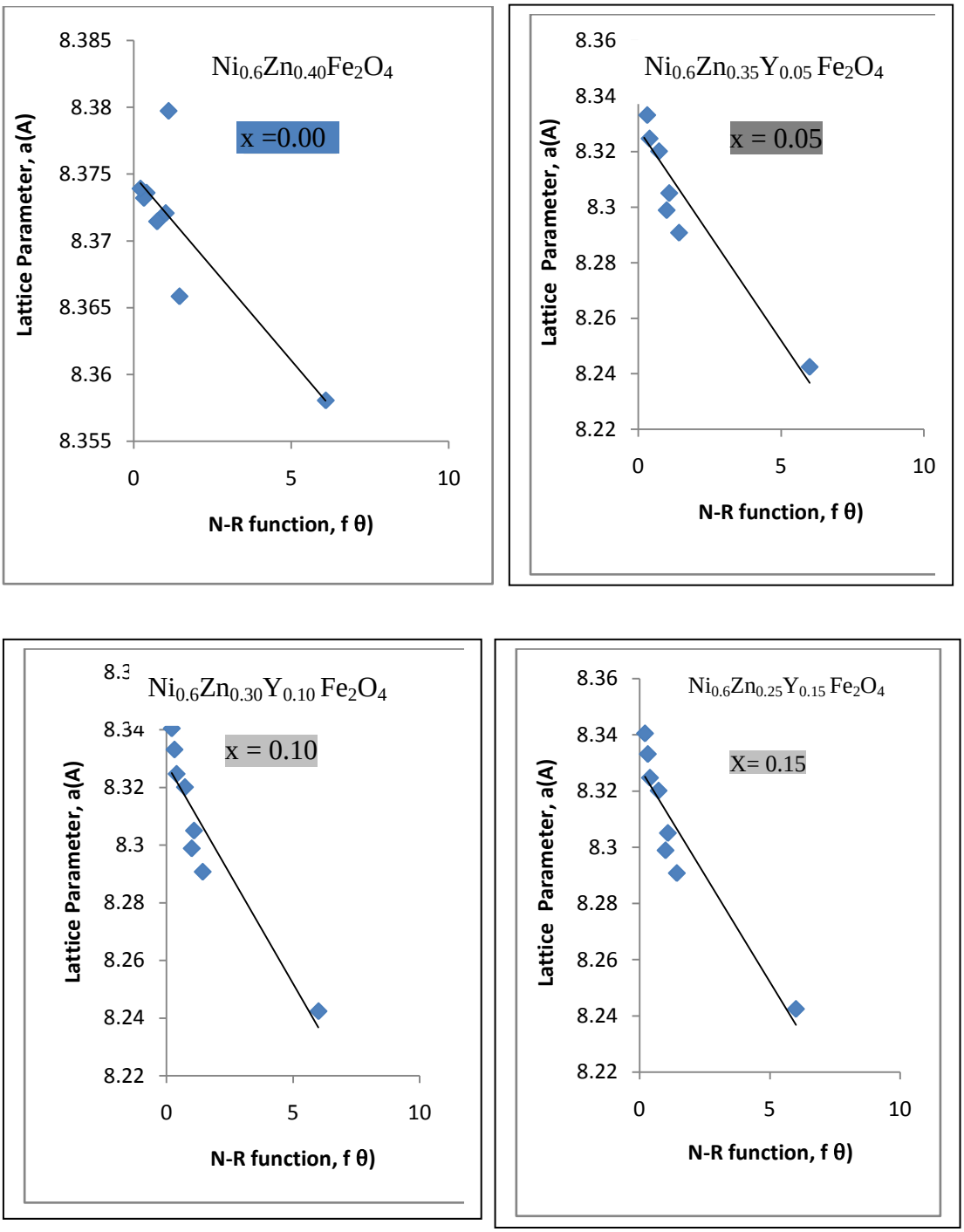

Figure 4.6 Variation of lattice parameter 'a' with N-R function and determination of exact lattice parameter a_0 of $Ni_{0.6}Zn_{0.40-x}Y_xFe_2O_4$ [x = 0.00, 0.05, 0.10, 0.15].

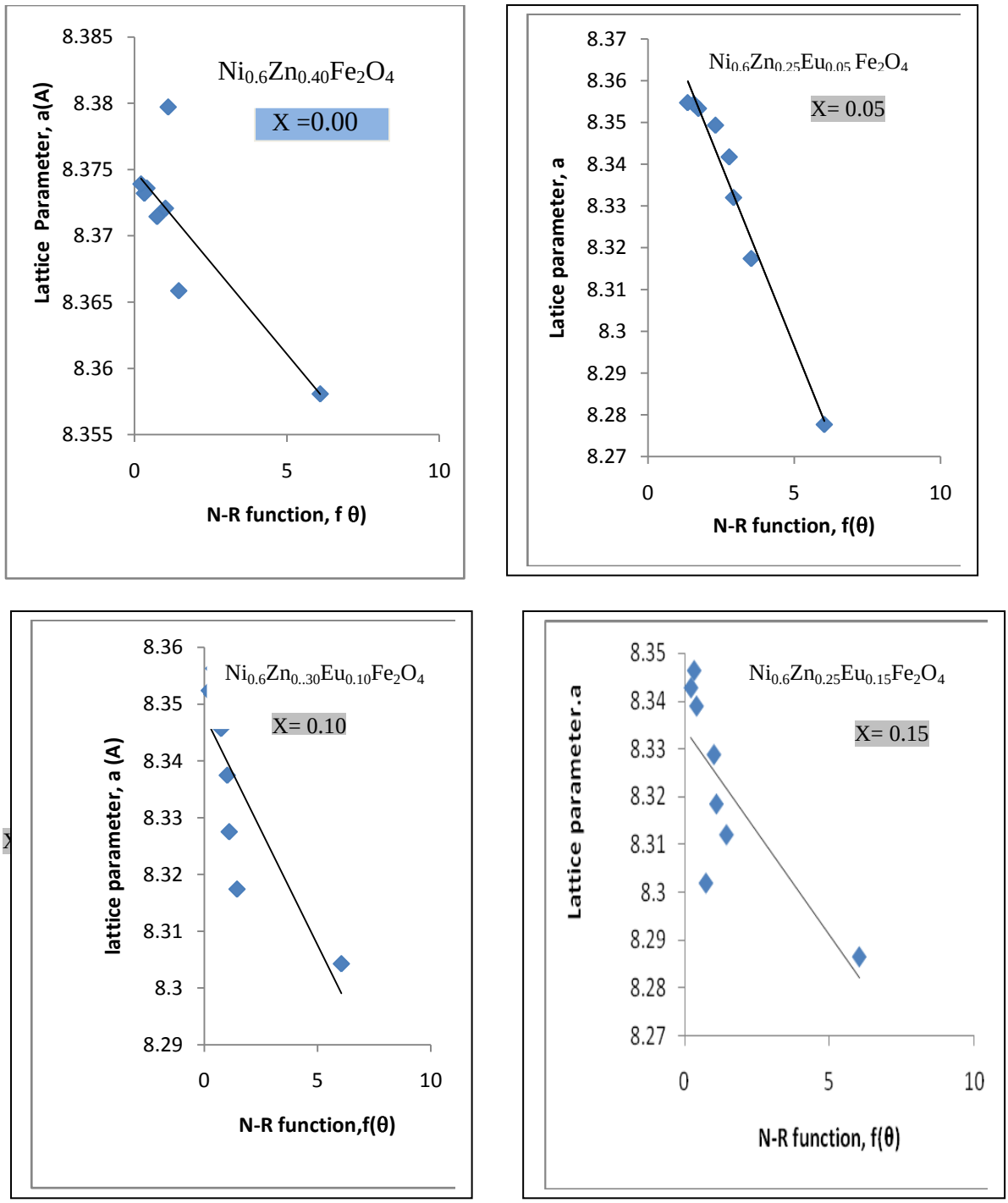

Figure 4.7 Variation of lattice parameter 'a' with N-R function and determination of exact lattice parameter a_0 of $Ni_{0.60}Zn_{0.40-x}Eu_xFe_2O_4$ [x = 0.00, 0.05, 0.10, 0.15].

4.1.3 Density and Porosity

The bulk density (d_B) was measured by usual mass and dimensional consideration whereas X-ray density (d_x) was calculated from the molecular weight and the volume of the unit cell for each sample by using the equation(3.5) and (3.6).The calculated values of the bulk density and theoretical (or X-ray) density of the present ferrite system are listed in Table- 4.1, Table-4.2 and TabIe-4.3. It is observed that bulk density is lower than the X-ray density shown in Figure4.8, Figue4.9 and Figure 4.10. This may be due to the existence of pores which were formed and developed during the sample preparation or sintering process. The bulk density slightly decreases with increasing rare earth ions (La^{3+}, Y^{3+} and Eu^{3+}) and the X-ray density increases continuously with increasing x-content.

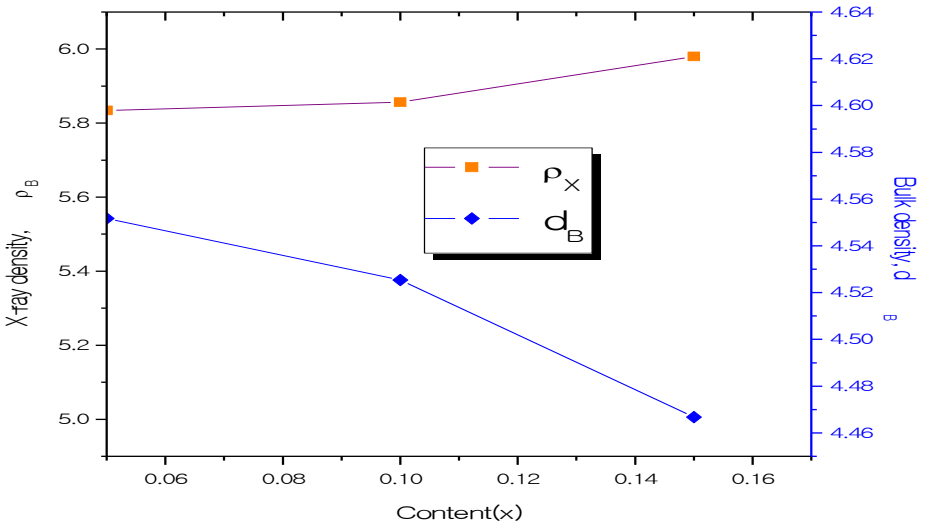

Figure 4.8 Variation of bulk density and X-ray density as a function of La content.

There are two possible existence statesof rare earth ions (La^{3+}, Y^{3+} and Eu^{3+}) in the Ni-Zn ferrites: Some of La^{3+}, Y^{3+} and Eu^{3+} entered the lattice and substituted the Zn^{2+}; other La^{3+}, Y^{3+} and Eu^{3+} diffused to the grain boundary during the sintering process. La^{3+}, Y^{3+} and Eu^{3+} ions entering the lattice can result in the increasing of the lattice parameter be-cause of La^{3+}, Y^{3+} and Eu^{3+} ions' larger radius than Zn^{2+}; But La^{3+}, Y^{3+} and Eu^{3+} congregating at grain boundary will reduce lattice parameter due to the vacancies left in the Ni-Zn lattice; As a combination of the two effect described above, a very small overall lattice parameter change can be observed. As for the

crystallite size reducing, two kind of La^{3+}, Y^{3+} and Eu^{3+} existence states both can constrain the growth of the grain. The La^{3+}, Y^{3+} and Eu^{3+} substitution in the lattice will induce lattice distortion, internal stress caused by this distortion hinders the growth of grains; If La^{3+}, Y^{3+} and Eu^{3+} diffused to the grain boundaries, that will also restrain the grain growth by lower down the grain mobility; That explains why the crystallite size of the substituted Ni-Zn ferrite is much smaller than un-doped ferrites[4.8,4.9]

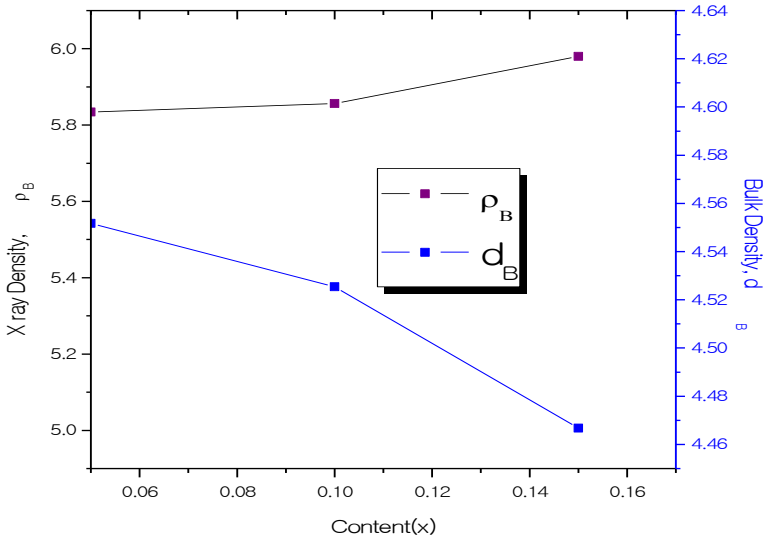

Figure 4.9 Variation of bulk density and X-ray density as a function of Y content.

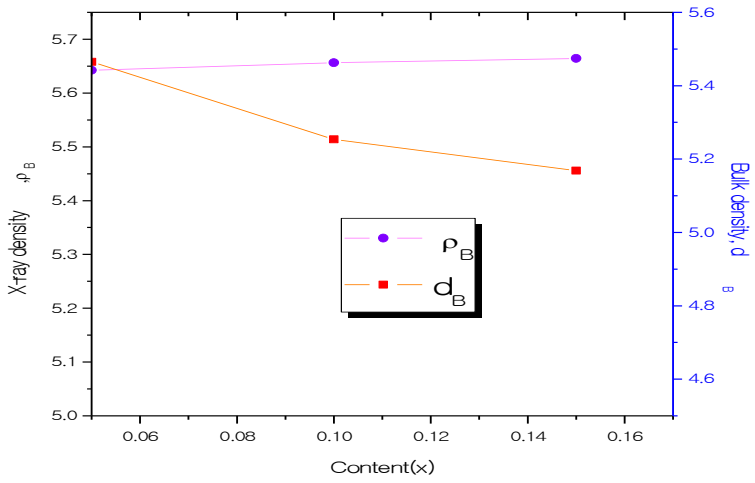

Figure 4.10 Variation of bulk density and X-ray density as a function of Eu content.

The enhancement of Bulk density is due to activated diffusion process triggered by the excess vacancies created by Zn^{2+} deficiency. Table-4.1, Table-4.2 and Table 4.3 show the results of lattice parameter, theoretical density, and bulk density shows the results of lattice parameter, theoretical density, and bulk density calculated porosity. It is observed all the samples that porosity increases monotonically with increasing La^{3+}, Y^{3+} and Eu^{3+}. Porosity also increased with the increasing of La, Y and Eu contents are shown in table-4.1, table-4.2 and table-4.3 respectively. Specimens contained some closed porosity. It was difficult to remove these closed porosities completely due to the evaporation of constituents specially Zn. It is known that the porosity of the samples come from two sources, intragranular porosity and intergranular porosity. The intergranular porosity mainly depends on the grain size [4.10]. At higher sintering temperatures the density is decreased because the intergranular porosity is increased resulting from discontinuous grain growth.The porosity which is intrinsic for any oxide material plays an important role in the deciding the magnetic and electrical properties.

Table- 4.1 Data of the lattice parameter (a), X-ray density (d_x), bulk density (d_B), porosity (P %), molecular weight (M) of $Ni_{0.40}Zn_{0.40-x}La_xFe_2O_4$ (x = 0.05, 0.10 and 0.15)ferrites sintered at 1250^0C/3hrs.

Sample Composition	a_0(Å)	$d_x$gm/cm^3	$d_B$in gm/cm^3	Porosity(%)
$Ni_{0.60}Zn_{0.35}Fe_2O_4$	8.375	5.0600	4.6201	8.6937
$Ni_{0.60}Zn_{0.35}La_{0.05}Fe_2O_4$	8.3675	5.8338	4.6517	13.5412
$Ni_{0.60}Zn_{0.30}La_{0.10}Fe_2O_4$	8.3600	5.85681	4.5254	13.9421
$Ni_{0.60}Zn_{0.25}La_{0.15}Fe_2O_4$	8.3125	5.9797	4.4668	14.3869

Table- 4.2 Data of the lattice parameter (a), X-ray density (d_x), bulk density (d_B), porosity (P %), molecular weight (M) of $Ni_{0.40}Zn_{0.40-x}Y_xFe_2O_4$ [x = 0.05, 0.10 and 0.15]ferrites sintered at 1250^0C/3hrs.

Sample Composition	a_0(Å)	d_x (gm/cm3)	d_B (gm/cm3)	Porosity (%)
$Ni_{0.60}Zn_{0.35}Fe_2O_4$	8.375	5.0600	4.6201	8.6937
$Ni_{0.60}Zn_{0.35}Y_{0.05}Fe_2O_4$	8.325	5.4938	5.7610	10.5362
$Ni_{0.60}Zn_{0.30}Y_{0.10}Fe_2O_4$	8.324	*5.5322*	5.5531	10.9623
$Ni_{0.60}Zn_{0.25}Y_{0.15}Fe_2O_4$	8.323	5.*7559*	5.4025	11.6542

Table- 4.3 Data of the lattice parameter (a), X-ray density (d_x), bulk density (d_B), porosity (P %), molecular weight (M) of $Ni_{0.40}Zn_{0.40-x}Eu_xFe_2O_4$ [x = 0.05, 0.10 and 0.15]ferrites sintered at 1250^0C/3hrs.

Sample Composition	a_0(Å)	d_x (gm/cm3)	d_B (gm/cm3)	Porosity (%)
$Ni_{0.60}Zn_{0.35}Fe_2O_4$	8.375	5.0600	4.6201	8.6937
$Ni_{0.60}Zn_{0.35}Eu_{0.05}Fe_2O_4$	8.3655	5.6423	5.4650	11.3245
$Ni_{0.60}Zn_{0.30}Eu_{0.10}Fe_2O_4$	8.3474	5.6565	5.2537	11.7668
$Ni_{0.60}Zn_{0.25}Eu_{0.15}Fe_2O_4$	8.3323	5.6644	5.1685	11.9595

4.2 Microstructures

Microstructure significantly affects the magnetic and electrical properties of ferrites. Figure 4.11(a, b, c, d) shows a set of microstructure where the sample (a) x = 0.00 shows the presence of a monophasic spinel phases whereas, the la substituted materials whose (b) x = 0.05 (c) x =0.10 and (d) x= 0.15 show a multiphasic microstructure consisting of a bigger matrix of ferrite grains and a smaller $LaFe_2O_3$ secondary phase at the grain junction / boundaries. The grain size of ferrite matrix phase as well as the $LaFe_2O_3$ phase increased with increasing the La^{3+} substitutions. The crystal grain growth depends on grain boundaries migrating and larger crystal grains swallowing the small ones. Grain growth is closely related to the grain boundary mobility. Recrystallization and grain growth involve the movement of grain

boundaries. It facilities the grain growth by increasing the rate of cations inter diffusion as a result of its segregation to the grain boundaries [4.11]. The behavior of grain growth reflects the competition between the driving force for grain boundary movement and the retarding force that drives the grain boundaries to grow over pores, thereby decreasing the pore volume and making the material dense.

Figure 4.12 (a, b, c, d) shows the microstructure of $Ni_{0.40}Zn_{0.40-x}Y_xFe_2O_4$ferrites sintered at 1250^0C/3hrs. It is clear that the microstructure of Ni-Zn-Y ferrite strongly depend on the amount of Y-content in the samples. As the Y-content increases, the grain size increases gradually. Figure 4.12(a) showed the presence of a monophasic homogeneous microstructure without Y content. Y doped specimens shown in figure 4.12(b, c, d) are a biphasic homogeneous microstructure constituted of dark ferrite matrix grain and small whitish grain at the grain junction/boundary. The grain size of matrix phase was maximum at x = 0.10 composition for Y content. Relatively lower grain size of ferrite matrix at x =0.10 composition shows in figure 4.12(c) might be due to the grain growth inhibition caused by $YFeO_3$ are clear visible.

Figure 4.13(a, b, c, d) shows the SEM microstructure of $Ni_{0.60}Zn_{0.40-x}Eu_xFe_2O_4$ferrites sintered at 1250^0C/3hrs. It is clear that the microstructure of Ni-Zn-Eu content in the samples. As the Eu content increases, the grain size increases gradually. It is also noticed from the microstructure that with increasing Eu-content grain grows bigger. This reflected in the permeability also increase with Eu content.

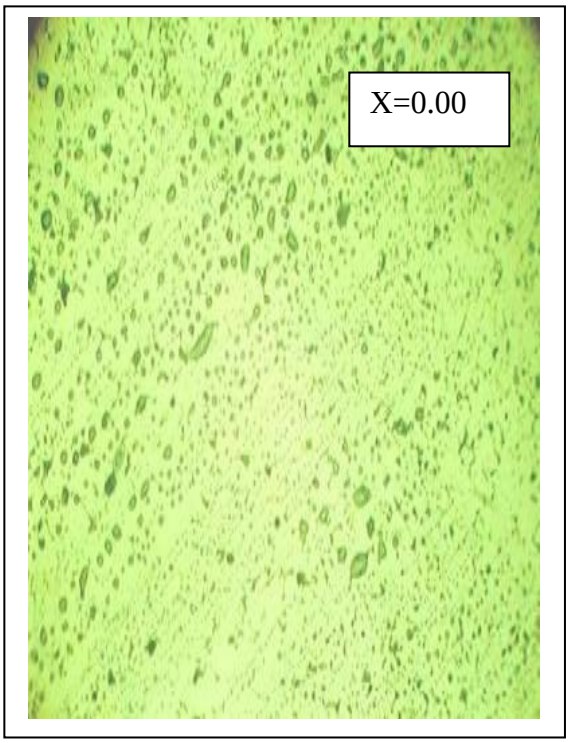

(a)

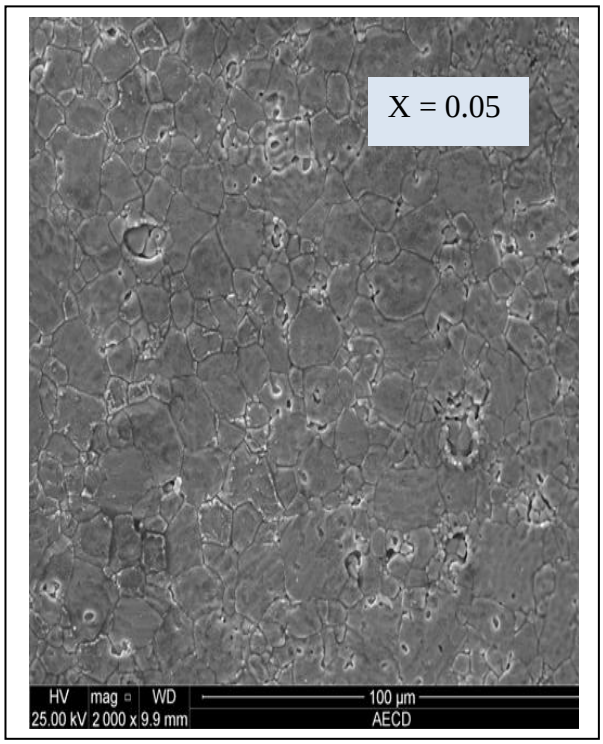

(b)

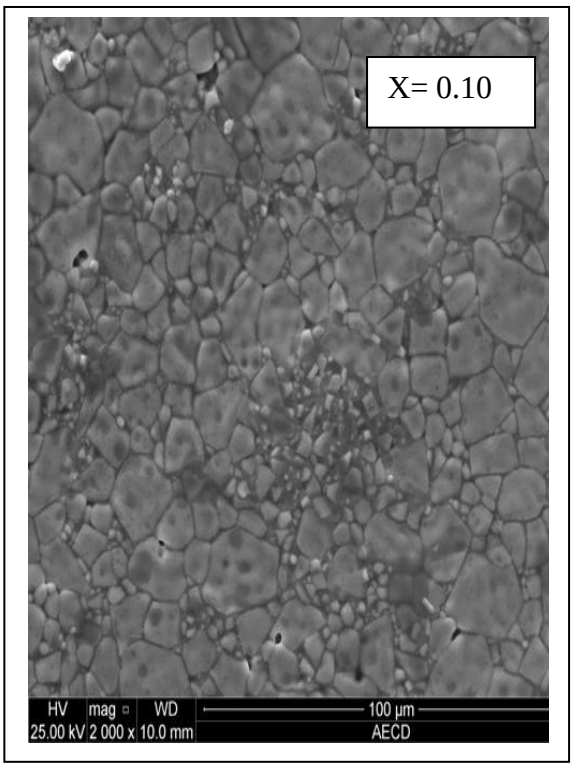

(c)

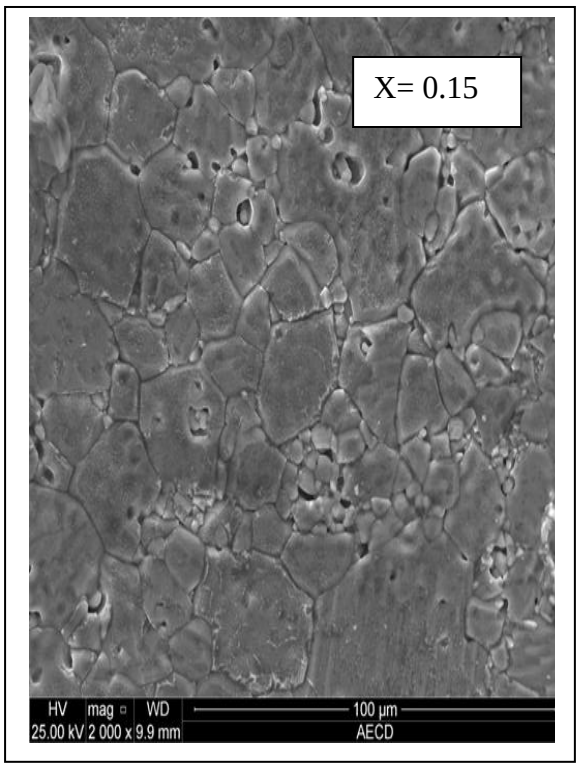

(d)

Figure 4.11(a, b, c, d) Variation of SEM photographs with La content (x) of $Ni_{0.40}Zn_{0.40-x}La_xFe_2O_4$ferrites whose x = 0.05, 0.10 and 0.15 sintered at 1250^0C/3 hrs

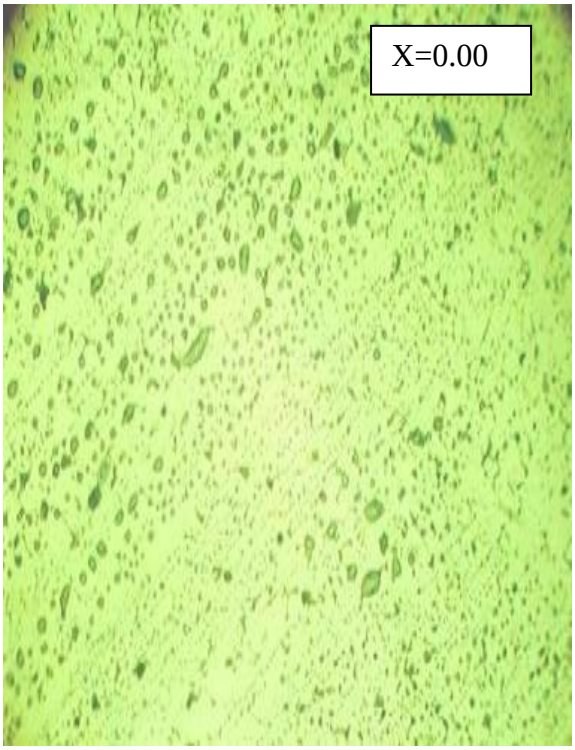

(a)

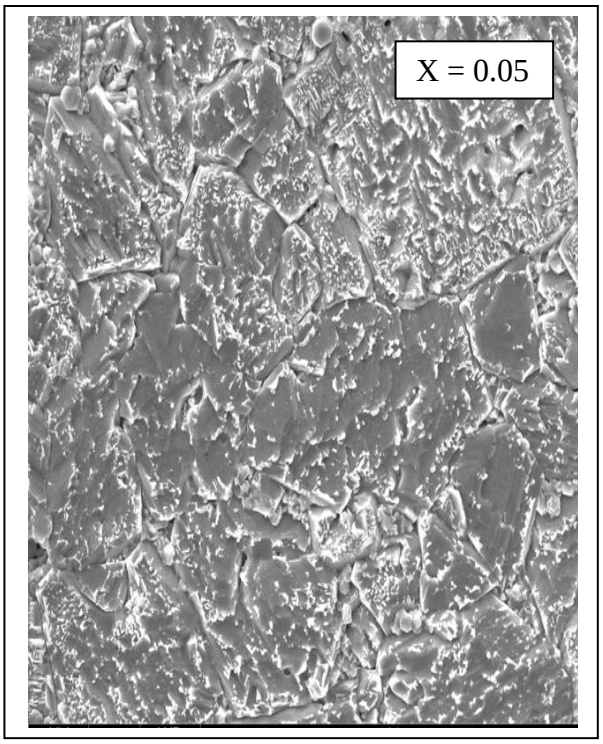

(b)

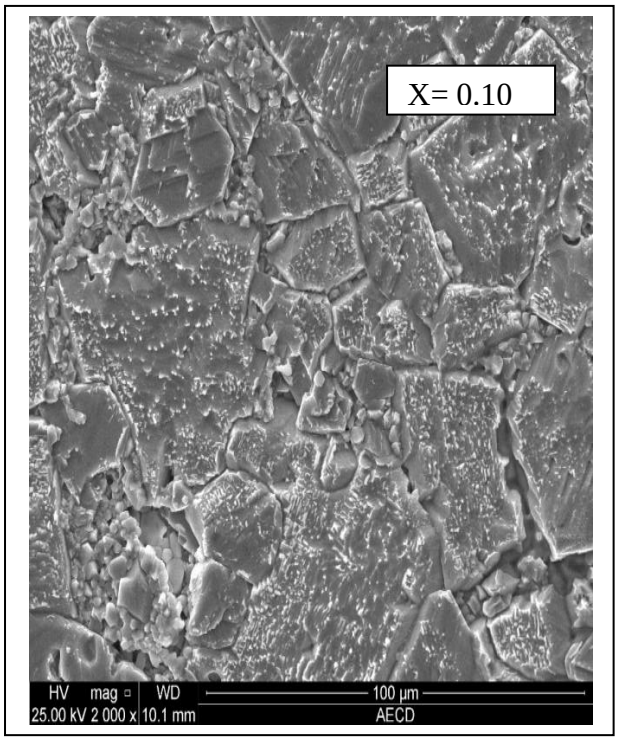

(c)

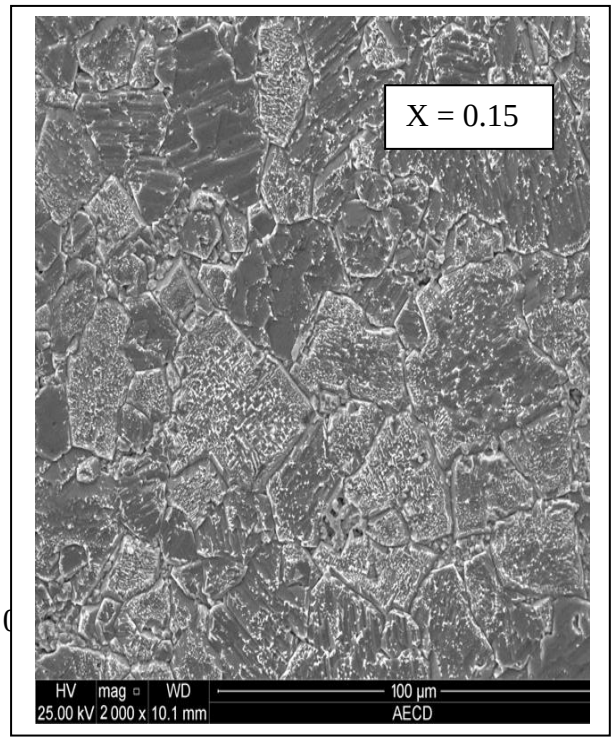

(d)

Figure 4.12 (a, b, c, d) Variation of SEM photographs with La content (x) of $Ni_{0.40}Zn_{0.40-x}Y_xFe_2O_4$ferrites whose x = 0.05, 0.10 and 0.15 sintered at 1250^0C/3 hrs

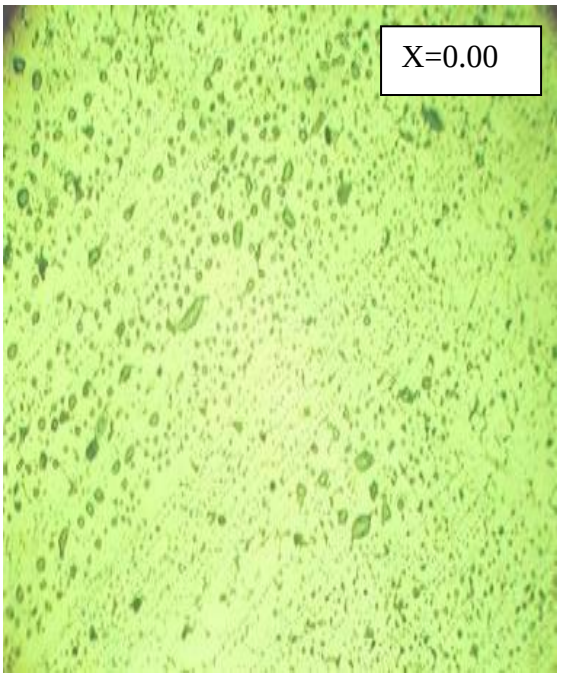

(a)

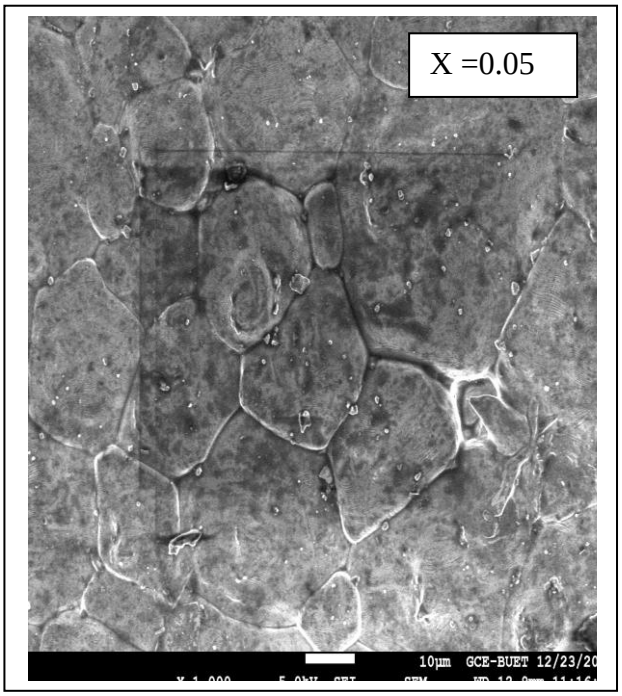

(b)

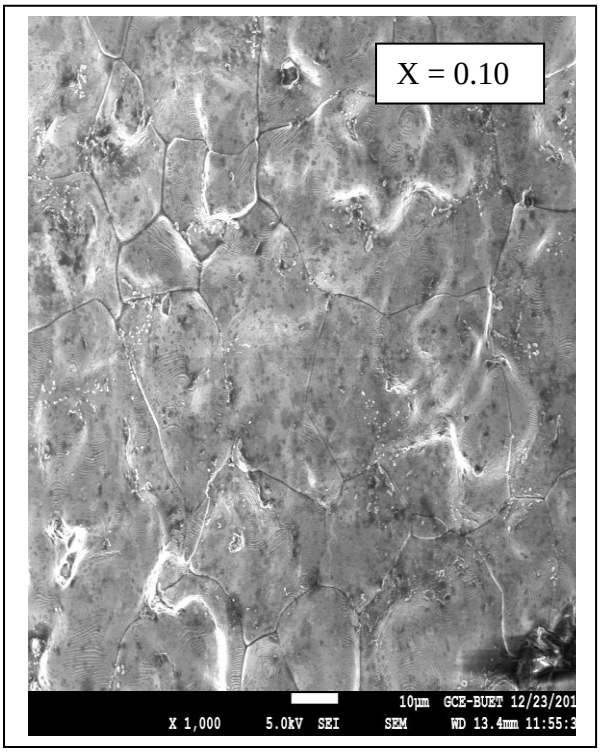

(c)

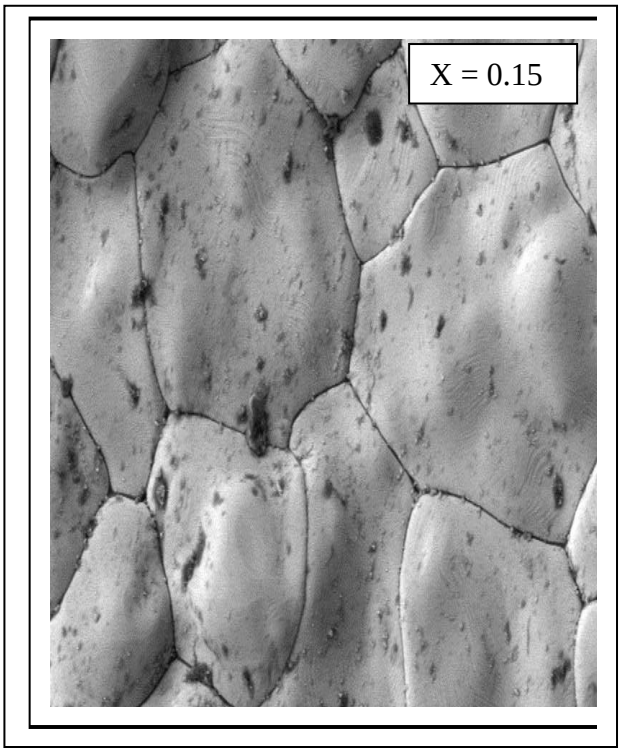

(d)

Figure 4.13 (a, b, c, d) Variation of SEM photographs with La content (x) of $Ni_{0.40}Zn_{0.40-x}Eu_xFe_2O_4$ferrites whose x = 0.05, 0.10 and 0.15 sintered at 1250^0C/3 hrs

Since permeability is directly proportional to grain size D and M_s which also increase with increasing M_s i.e. $\mu_i \infty \frac{M_s^2}{\sqrt{K_1}} D$, The increase in grain size with Eu-content is clearly visible. Figure 4.13(a) shows a monophasic and homogeneous microstructure whereas figure 4.13(b, c, d) shows a biphasic microstructure constituted of a matrix of grains of a second phase ($EuFeO_3$). Energetically, small grains are less stable than large grains due to their higher specific surface areas. As a consequence, liquid phase layers would be dissolved in the liquid phase layers. It is observed that an increase in the amount of Eu(x = 0.15) content result in an increase in the coverage of the grains by the $EuFeO_3$ phase and this is beneficial to grain growth.

4.3 Magnetic Properties

4.3.1 Temperature Dependence of Initial Permeability

Curie temperature, Tc is a basic quantity in the study of magnetic materials. It corresponds to the temperature at which magnetically ordered material becomes magnetically disorder. Figuer4.14 shows the temperature dependence of initial permeability, μ', for the toroid shaped samples of $Ni_{0.40}Zn_{0.40-x}La_xFe_2O_4$ (where x= 0.05, 0.10 and 0.15)ferrites sintered at 1250^0C/3hrs which is measured manually by using WAYNE KERR IDUCTANCE ANALYZER 3255B, a small oven and a thermocouple based thermometer. Curie temperature also signifies the strength of theexchange interaction between the magnetic atoms exchange interaction between the magnetic atoms. It is observed from the Figure 4.14 that the permeability falls sharply when the magnetic state of the ferrite samples changes from ferromagnetic to paramagnetic state. When the anisotropy constant reaches to zero just below the Curie temperature, T_c the initial permeability μ' attains its maximum value known as Hopkinson's peak[4.12] and then drops of sharply to minimum value at Curie point. The sharpness of the permeability drop at the Curie point can be used as a measure of degree of compositional homogeneity according to Globus [4.13], which has also been confirmed by XRD that no impurity phases could be detected. It is observed from the Figure 4.15 and table 4.4 that T_c increases continuously with increase of La-content.

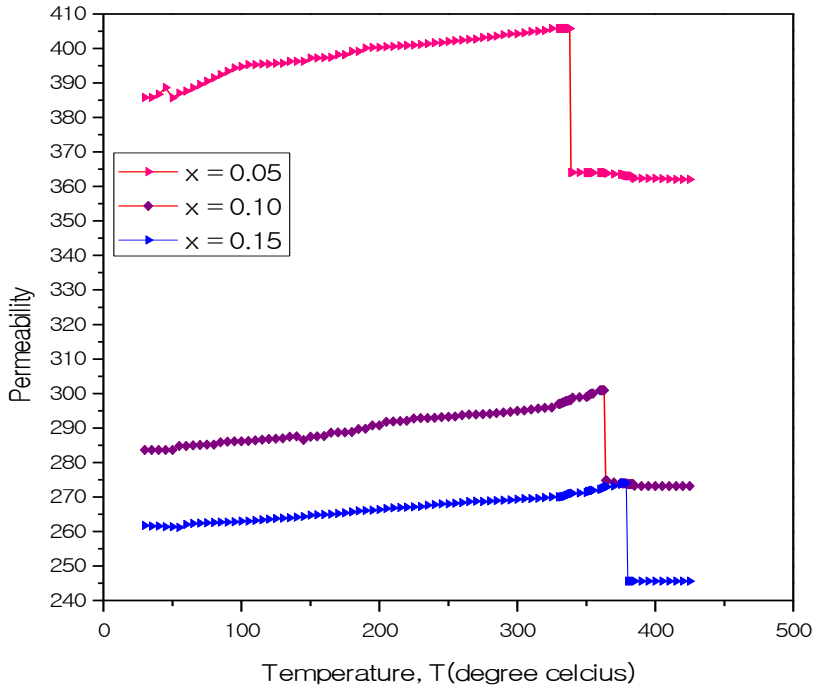

Figure 4.14 Variation of permeability, μ′with temperature of $Ni_{0.60}Zn_{0.40-x}La_xFe_2O_4$ where x =0.05, 0.10 and 0.15 ferritessintered at 1250°C/3hrs

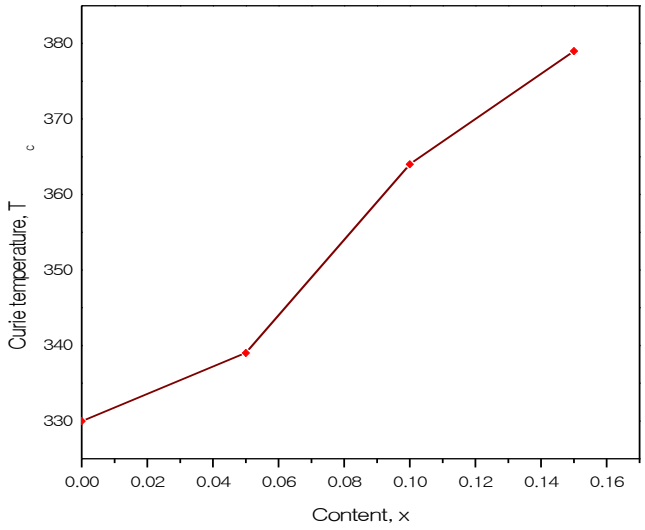

Figure 4.15 Variation of T_C with La of $Ni_{0.60}Zn_{0.40-x}La_xFe_2O_4$ where X = 0.05, 0.10 and 0.15 ferrites sintered at 1250°C/3 hrs.

Table4.4 Data of Curie temperature (T_C) of $Ni_{0.60}Zn_{0.40-x}La_xFe_2O_4$ [x = 0.05, 0.10 and 0.15] ferrites.

Content X	T_s=1250°C
	T_c(°C)
0.00	330
0.05	339
0.10	364
0.15	379

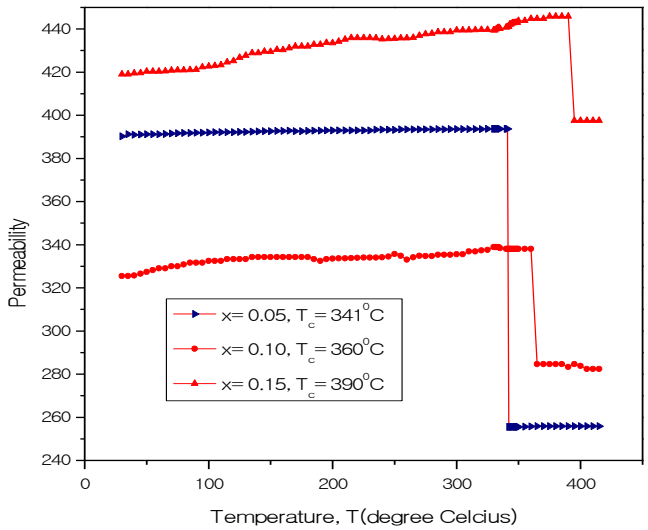

Figure 4.16 Variation of permeability, μ′with temperature of $Ni_{0.60}Zn_{0.40-x}Y_xFe_2O_4$ where x =0.05, 0.10 and 0.15 ferrites sintered at 1250°C/3 hrs.

Figure 4.16shows the temperature dependence of initial permeability μ' of the toroid shaped sample with composition $Ni_{0.40}Zn_{0.40-x}Y_xFe_2O_4$(wherex= 0.05, 0.10 and 0.15)ferrites which measured at a constant frequency 100 KHz of an AC signal by using Impedance Analyzer. Since the initial permeability is directly related to the

magnetization and the ionic structure, the thermal spectra of permeability can be taken as a test of the formation and homogeneity of ionic structure of the samples. It is observed that the permeability falls sharply that μ' attains its maximum value and then drops off to minimum value near T_c is shown in table 4.5, T_c increases with increases Y content is shown in Figure 4.17.

Figure 4.18 shows the T_c is obtained from the initial permeability, μ' versus temperature profiles of composition $Ni_{0.40}Zn_{0.40-x}Eu_xFe_2O_4$ (where $_x$= 0.00, 0.05, 0.10 and 0.15). It is found that μ' increases with the increase of temperature, while it falls abruptly close to Curie temperature. The abrupt fall of permeability indicates the homogeneity and the single phase of the studied sample which have also been confirmed by XRD patterns for each sample. In Figure 4.19 the variation of T_c as a function of Eu contents of Ni-Zn-Eu ferrites. It is observed that T_c increases continuously with increases of Eu^{3+} content as shown in Table 4.6

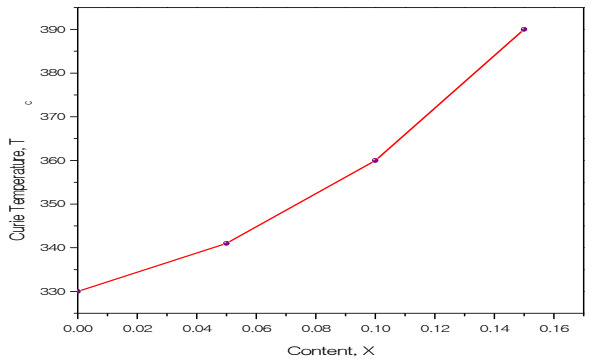

Figure 4.17 Variation of T_C with Lanthanum Content (x) of $Ni_{0.60}Zn_{0.40-x}La_xFe_2O_4$ [x =0.05, 0.10 and 0.15] ferrites sintered at 1250°C/3hrs

Table-4.5 Data of Curie temperature (T_C) of $Ni_{0.60}Zn_{0.40-x}Y_xFe_2O_4$ [x = 0.05, 0.10 and 0.15]ferrites

Content X	T_s=1250°C
	T_c(°C)
0.00	330
0.05	341
0.10	360
0.15	390

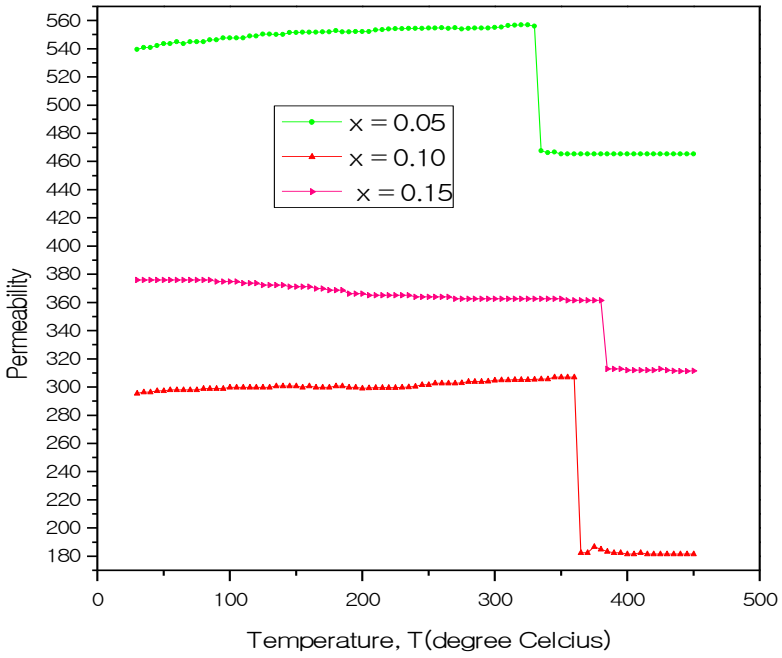

Figure 4.18 Variation of permeability, μ′with temperature of $Ni_{0.60}Zn_{0.40-x}Y_xFe_2O_4$ [x =0.05, 0.10 and 0.15]ferrites sintered at 1250°C/3 hrs.

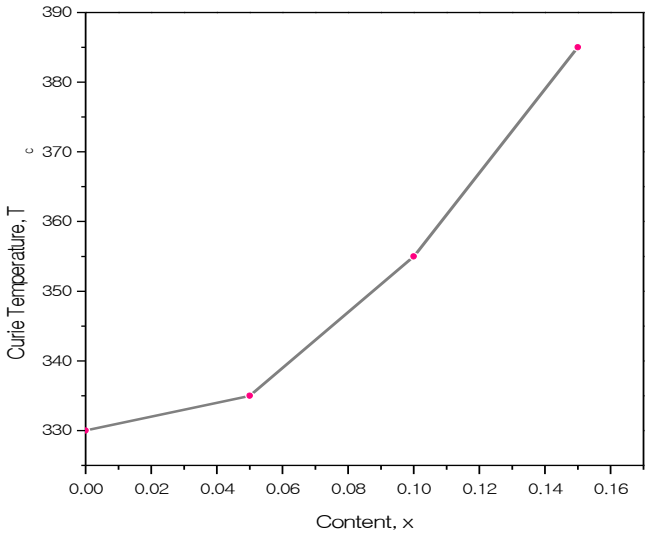

Figure 4.19 Variation of T_C with Lanthanum Content (x) of $Ni_{0.60}Zn_{0.40-x}La_xFe_2O_4$ [x =0.05, 0.10 and 0.15] ferrites sintered at 1250°C/3 hrs.

Table-4.6 Data of Curie temperature T_C of $Ni_{0.60}Zn_{0.40-x}Eu_xFe_2O_4$ [x =0.05, 0.10 and 0.15]ferrites.

Content X	T_s=1250°C
	T_c(°C)
0.00	330
0.05	335
0.10	360
0.15	385

4.3.2 Frequency Dependence of Complex Permeability

The complex permeability is given by $\mu = \mu' - i\mu''$, μ' is the real permeability (in phase) and μ'' the imaginary permeability (90^0 out of phase). Complex permeability has been determined as a function of frequency, f up to 100 MHz at room temperature for all the samples of series [$Ni_{0.40}Zn_{0.40-x}RE_xFe_2O_4$ (RE = La, Y, Eu and x= 0.00, 0.05, 0.10 and 0.15] ferrites by using the conventional technique based on the determination of the complex impedance of circuit loaded with toroid shaped sample.

Figure 4.20 and Figure 4.21 show the variation of the complex permeability spectra with frequency of the system $Ni_{0.40}Zn_{0.40-x}La_xFe_2O_4$ for the different values of x at sintering temperature1250^0C/3hrs. La^{3+} has no unpaired electrons and it behaves as diamagnetic. The substitution of ferromagnetic Fe^{3+} ($5\mu_B$) by diamagnetic La^{3+} in the spinel was not metal for increasing permeability. It has been suggested that the substitution of La^{3+}ions moved Ni^{2+} and Zn^{2+} ions from 'B' to 'A' sites causing A such lattice dilution and increased the magnetic permeability in Ni-Zn ferrites. However, in the present case La^{3+} incorporation into the lattice is very small and hence the increased permeability with increasing La^{3+} ions due to its incorporation. The increased permeability with increasing La^{3+} ions due to the following reasons: (i) increased grain size (ii) increased density (iii) decreased magnetocrystalline anisotropy (iv) change in stress and (v) change of the Zn containing nonmagnetic precipitated compound due to the solid solution formation of Zn in La Fe_2O_3etc.

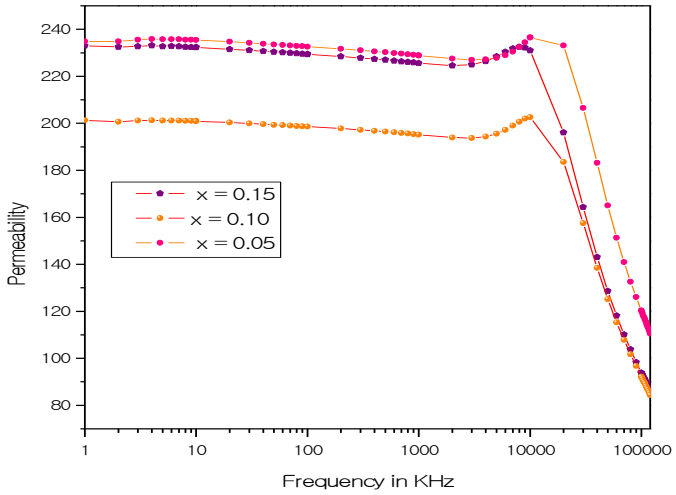

Figure 4.20 Variation of initial permeability with frequency of $Ni_{0.60}\ Zn_{0.40-x}La_xFe_2O_4$ [x = 0.05, 0.10, 0.15]ferrites sintered at 1250^0C/3hrs.

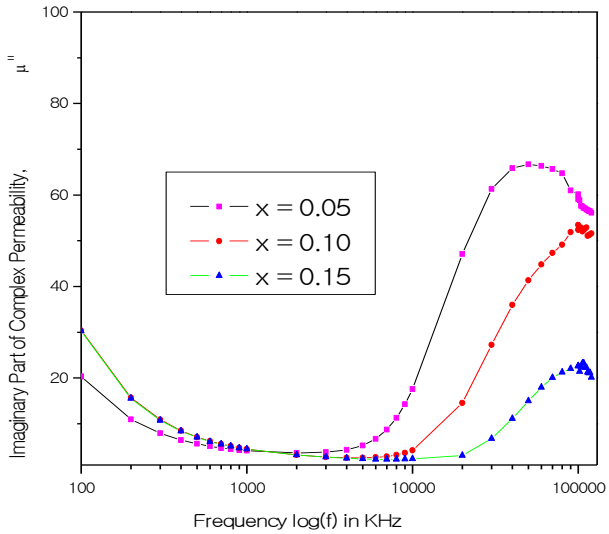

Figure 4.21 Complex imaginary permeability μ" with frequency of $Ni_{0.60}Zn_{0.40-x}\ La_xFe_2\ O_4$[x=0.05, 0.10, 0.15] ferrites sintered at 1250^0C/3hrs.

The La substituted compositions are different in Fe and hence Fe^{2+} ions are expected to be at minimum. The magnetic anisotropy field in ferrites results mainly from Fe^{2+} ions [4.15]. This decrease in anisotropy increases the permeability. From

this Figure 4.20, it is seen that the real part of the permeability μ' remained almost constant until the frequency is raised to a certain value within the range 10- 60MHz and then drop to a very low values at higher frequencies. The imaginary part of μ" gradually increased with the frequency and attain a broad maximum at a certain frequency whose the real part of permeability rapidly decreased as shown in Figure 4.21. Figure 4.22 and Figure 4.24 shows the variation of the real part of permeability with frequency of the system $Ni_{0.40}Zn_{0.40-x}Y_xFe_2O_4$ [x = 0.05, 0.10 and 0.15] and $Ni_{0.40}Zn_{0.40-x}Eu_xFe_2O_4$[x = 0.05, 0.10 and 0.15] at constant sintering temperature1250^{0}C/3hrs respectively. The initial permeability μ' decreases with increasing both rare earth content Y and Eu, which is consistent with the decrease in density with Zn-content. The initial permeability is closely correlated to the densification of the samples with Y and Eu-content. The decrease of permeability with increasing Y or Eu may be explained on the basis of intragranular pores entrapped within the grain which create constraint on the domain wall mobility.

As a result initial permeability decreases figure 4.22 shows that the permeability of the compositions $Ni_{0.40}Zn_{0.40-x}Y_xFe_2O_4$ [x = 0.05, 0.10 and 0.15] are stable within the range 10 to 30MHz, and figure 4.24 shows that the permeability of the composition $Ni_{0.40}Zn_{0.40-x}Eu_xFe_2O_4$ [x = 0.05, 0.10 and 0.15] are stable within the range 20 to 40 MHz, the maximum frequency limit of the instrument. Figure 4.23 and Figure 4.24 shows, the imaginary component μ" first rises slowly and then increases quite abruptly making a peak at a certain frequency where the real component μ' is falling sharply. This feature is well known as the ferromagnetic resonance [4.16]. At low frequencies, a ferrite inductor is a low loss constant self induction [Figure 4.20, Figure 4.22 and Figure 4.24] where μ' is highest and the core is mostly inductive; rejecting the electromagnetic interference (EMI) signal to the source. At high frequencies where the μ" parameters become more significant, the inductors show high impedance and become resistive and dissipate interfering signals rather than reflecting these to the source [4.17]. When frequency is low, permeability is high and when frequency is high permeability is low. Thus, an effective limit of product of frequency and permeability is established. So, that effect of rare earth content of high frequency and high permeability are mutually incompatible.

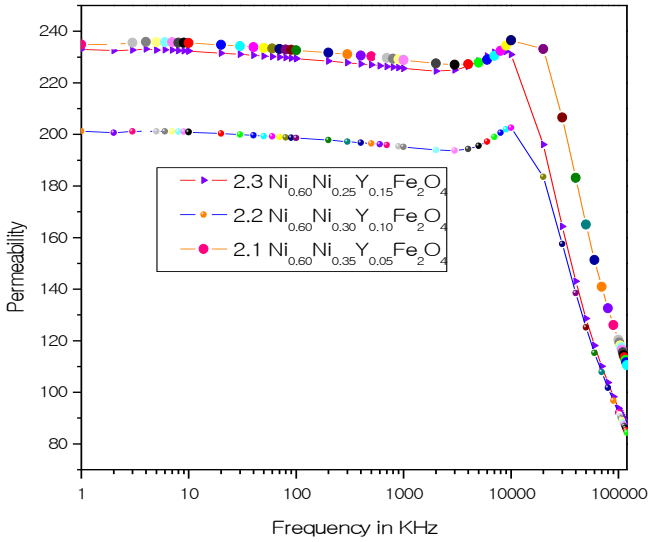

Figure 4.22 Variation of initial permeability with frequency of $Ni_{0.60}$ $Zn_{0.40-x}Y_xFe_2O_4$ [x = 0.05, 0.10, 0.15]ferrites sintered at 1250^0C/3hrs

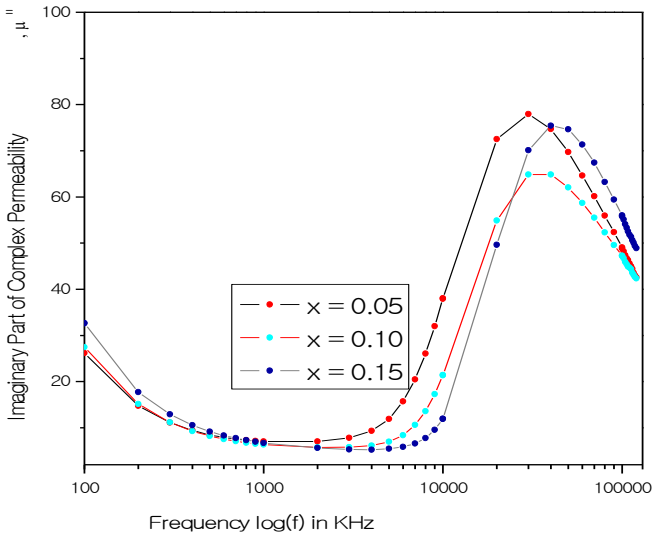

Figure 4.23 Complex imaginary permeability μ'' with frequency of $Ni_{0.60}Zn_{0.40-x}Y_xFe_2O_4$[x=0.05, 0.10, 0.15] ferrites sintered at 1250^0C/3hrs.

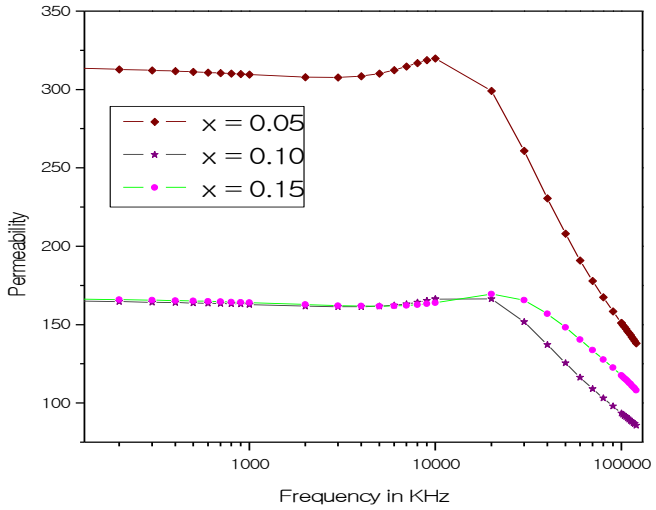

Figure 4.24 Variation of initial permeability with frequency of $Ni_{0.60}\ Zn_{0.40-x}Eu_xFe_2O_4$ [x = 0.05, 0.10, 0.15] and Eu ferrites sintered at 1250^0C/3hrs.

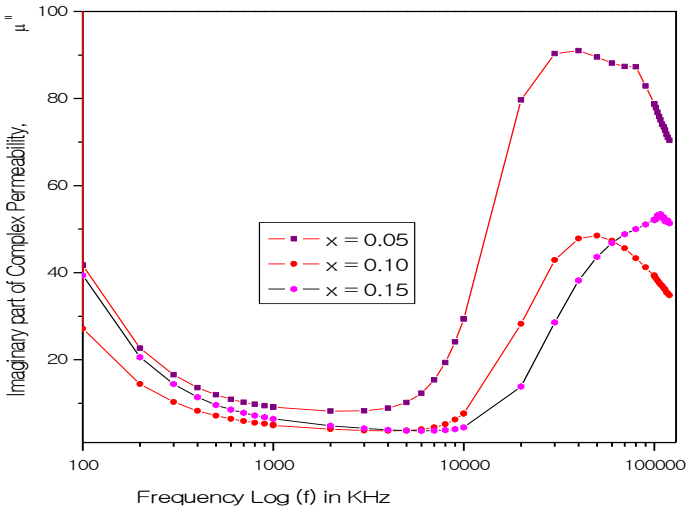

Figure 4.25 Complex imaginary permeability μ'' with frequency of $Ni_{0.60}Zn_{0.40-x}Eu_xFe_2O_4$[x=0.05, 0.10, 0.15] ferrites sintered at 1250^0C/3hrs.

4.3.3 Frequency Dependence of Quality Factor

The frequency dependence of $Ni_{0.60}Zn_{0.40-x}RE_xFe_2O_4$ [RE La, Yand Eu] ferrites sintered at 1250^0C/3hrs have been calculated from the relation Q = 1/ tanδ; where tanδ is the loss factor is used to measure the merit of the magnetic materials. Figures 4.26, 4.27 and 4.28 show the frequency dependence quality factors (Q-factors) of samples are$Ni_{0.60}Zn_{0.40-x}La_xFe_2O_4$, $Ni_{0.60}Zn_{0.40-x}Y_xFe_2O_4$ and $Ni_{0.60}Zn_{0.40-x}Eu_xFe_2O_4$ sintered at 1250^0C for 3 hours respectively. Q-factor increases with an increase of frequency showing a peak and then decreases with further increase of frequencies. It is seen that Q-factor again deteriorates beyond 2 MHz for La (Figure 4.26), 1MHz for Y (Figure 4.27) and 4MHz for Eu (Figure 4.28) i.e. the loss tangent is minimum around 1 to 4MHz. The loss is due to the loss of domain wall motion with respect to the applied alternating magnetic field and is attributed to various domain defects [4.18] which include non- uniform and non repetitive domain wall motion, domain wall bowing, and localized variation of flux density, nucleation and annihilation of domain walls.

The peak corresponding to maxima in Q-factor shifts to lower frequency range as La or Y content increases but Eu not significantly shifts. Sample with x = 0.15 possesses the maximum value of Q-factor for all the samples La, Y and Eu. The low frequency dispersions are associated with domain wall dynamics [4.19] and high frequency to spin rotation. Both of these samples are shown here for a better understanding for the merit of the prepared materials for an induction device application. This phenomenon is associated with the ferromagnetic resonance within the domains and at the resonance maximum energy is transferred from the applied magnetic field to the lattice resulting in the rapid decrease in Q-factor. Ni-Zn-La, Ni-Zn-Y and Ni-Zn-Eu ferrites have been found to demonstrate reasonably good permeability at room temperature covering stable wide range of frequency indicating the possibilities for applications as high frequency up to several MHz induction and/or core materials. These mean that Ni-Zn-RE (La, Y and Eu) ferrite materials are suitable for high frequency applications with high permeability.

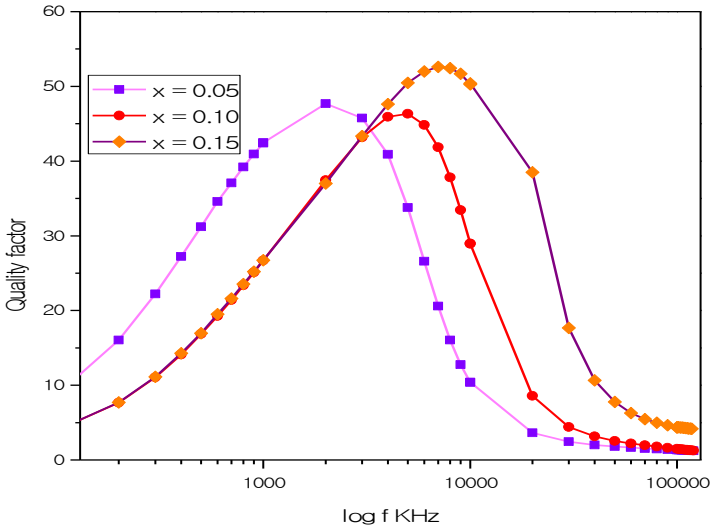

Figure 4.26 Variation of relative quality factor, as a function of frequency of $Ni_{0.60}Zn_{0.40-x}La_xFe_2O_4$ [x= 0.05, 0.10 0.15] ferrites sintered at 1250^0C/3hrs.

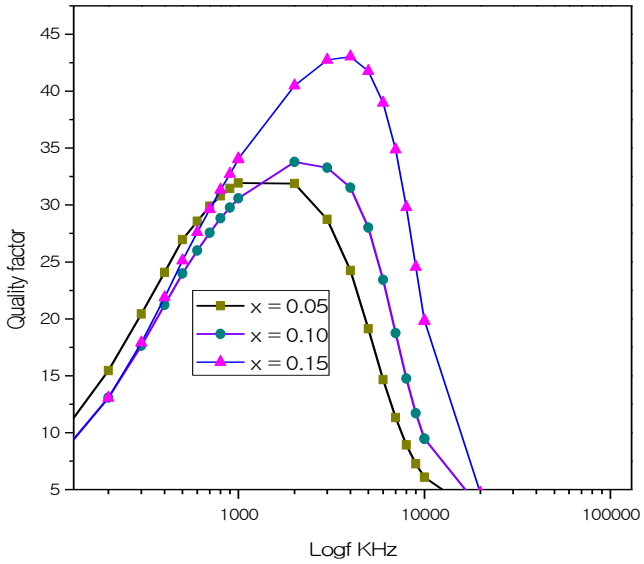

Figure 4.27 Variation of relative quality factor, as a function of frequency of $Ni_{0.60}Zn_{0.40-x}Y_xFe_2O_4$ [x= 0.05, 0.10 0.15] ferrites sintered at 1250^0C/3hrs.

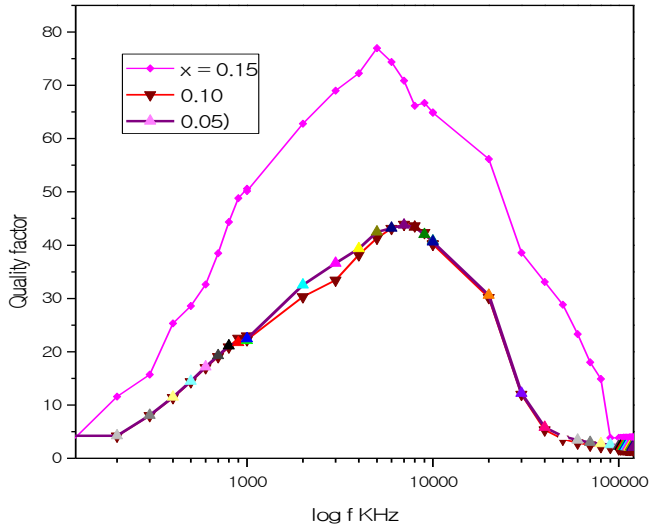

Figure 4.28 Variation of relative quality factor, as a function of frequency of $Ni_{0.60}Zn_{0.40-x}Eu_xFe_2O_4$ [X = 0.05, 0.10 0.15] ferrites sintered at 1250^0C/3hrs.

4.4 Variation of Saturation Magnetization at Room Temperature

Magnetization as a function applied field up to 20 KOe was measured with vibrating sample magnetometer (VSM) at room temperature of three samples $Ni_{0.40}Zn_{0.40-x}La_xFe_2O_4$, $Ni_{0.40}Zn_{0.40-x}Y_xFe_2O_4$ and $Ni_{0.40}Zn_{0.40-x}Eu_xFe_2O_4$ ferrites sintered at 1250^0C/3hours are shown in Figures 4.29, Figure-4.30 and Figure 4.31 respectively. It is observed that the magnetization increases sharply at very low field (H < 1 KOe) which corresponds to magnetic domain reorientation that thereafter increases slowly up to saturation due to spin rotation. This magnetization process is connected with soft magnetic behavior of magnetic material. The slow process of magnetization toward the saturation value is connected with the magnetic anisotropy effect. Actual saturation could not be attained even with magnetic field as high as 20 KOe. Saturation Magnetization (M_s) values of different compositions are given in table 4.7 that M_s is increase with increasing rare earth elements (La, Y and Eu) with x-content.

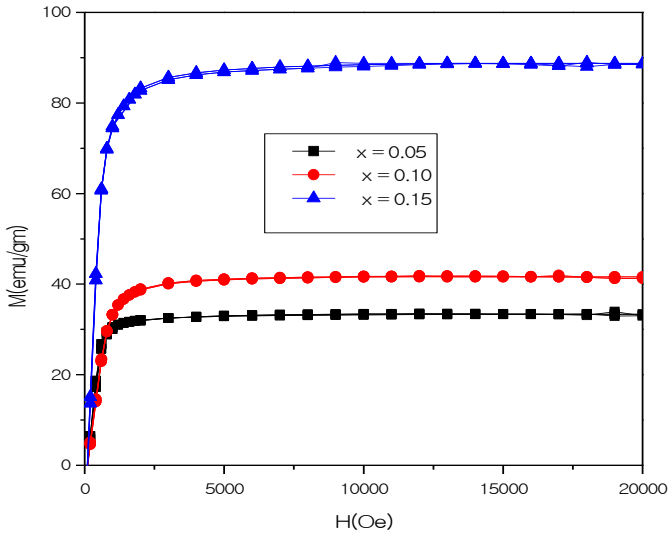

Figure 4.29 Variation of magnetization at room temperature as a function of applied field on $Ni_{0.40}Zn_{0.40-x}La_xFe_2O_4$ [x= 0.05, 0.10 and 0.15] ferrites sintered at 1250^0C/3hrs.

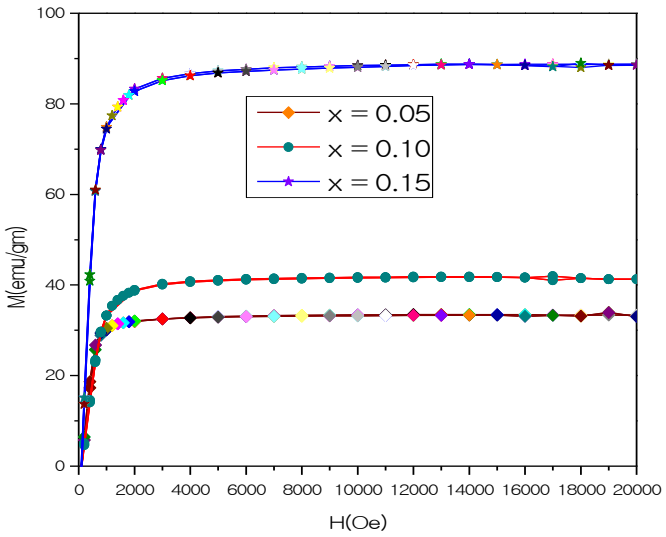

Figure 4.30 Variation of magnetization at room temperature as a function of applied field on $Ni_{0.40}Zn_{0.40-x}Y_xFe_2O_4$ [x= 0.05, 0.10 and 0.15] ferrites sintered at 1250^0C/3hrs.

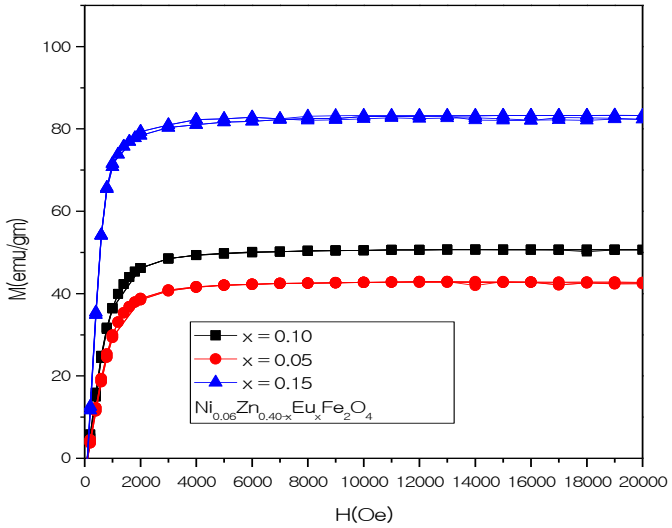

Figure 4.31 Variation of magnetization at room temperature as a function of applied field on $Ni_{0.40}Zn_{0.40-x}Eu_xFe_2O_4$ [x= 0.05, 0.10 and 0.15] ferrites sintered at 1250^0C/3hrs.

Table 4.5 Data of Saturation Magnetization (M_s) of $Ni_{0.60}Zn_{0.40-x}RE_xFe_2O_4$ [RE= La, Y, Eu and x =0.05, 0.10, 0.15]ferrites

	Name of the samples	Saturation magnetization(M_s)
RE = La	$Ni_{0.60}Zn_{0.35}La_{.05}Fe_2O_4$	32
	$Ni_{0.60}Zn_{0.30}La_{.10}Fe_2O_4$	38
	$Ni_{0.60}Zn_{0.25}La_{.15}Fe_2O_4$	84
RE = Y	$Ni_{0.60}Zn_{0.35}Y_{.05}Fe_2O_4$	32
	$Ni_{0.60}Zn_{0.30}Y_{.10}Fe_2O_4$	40
	$Ni_{0.60}Zn_{0.25}Y_{.15}Fe_2O_4$	82
RE = Eu	$Ni_{0.60}Zn_{0.35}Eu_{.05}Fe_2O_4$	40
	$Ni_{0.60}Zn_{0.30}Eu_{.10}Fe_2O_4$	50
	$Ni_{0.60}Zn_{0.25}Eu_{.15}Fe_2O_4$	80

The observed variation in $M_s$can be explained on the basis of cation distribution and the exchange interactions between A and B sites. The initial increase in M_s with increasing rare earth (La, Y, Eu) is due to the increase of resultant sub lattice magnetic moment which can be explained on the basis of Neel's two sub lattice model. Neel [4.20] considered three types of exchange interactions between unpaired electron of two ions lying in A and B sites. In perfect ferrites, the A - A, B - B and A - B nearest neighbor exchange coupling are normally anti ferromagnetic and the A - B exchange coupling is usually heavily predominant.

The net magnetization is therefore the difference between the magnetic moments of B and A sub lattices, i.e. $M = M_B - M_A$ and will normally be parallel to the B-sub lattice magnetization because the number of cations on B-sites is twice the number of cations on A-sites. The magnetization of each composition depends on the distribution of Fe^{3+} ions between the two sub lattices A and B, where the Ni^{2+} and Zn^{2+} ions are non magnetic. It is mentioned that $Ni_{0.60}Zn_{0.40-x}RE_xFe_2O_4$ (RE = La, YandEu) ferrites are known as mixed ferrites, where Ni^{2+} andFe^{3+} ions are located on B-sites andZn^{2+}ions show a strong preference for tetrahedral A-site due to its electronic configuration.Ahmed et al. [4.15] worked on $(Ni_{1-x}Zn_x)La_yFe_{2-y}O_4$ ferrite system and reported La^{3+} could not enter into theoctahedral site but form small aggregates on the grain boundary. Similarly, the rare earth ions Y and Eu could not enter into the B site and accumulate on the grain boundary.

4.5 Electrical Transport Property

4.5.1 Temperature Dependence of Resistivity

Resistivity is an important electrical property of ferrite materials. The electrical properties of ferrite materials depend upon the method of preparation, chemical composition, grain size and sintering temperature. The temperature dependence of electrical resistivity of ($Ni_{0.60}Zn_{0.40-x}$ RE $_x$ Fe_2O_4) (RE = La, Y, Eu) ferrites sintered at 1250^0C/3hrs.

Ferrites of different compositions have been investigated. The above equation shows the variation of AC resistivity as a function of temperature. The relationship between resistivity and temperature may be expressed by Arrhenius relation [4.22] as

$$\rho = \rho_0 e^{\frac{E_a}{k_B T}}$$

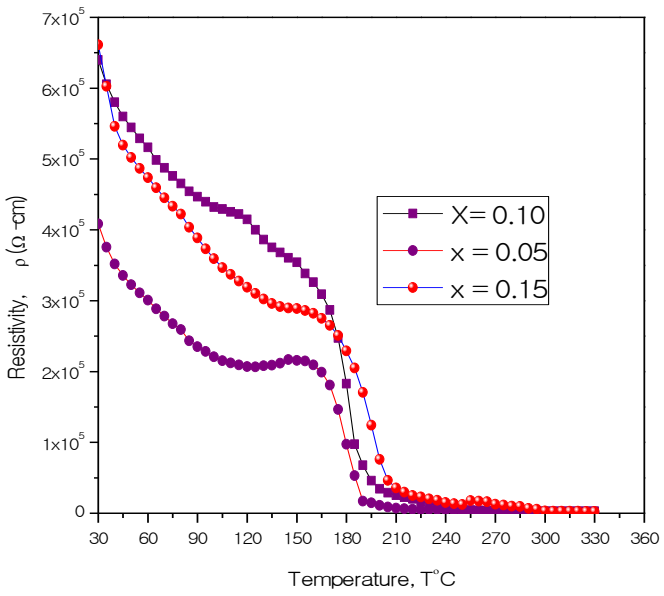

Figure 4.32 AC resistivity as a function of Temperature of $Ni_{0.60}Zn_{0.40-x}La_xFe_2O_4$[x = 0.05, 0.10, 0.15] ferrites sintered at 1250^0C/3hrs.

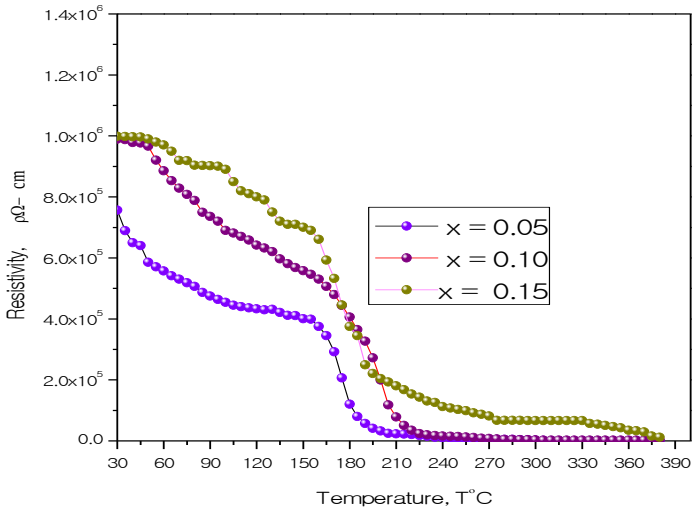

Figure 4.33 AC resistivity as a function of Temperature of $Ni_{0.60}Zn_{0.40-x}Y_xFe_2O_4$[x = 0.05, 0.10, 0.15] ferrites sintered at 1250^0C/3hrs.

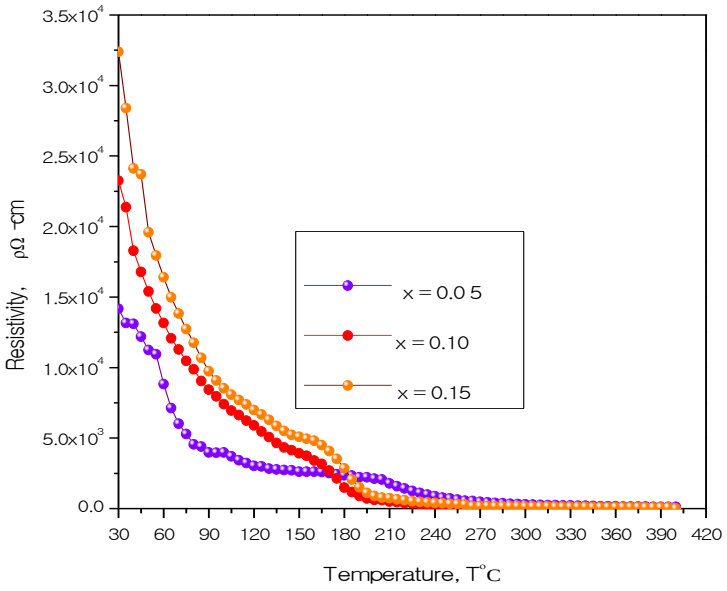

Figure 4.34 AC resistivity as a function of Temperature of $Ni_{0.60}Zn_{0.40-x}Eu_xFe_2O_4$[x = 0.05, 0.10, 0.15] ferrites sintered at 1250^0C/3hrs.

Where, T is the absolute temperature, K_B the Boltzmann constant and Ea is the activation energy. It is seen that the electrical resistivity decreases for all the studied samples according to equation exhibiting the semiconducting nature of the samples. From figure 4.32, figure 4.33 and figure 4.34 one can observe that in the investigated temperature range, the resistivity decreased.

The resistivity increased with incorporationrare earthsuch as La, Y and Eu in Ni-Zn ferrite. The conduction in ferrite was considered to occur by the electro hoping between Fe^{3+} and Fe^{2+} ions that are located at the octahedral site of the spinel ferrite structure. The specimens at x = 0.15 showed highest resistivity among all, which might be attributed to the presence of lower amount of Fe^{2+} ions in the ferrites. As described earlier, La, Y and Eu substituted compositions were deficient in Fe content and crystallization of $LaFeO_3$, $YFeO_3$ and $EuFeO_3$ at their grain boundaries impeded the oxidation of Fe^{3+}ions inside the grains. This might be a reason of increased resistivity in them. The resistivity of all the compositions decreased with the increasing temperature. The resistivity was primarily dependant on the temperature but temperature > 180^0C all the samples are independent.

4.5.2 Frequency Dependence of Dielectric Constant

Figure 35, Figure 36 and Figure 37 show the variation of dielectric constant, ε' with frequency for different composition of $Ni_{0.60}Zn_{0.40-x}La_xFe_2O_4$,$Ni_{0.60}Zn_{0.40-x}Y_xFe_2O_4$ and$Ni_{0.60}Zn_{0.40-x}Eu_xFe_2O_4$ where x =0.05, 0.10, 0.15) ferrites sintered at 1250^0C/3hrs for 1MHz to 100MHz at room temperature. It can be seen from the figure that the dielectric constant is found to decrease continuously with increasing frequency for all the specimens exhibiting a normal dielectric behavior of ferrites. The dielectric dispersion is rapid at lower frequency region and it remains almost independent at high frequency side. The incorporation of rare earth elements (La, Y, Eu) into these ferrites has no pronounced effect on the dielectric constant in high frequency, but significantly decreases the dielectric constant in the low frequency range.

The dielectric behavior of ferrites may be explained on the basis of the mechanism of the dielectric polarization process and is similar to that of the conduction process. The electronic $Fe^{2+} \leftrightarrow Fe^{3+}$gives the local displacement of electrons in the direction of applied electric field, which induces the polarization in ferrites [4.23].The magnitude of exchange depends on the concentration Fe^{2+}/Fe^{3+} in pairs present on B-site for the present ferrite. All the samples have high value of ε' in the order of 10^5 at low frequencies. This could be explained using Koop's phenomenological theory [4.24] which was based on the Maxwell-Wagner model [4.25 – 4.26] for the inhomogeneous double layer dielectric structure. The first layer is the fairly well conducting large ferrite grain which is separated by the second thin layer of the poorly conducting grain boundaries. The grain boundaries of the lower conductivity were found to be ferrite at lower frequencies while ferrite grains of high conductivity are effective at high frequency.

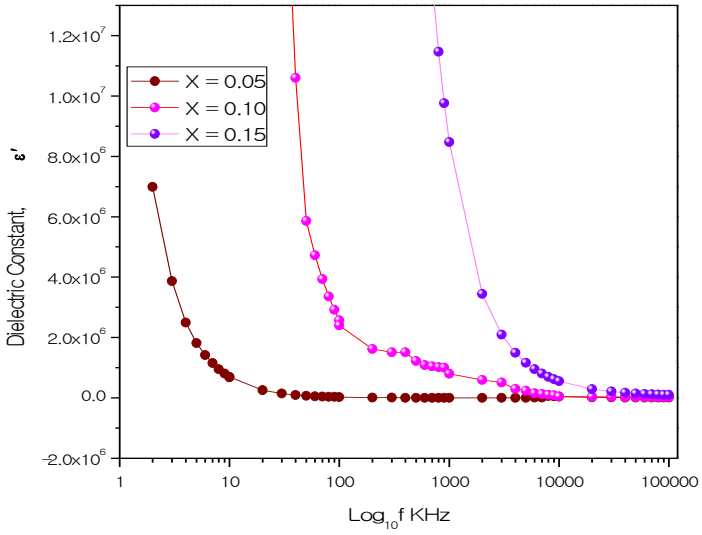

Figure4.35 Dielectric constant as a function of frequency of the ferrite system of $Ni_{0.40}Zn_{0.40-x}La_xFe_2O_4$ [x= 0.05, 0.10 and 0.15] ferrites sintered at 1250^0C/3hrs.

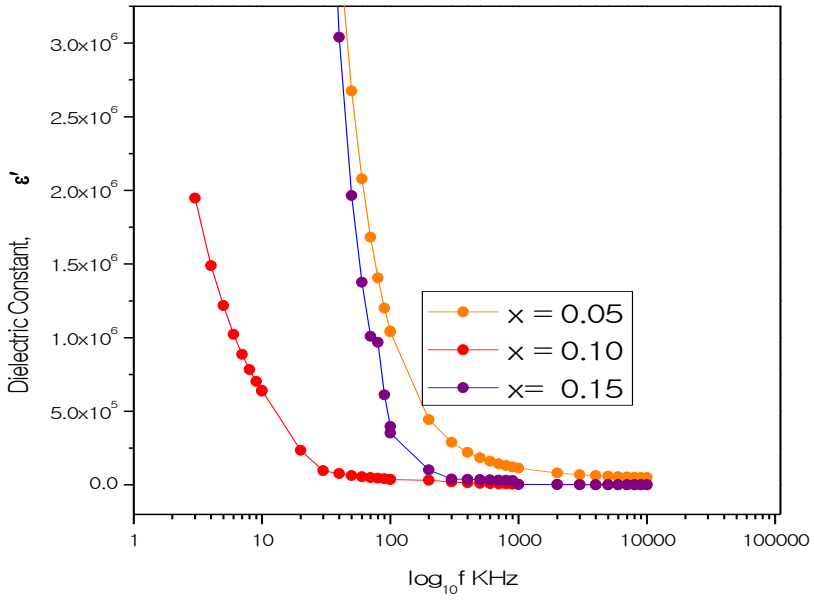

Figure 4.36 Dielectric constant as a function of frequency of the ferrite system of $Ni_{0.40}Zn_{0.40-x}Y_xFe_2O_4$ [x= 0.05, 0.10 and 0.15] ferrites sintered at 1250^0C/3hrs.

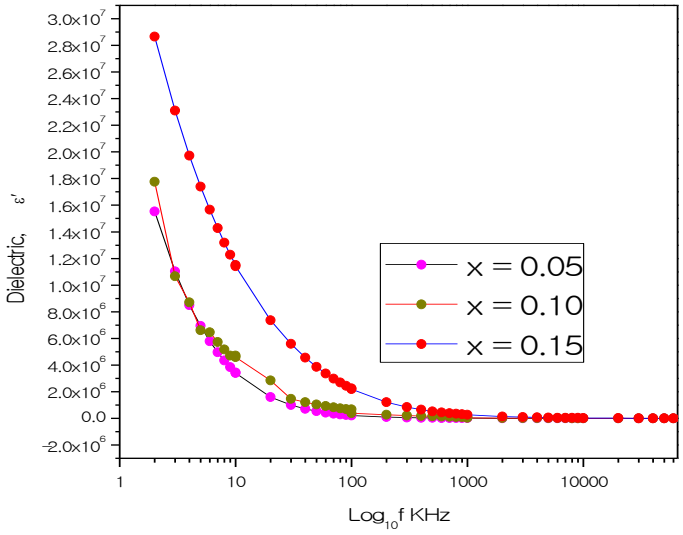

Figure 4.37 Dielectric constant as a function of frequency of the ferrite system of $Ni_{0.40}Zn_{0.40-x}Eu_xFe_2O_4$ [x= 0.05, 0.10 and 0.15] ferrites sintered at 1250^0C/3hrs.

CONCLUSIONS

5.1 Conclusions

The synthesis characterization and detail study of structural, magnetic and electric properties have been carried out on $Ni_{0.60}Zn_{0.40-x}La_xFe_2O_4$, $Ni_{0.60}Zn_{0.40-x}Y_xFe_2O_4$ and $Ni_{0.60}Zn_{0.40-x}Eu_xFe_2O_4$ ferrites samples [x = 0.05, 0.10 and 0.15], double sintering ceramic method, sintered at 1250^0C for 3 hours.

The XRD patterns confirmed the Ni-Zn ferrite sample is spinel cubic and the Ni-Zn- RE ferrites are pluriphasic (cubic and orthorhombic). The rare earth (RE) substitution for Fe in the ferrite mainly produced secondary phase $REFeO_3$. The lattice parameter decreases with increasing RE (La, Y and Eu) contents obeying Vagard's law. The bulk density is lower than the actual density of the sample. Bulk density is decreasing slowly with increasing RE (La, Y and Eu). The porosity of the Ni-Zn-RE samples decreases with increasing La, Y and Eu contents.

The microstructure clearly shows multiphase consisting of a bigger matrix of ferrite grains and a smaller $REFeO_3$ [RE = La, Y and Eu] secondary phase at the grain boundaries. The grain size of ferrite matrix phase as well as the La FeO_3 phase increased with increasing La^{3+}substitutions. Y doped Ni-Zn-Y ferrites are biphasic homogeneous microstructure constituted of dark ferrite matrix grains and small whitish grain at the grain junction. The microstructure of Ni-Zn-Eu ferrites shows the bigger grain growth with increasing Eu contents.

The Curie temperature is found to increase with successive addition of magnetic La, Y and Eu elements in the Ni-Zn-RE ferrites [RE = La, Y and Eu] due to strengthening of A-B exchange interaction as La, Y and Eu replace the nonmagnetic Zn. The abrupt fall off permeability indicates homogeneity of the samples.

Grain size has a great influence on the domain wall contribution and hence on permeability decreases with increasing La contents. With increasing frequency the initial permeability remains constant up to 10 MHz to 60 MHz for Ni-Zn-La ferrites. The imaginary part μ'' of permeability increases slowly and attain a broad maximum within the frequency range up to 10-60 MHz for Ni-Zn-La ferrites. The initial permeability for Ni-Zn-Y ferrite remains constant up to 10-30MHz and the broad maximum also takes place at the frequency range 10-30 MHz. Similarly, for Ni-Zn-Eu ferrites the initial permeability remains stable up to the frequency 20-40 MHz. The

ferromagnetic resonance occurs at the frequency range 20-40MHz which is confirmed by the imaginary part of the permeability.

The saturation magnetization increases with increasing the RE [La, Y and Eu] by replacing the nonmagnetic Zn content in Ni-Zn-RE ferrites. RE substitution in the Ni-Zn-RE ferrites leads to increase of Fe^{3+} ions on the B-sites and consequently decreases Fe^{3+} ions on A-sites. So, the net magnetization increases accordingly RE based ferrite on Neel's two sublattice collinear models. Ferrimagnetism in ferrite is largely governed by the spin coupling of 3d electrons. If the RE ions enter the spinel lattice, the RE-Fe interactions also appears 4f-3d coupling, which can lead to changes in the magnetization and Curie temperature.

AC resistivity increases with increasing RE content which is attributed to the fact that the incorporation of Zn replacing by RE in B-site of Ni-Zn-RE ferrites may decrease the concentration of Fe^{3+}/Fe^{2+} ion pairs. The occupation of RE ions on B-sites impedes the motion of Fe^{2+} in the conduction process in ferrite, thus causing an increase in resistivity. Resistivity of all compositions decreases with increasing temperature. Temperature $>180^0$C all the samples are independent of temperature.

Dielectric constant ε' decreases with increasing frequency exhibiting normal dielectric behavior of Ni-Zn-RE [La, Y and Eu] ferrites. The dielectric dispersion is rapid at lower frequency region and remains almost independent at high frequency. The dielectric behavior of ferrites may be explained on the basis of the mechanism of the dielectric polarization process and is similar to that of the conduction process.

5.2 Scope for Future Work

With the development and advancement of ferrites a tremendous surge in research on miniaturization and high efficiency electronic devices is one rise soft ferrite materials are extensively used in inductors which form a basic requirement in high technology areas. Most effective rare earth in Ni -Zn ferrites adequately suit these demands and are considered to shape the future of advanced technology.

The scopes of the future works are proposed as:

(i) Different multiphase ferrite systems to investigate the effect on different sintering temperature are improving electromagnetic properties.

(ii) Fabrication and characterization of multilayer chip inductor using improved Ni- Zn-RE ferrites as stated.

(iii) AC and DC electrical properties may be studied.

(iv) SEM can be studied for better understand surface nature and domain wall motion. Formation of secondary phase in ferrites with substitution RE shows a biphasic microstructure constituted of a matrix of dark grains and a second orthoferrite phase.

Therefore future work addition of small amount of RE ions to ferrite samples produces a change in their magnetic and electrical as well as structural properties depending upon the type and the amount of RE elements. Substitution rare earth in ferrites has been used as attractive approaches to enhance the electromagnetic properties.

REFERENCE

CHPATER-I

[1.1] Louh R. F., Reynolds T. G. and Buchanan R. C. "Ceramic Materials for Electronics", 3rd edition, edited by R. C. Buchanan, Marcel Dekker Inc. 2004.

[1.2] Kulikowski J., " Soft magnetic ferrites development of stagnation", J. Magn. Magn. Matter, 41, 56-62, 1984.

[1.3] Snoek J. L., "New development of Ferromagnetic Materials", Elsevier Publ. Co. N.Y. 1984.

[1.4] Ahmed T. T., Rahman I. Z and. Tofial S. A. M, "Effect of Copper in distribution on the magnetization of nano scaled Ni-Zn ferrites." J. Magn. Magn. Matter, 272-276, 2250-2252, 2004.

[1.5] Khan Z. H., Mahbubur Rahman M., Sikder S. S., M. A. Hakim, D. K. Saha, "Complex Permeability of Fe deficient Ni-Cu-Zn ferrites", Journal of Alloys and Compounds, 548, 208-215, 2013.

[1.6] Seo S. H. and Oh J. H. , " Effect of MoO_3 Addition of Sinterial behaviors and Magnetic properties of Ni-Cu-Zn Ferrite for Multilayer Chip inductors", IEE Transactions on Magnetics, 35, 5, 1999.

[1.7] Kin O. Low, Frank Sale R., "Electromagnetic properties of gel-derived Ni-Cu-Zn ferrites." J. Magn. Magn. Mater. 246, 30-35, 2002.

[1.8] Hakim M. A., Manjurul Haque M., Huq M., Manjura Hoque Sk. and Norbblad P., "Reentrant Spin Glass Behavior of Diluted Mg-Zn Ferrites", CP 1003, Magnetic Materials International Conference on Magnetic Materials, AIP.P-295, ICMM - 2007.

[1.9] Manjurul Haque M. and Huq M. and Hakim M. A., "Thermal hysteresis of Permeability and Transport properties of Mn Substituted Mg-Cu-Zn ferrites", Journal of Physics D: Applied Physics, 41, 1-10, 2008.

[1.10] Manjurul Haque M., Huq M. and Hakim, "Influence of CuO and Sintering Temperature on the microstructure and magnetic properties of Mg-Cu-Zn ferrites"; J. Magn. Magn.Mater.320, 2792-2799, 2008.

[1.11] Rezlescu N., Rezlescu E., Pasnicu C., Craus M. L., " Effect of the Rare Earth Metal of Some Properties of a Nickel-Zinc Ferrite," J. Phys Condensed Matter, 6, 5707, 1994.

[1.12] Solyman S., Cera Intern. 32, 755, 2006.

[1.13] Satter A. A. and EI-Shokrofy K. M., J. Physics. IV CI, 245, 1997.

[1.14] Ahmed M. A., Oskasha N. and Sayed M. M. E., Cera Intern, 33, 49, 2007.

[1.15] Bogoroditzkii N., Pasynkov V. V., Basili R. R. and Volokobinskii Y. M. Sov Phys. Doxlady, 10, 85, 1965.

[1.16] Li F. S., Wang L., Wang J. B., Zhou Q. G., Zhou X. Z., Kunkel H. P., Williams G., J. Magn. Magn. Mater. 268, 332, 2004.

[1.17] Neel L., Ann. Phys. Paris, 3, 137, 1948.

[1.18] Herzer G., Venqnez M., Krobel M., Zhokov A. Reininser T. and Davies H. A. "Present and Future Application of Nanocrystalline Magnetic Materials". J. Magn. Magn. Mater, 294, 252, 2005.

[1.19] Rezlescu N. and Rezlescu E., Solid State Commun., 88(2), 139, 1993.

[1.20] Sun G. L. , Li J. B., Sun J. J. and Yans X. Z. , J. Magn. Magn. Mater, 281, 173, 2004.

[1.21] Guo D., Fan X., Chai G., Jians C., Lix. and Xue D., "Structural and Magnetic Properties of Ni-Zn Ferrite Films with High Saturation Magnetization Deposited by Magnetron Sputtering."Appl. Surf. Sci., 256, 2319-2332, 2010.

[1.22] Naughton T. B. and Clark R. D., "Lattice Expansion and Saturation Magnetization of Nickel –Zinc Ferrite Nanoparticles Prepared by Aqueous Precipitation", Am, Ceram., Soc., 90, 3541-3546, 2007.

[1.23] Sun J., Li J. and Sun G., J. Magn. Magn. Mater, 25, 20, 2002.

[1.24] Costa A. C. F. M., Morelli M. R. and Kiminami R. H. G. A., J. Mat. Sci. 39, 1773, 2004.

[1.25] Khan Z. H. , Mahbubur Rahman M., Sikder S. S. , Hakim M. A., Shireen Akhter, Das H. N. and Anjuman B. " Thermal Hysteresis of Cu Substituted $Ni_{0.28}Cu_{0.10+x}Zn_{0.62-x}Fe_{1.98}O_4$ Ferrites." Advanced Chemistry Letters, 2, 1 - 6, 2013.

[1.26] Low K. O. and Sale F. R., J. Magn. Magn. Mater. 30, 246, 2002.

[1.27] Haque M. M., Huq M. and Halcim M. A., "Effect of Zn^{2+} Substitution on the Magnetic Properties of $Mg_{1-x}Zn_x Fe_2O_4$ Ferrites", Physica, B404, 3915, 2009.

[1.28] Roy P. K. and Bena J., "Electromagnetic Properties of Samarium Substituted Ni-Cu-Zn Ferrite Prepared by Auto Combustion Method" J. Magn. Magn. Mater, 321(4), 247-251, 2009.

[1.29] Roy P. K., Nayak B. B. H. and Bera J., " Study on Electro –magnetic Properties of La Substituted Ni-Cu-Zn Ferrite Synthesized by Auto Combination Method." J. Magn. Magn. Mater, 320, 1128-1132, 2008.

[1.30] Sattar A. A. ,Wafix A. H. , Shokrofy K. M. E. and Tabby M. M. E., Phys. Stat. Sol. (a), 171, 563, 1999

[1.31] Ahmed M. A., Okasha N. and Sayed M. M. E, Cera Intern. 33(1), 49, 2007.

[1.32] Saroaut Noor, Sikder S. S., Samirullah M., Hakim M. A. and Shireen Akhter, " Effect of Cd Properties of Co-Cd Ferrites". Journal of Bangladesh Academy of Science.35,229-235, 2011.

[1.33] Saroaut Noor, Mahbub Rahman M., Sikder S. S., and Hakim M. A., "Effect of Cd Substitution on Structural and Transparent Properties of Co-Ferrites." Jahangirnagar University J. of Sci.34, 2, 01-11, 2011.

[1.34] Saroaut Noor, Hakim M. A., Sikder S. S., Manjura S. Haque, Kazi Hanium Maria and Per Nordblad, " Magnetic Behavior of Cd^{2+} and Substituted Cobalt Ferrites." Journal of Physics and Chemistry of Solids, 73, 227-231, 2011.

[1.35] Zhao L. Cui Y., Yang H., Yu L., Jin W, and Feng S. Mat.Lett.60, 104, 2006.

[1.36] Zhao L., Yang H., Zhao X., Yu L. Cui Y. and Feng S., Matt. Lett., 60, 1, 2006.

[1.37] Abdeen A. M., "Electrical conduction in Ni-Zn ferrites", J. Magn. Magn. Mater., 185 199, 1998.

[1.38] Ahmed M. A., Ateia E., Salah L. M., Gamal A. A. E., Mat. Chem. Phys. 92, 310, 2005.

[1.39] Sun G. L., Li J. B., Sun J. J., Yang X. Z.; J. Magn. Magn. Mater., 281 173, 2004.

[1.40] Ajmal M., Maqsood A., All. Compd. 54, 2008.

[1.41] Nakamura T., "Low Temperature Sintering of Ni – Cu- Zn ferrite and its Permeability Spectra", J. Magn. Magn. Mater., 168 , 285 – 291, 1997.

[1.42] Nakamura T., Tsutaka T., Hatake Yana K., "Frequency dispersion of permeability in ferrite composite materials", J. Magn. Magn. Mater, 138 319, 1994.

[1.43] Rezlescu N., Rezlescu E., Popa P. D., Rezlescu L., J. Alloys Compds. 657, 275, 1998.

[1.44] Gabal M. A., Asiri A.M., Alangari Y. M., J. Ceram. Inter. 37, 2625, 2011.

[1.45] Jcoba S. E., Dukalde S., Bertorella H. R., J. Magn. Magn.Mater., 253, 272, 2004.

CHAPTER-II

[2.1] Rare Earth Elements - Critical Resources for High Technology: United States Geological Survey, Fact Sheet 087-02.

[2.2] Rare Earths**:** United States Geological Survey, Mineral Commodity Summaries, 2014.

[2.3] Rezlescu N., Rezlescu E., Pasnicu C., Craus M. L., J. Phys. Cond. Matter 6,5707, 1994.

[2.4] Satter A. A. and El- Shokrofy K. M. J. Phys, IV ed. 245, 1997.

[2.5] Jing J., Liang-Chao L., Feng X., Chin. J. Chem. 24, 1804, 2006.

[2.6] Jing J., Liang-Chao L., Feng X., J. Rare Earths.25, 79, 2007.

[2.7] Vanuitert L. G., J. Chemi. Phys. 23, 1883, 1955.

[2.8] Kolekar C. B., Kamble P.N., Vaingankar A.S., J. Bull. Mater. Sci. 18(2), 133, 1995.

[2.9] Jie S., Lixi W., Naicen X., Qitu Z., J. Rare Earths, 28, 445, 2010.

[2.10] Bahadur D. Giri J. Nayak B.B, Sriharsha T., Pradhan P., Prasad NK, *et. al*, J. Pramana Phys. 65, 663, 2005.

[2.11] Smit J., Wijn H. P., J. Ferrites, John Wiley and Sons, New York, 1959.

[2.12] Standley K. J.; "Oxide Magnetic Materials" 2 ed., Oxford University Press, 1972.

[2.13] Valenzuela R.; Magnetic Ceramics, Cambridge University Press, 1994.

[2.14] Murdock E. S., Simmons R. F., Davidson R. Roadmap for 10 Gbit/in2 Media: Challenges. IEEE Trans. Magnetics, 28, 5, 3078, 1992.

[2.15] Livingston T. D., "Driving force", The Natural Magic of Magnet, Harvard University Press: Cambridge, 1996.

[2.16] Culity B. D., " Introduction to Magnetic Materials", Addison- Wesley Publishing Com; 1972.

[2.17] Standly K. J, "Oxide Magnetic Materials", 2nd ed., Oxford University Press, 1972

[2.18] Verway E. J. and Heilmann E. L., Journal of Chem. Physics.15(4), 174, 1947.

[2.19] Van Uitert L. G., J. Chem. Phys. 24(2), 1956.

[2.20] Virginia Fuentes, Aburto S. and Velenzuela R., " Sub lattice in Nickel Ferrite." J. Magn. Magn. Mater., 69, 233, 1987.

[2.21] Anderson P.W.; In Magnetism, Vol 1, Eds, G. T. Rado and H. Shul; Academic Press, New York, 1963.

[2.22] Neel L., "Magnetic properties of Ferrites: Ferrimagnetisms and antiferromagntism"; Anneals de Physics, E3, 137-198, 1948.

[2.23] Romein F.C. , Philips Rep., 8, 304, 1953.

[2.24] Yafet Y. and Kittel C., "Antiferromagnetic arrangements in ferrites", Phys. Rev. 87, 290, 1952.

[2.25] Leyons D. H., Keplan T. A., Dwight K. and Menyuk N., "Classical theory of the ground spin state in cubic Spinels", Phys. Rev. 126, 540, 1962.

[2.26] Samokhvalov A. A. and Rustamov A. G.; SOV. Phys. Solid State, 6, 749, 1964.

[2.27] Bossmann A. J. and Crevecoeur C., "Mechanism of the electrical conduction in Li-doped NiO" , Phys. Rev. 144,763, 1966.

[2.28] Viswanathan B., Muthy V. R. K., "Ferrite Materials Science and Technology", Spring Vertay, Noarosa Publishing House, New Delhi, 1990.

[2.29] Jonker G. H.; J. Phys. Chem. Solids, 9, 165 – 175. 1959.

[2.30] Van Santan J. H. and Jonker G. H.; Physica, 19, 120, 1953.

Chapter III

[3.1] Kong L. B., Li Z. W., Lin G. Q. and Gan Y. B., "Magneto-Dielectric properties of Mg-Cu-Co ferrites Ceramic: II Electrical, dialectical and magnetic properties", J. Am. Ceram. Soc., 90(7), 2014, 2007.

[3.2] Sharma S. K., Kumar R., Kumar S. Knobel M., Menses C.T., Kumar V. V. S., Reddy V. R. , Singh M. and Lee C. G., " Role of inter particle interactions on the magnetic behavior of $Mg_{0.95}Mn_{0.05}Fe_2O_4$ ferrite nano particles", J. Phys. Conden. Matter., 20, 23, 2008.

[3.3] Zahi S., Hashim M. and Daud A. R.; "Synthesis magnetic and microstructure of Ni-Zn ferrite by Sol-gen technique"; J. Magn. Magn. Mater., 308, 177, 2007.

[3.4] Hakim M. A., Saha D. K. and Fazle Kibria A. K. M., "Synthesis and temperature dependent structural study of nanocrystalline Mg- ferrite materials", Bang. J. Phys., 3, 57, 2007.

[3.5] Bhaskar A., Rajini Kanth B. and Murthy S. R., "Electrical properties of Mn added Mg-Cu- Zn ferrites prepared by microwave sintering method", J. Magn. Magn. Mater., 283, 109, 2004.

[3.6] Yue Z., Zhou J., Li L. and Gui Z.; "Effects of MnO_2 on the electro-magnetic properties of Ni-Cu-Zn ferrites prepared by sol-gel auto combustion", J. Magn. Magn. Mater., 233, 224, 2001.

[3.7] Chen C. W.; Magnetism and Metallurgy, Soft Mag. Mat., North-Holland Pub. Com. XV, 288, 1977.

[3.8] Goldman A; Handbook of Modern Ferromagnetic Materials, Kulwer Acad. Pub, Boston, U. S. A., 1999.

[3.9] Tahir Abbas, Islam M. U. and Ashraf Ch M., Mod. Phy. Letts. B 9(22), 1419, 1995.

[3.10] Smit J. and Wijin H. P.; Ferrites, Wiely New York, 250, 1959.

[3.11] Forner S.; "Versatile and sensitive Vibrating Sample Magnetometer", Rev. Sci. Instr. 30, P.548, 1959

Chapter IV

[4.1] Ben Tahar L., Artus M., Ammar S., Smiri L.S., Herbst F., Vaulay M. J., Richard V., Greneche J. M., Villian F., Fievert F., " Magnetic Properties of $CoFe_{1.9}Re_{0.1}O_4$" nanoparticles (RE = La, Ce, Nd, Sm, Eu, Gd, Tb, Ho) prepared in Poyol", J. Magn. Magn. Mater. 323, 2420, 2008.

[4.2] Mansour Al-Haj, "Structural Characterization and Magnetization of $Mg_{0.7}$ $Zn_{0.3}Sm_x$ $Fe_{2-x}O_4$ Ferrites". J. Magn. Magn. Mater., 299, 435, 2000.

[4.3] Sun J., Li J., Sun G., "Effects of La_2O_3 and Gd_2O_3 on some properties of Ni-Zn Ferrites." J. Magn. Magn. Mater., 250, 20, 2002.

[4.4] Ahmed M. A., Ateia E., Salah Z. M., Gmal El. A. A. " Structural and Electrical Studies of La^{3+} substituted Ni-Zn ferrites Mater." Chem. Phys. 92, 310, 2005.

[4.5] Satter A. A., and Shokrofy El., K., M... J. Phys IV CI P. 245, 1997.

[4.6] Nelson J. B., Riley D. P, "An experimental investigation of extrapolation methods in the derivation of accurate unit-cell dimension of crystals"; Proc. Phys. SOC London 57,160,1945.

[4.7] Vagards L., "Die constitution der mischkristalle und die raumfullung der atome", Z. Phys. 5, 17, 1921.

[4.8] Sun G., Li J., Sun J.and Yang X., "The Influences of Zn^{2+} and Some Rare-Earth Ions on the Magnetic Proper-ties of Nickel-Zinc Ferrites," Journal of Magnetism and. Magnetic Materials, 281,173-177, 2004.

[4.9] Jacobo S. E., Fano W. G. and Razzitte A. C., "The Effect of Rare Earth Substitution on the Magnetic Properties of $Ni_{0.5}Zn_{0.5}M_xFe_{2-x}O_4$ (M: Rare Earth)," Physica B, 320, 261-263, 2002.

[4.10] Yang Z. H., Gong Z., Q., Li H. X., Ma Y. T. and Yang Y. F., " Synthesis of Ni-Zn Ferrites and Its Microstructure and Magnetic Properties." Journal of Central South University of Technology, 13, 618-623, 2006.

[4.11] Mendelson, M. I., "Average Grain Size in Polycrystalline Ceramics." J. Am. Ceram, Soc. 52, 8,443-446, 1969.

[4.12] Cullity B. D., Graham C. D., "Introduction to Magnetic Materials."2nd ed., 2009.

[4.13] Globus A., Monjaras R. V., "Influence of the Deviation from Stoichiometry on the Magnetic Properties of Zn Rich Ni-Zn Ferrites", IEEE Trans. Magn. 11(5), 1300-1302, 1975

[4.14] Brockman F. G., Dowling P. H. and Steneck W. G., "Dimensional effects resulting from a high dielectric constant found in a ferromagnetic ferrite", Phys. Rev. 77 85, 1950.

[4.15] Gorter E. W. Philips Res. Rep. 9, 295, 1954.

[4.16] Brockman F. G., Dowliay P. H., Stenneck W. G., " Dimensional Effects Resulting from a High Dielectric Constant Found in Ferromagnetic Ferrite". Phys. Rev. 77, 85, 1950.

[4.17] Snelling E. C.; "Soft Ferrites; Properties and Applications".Ed., Butterworth, London, 1988.

[4.18] Overshott K.; "The causes of the Anomalous Loss in Amorphous Ribbon Materials". IEEE Trans. Magn. 17, 2698, 1981.

[4.19] Gorter E. W., "Saturation Magnetization and Crystal Chemistry of Ferrimagnetic Oxides". Philips, Res. Rep. 9, 295, 1954.

[4.20] Neel I., Ann. Phys. 3, 137, 1948.

[4.21] Ahmed M. A., Ateia E., Salah L. M. Gamal A. A. E; Mat. Chem. Phys. 92 310. 2005.

[4.22] Smit J., Wijn H. P. J.; Ferrites, Philips Tech. Library (Netherlands) 1959.

[4.23] Zhenxing Yue, Zhou Ji, Longtu Li, Xiaolui Wang and Zhilun Gui, "Effect of copper on the electromagnetic properties of Mg-Zn-Cu ferrites prepared by Sol-gel auto-combustion method"; Mater. Sci. Eng. B 86, 64, 2001.

[4.24] Maxwell J.; 1873, Electricity and Magnetism, Vol.1 Oxford University Press. London Wanger K, Ann. Phys. 40, 817, 1913.

JOURNAL PAPERS/CONFERENCE PUBLICATIONS

[1] M. A. Hossain, M. N. I. Khan and S. S. Sikder: "Study of the Variation of Resistivity, Permeability and Curie Temperature of Rare Earth Metal lanthanum (la) Substitution on $Ni_{0.60}Zn_{0.40-x}La_x$ Fe_2O_4 (x=0.05, 0.10, 0.15) Ferrites ". American Scientific Research Journal for Engineering, Technology, and Sciences (ASRJETS) (USA).Volume 14, No 2, pp 72-79, 2015.

[2] M. A. Hossain, M. N. I. Khan and S. S. Sikder: "Effect of Resistivity, Permeability and Curie temperature of Rare Earth Metal Europium (Eu) Substitution on $Ni_{0.60}Zn_{0.40-x}Eu_x$ Fe_2O_4 (x=0.05, 0.10, 0.15) Ferrites". ARPN Journal of Science and Technology (Malaysia).VOL. 5, NO. 10, October 2015.

[3] M. A. Hossain, M. N. I. Khan and S. S. Sikder:"Study of the Variation of Resistivity, Permeability and Curie Temperature of Rare Earth Metal Yttrium (Y) Substitution on $Ni_{0.60}Zn_{0.40-x}Y_x$ Fe_2O_4 (x=0.05, 0.10, 0.15) Ferrites" IEEE XPlore, Proceedings of International Conference on Electrical Information and Communication Technology (EICT 2015).

[4] M. A. Hossain, M. N. I. Khan, S. S. Sikder, S. M. Hoque and D. K. Saha, 2016: **"**Structural and Magnetic Behaviors of Rare Earth substituted $Ni_{0.60}Zn_{0.40-x}Eu_xFe_2O_4$Ferrites", Presented at International Conference on Physics-2016, Bangladesh Physical Society, Dhaka, 10-12 March 2016.

[5] M. A. Hossain, S. S. Sikder, M. N. I. Khan and D. K. Saha 2016: Structural and Magnetic properties of La Substituted Ni-Zn Ferrites: **"**Presented at International Conference on Physics-2016, Bangladesh Physical Society", Dhaka, 10-12 March 2016.

[6] M. A. Hossain, M. N. I. Khan and S. S. Sikder: 2016: "Structural and Magnetic Properties of Yttrium (Y) Substituted Ni-Zn Ferrites"**,** Presented at Conference on Weather Forecasting and Advances in Physics**:** Bangladesh Perspective, Khulna University of Engineering & Technology, Khulna, 20th May 2016.

[7] M. A. Hossain, M. N. I. Khan,S. S. Sikder: "Complex Permeability of La, Y, Eu incorporation Ni-Zn Ferrites".Presented at National Conference on Physics-2017, Bangladesh Physical Society, Dhaka, 5-7 February 2017.

M. Phil. Thesis | Md. Alamgir Hossain | January-2017